Title

Theoretical estimates of equilibrium sulfur isotope effects among aqueous polysulfur and associated compounds with applications to authigenic pyrite formation and hydrothermal disproportionation reactions

Authors

Eldridge, Daniel L
Kamyshny, Alexey
Farquhar, James

Publication Date

2021-10-01

DOI

10.1016/j.gca.2021.05.051

Peer reviewed

Journal Pre-proofs

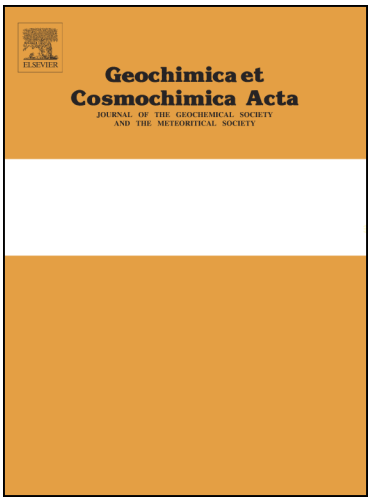

Theoretical estimates of equilibrium sulfur isotope effects among aqueous polysulfur and associated compounds with applications to authigenic pyrite formation and hydrothermal disproportionation reactions

Daniel L. Eldridge, Alexey Kamyshny Jr., James Farquhar

PII: S0016-7037(21)00332-X
DOI: https://doi.org/10.1016/j.gca.2021.05.051
Reference: GCA 12235

To appear in: *Geochimica et Cosmochimica Acta*

Received Date: 25 August 2020
Accepted Date: 25 May 2021

Please cite this article as: Eldridge, D.L., Kamyshny, A. Jr., Farquhar, J., Theoretical estimates of equilibrium sulfur isotope effects among aqueous polysulfur and associated compounds with applications to authigenic pyrite formation and hydrothermal disproportionation reactions, *Geochimica et Cosmochimica Acta* (2021), doi: https://doi.org/10.1016/j.gca.2021.05.051

Theoretical estimates of equilibrium sulfur isotope effects among aqueous polysulfur and associated compounds with applications to authigenic pyrite formation and hydrothermal disproportionation reactions

Daniel L. Eldridge[a,b,c,*], Alexey Kamyshny Jr.[d], James Farquhar[e]

[a] *Earth and Environmental Sciences Area, Lawrence Berkeley National Laboratory, 1 Cyclotron Road, Berkeley, CA 94720 USA*
[b] *Department of Earth and Planetary Science, University of California, Berkeley, CA 94720 USA*
[c] *Geophysical Laboratory, Carnegie Institution of Washington, 5251 Broad Branch Road NW, Washington, DC 20015 USA*
[d] *Department of Geological and Environmental Sciences, Ben-Gurion University of the Negev, P.O. Box 653, Beer Sheva 84105 Israel*
[e] *Department of Geology and ESSIC, University of Maryland, College Park, MD 20740 USA*

Abstract

Inorganic polysulfur compounds (polysulfides, S_x^{2-}; polysulfur radical ions, $S_x^{\cdot -}$; thiosulfate, $S_2O_3^{2-}$; polythionate, $S_xO_6^{2-}$; elemental sulfur, e.g. S_8) participate in numerous geochemical processes related to the sulfur cycle. These include authigenic pyrite formation in sediments undergoing early stages of diagenesis, reactions associated with magmatic-hydrothermal processes, and numerous other aquatic sulfur redox processes (e.g., pyrite and sulfide oxidation). Sulfur isotope fractionations among many of these and associated compounds (e.g., H_2S, HSO_4^-) are either unknown or unconstrained over wide ranges of temperatures. We present theoretical estimates of equilibrium sulfur isotope fractionation factors among aqueous polysulfur compounds (including select polysulfides, polysulfur radical anions, and polythionates) and select aqueous sulfide and sulfate compounds that correspond to all three stable isotope ratios of sulfur ($^{33}S/^{32}S$, $^{34}S/^{32}S$, $^{36}S/^{32}S$). Our estimates are based on electronic structure calculations

*Corresponding author
Email address: danieleldridge@lbl.gov (Daniel L. Eldridge)

performed at the B3LYP/6-31+G(d,p) level of theory and basis set implemented in concert with an explicit solvation model whereby molecules are encapsulated in water clusters of varying size (30-52 H_2O) to simulate the aqueous solvation environment. These calculations yield relatively small magnitude fractionation factors between aqueous polysulfides, polysulfur radicals, and reduced sulfur moieties in polythionates relative to the aqueous sulfide compounds but reveal numerous crossovers that result in non-intuitive temperature dependencies. Our predictions of $^{34}S/^{32}S$-based fractionation factors among aqueous sulfur compounds generally agree with previous experimental constraints where available within estimated uncertainties (e.g., $HSO_4^-/H_2S_{(aq)}$, $H_2S_{(aq)}/HS^-$, HSO_4^-/S^0, $H_2S_{(aq)}/S^0$). We use our calculations to explore equilibrium isotope fractionations among polysulfur and sulfide compounds that are precursors to authigenic pyrite in the framework of established mechanisms (e.g., the polysulfide mechanism). We examine possible explanations for why pyrite formation may be associated with relatively small isotope fractionation with respect to precursor aqueous sulfur compounds. We additionally use our theoretical calculations to constrain multiple sulfur isotope ($^{33}S/^{32}S$, $^{34}S/^{32}S$, $^{36}S/^{32}S$) mass balance models associated with the abiotic hydrolytic disproportionation of intermediate sulfur compounds (SO_2, S_8, $S_3^{\cdot-}$) relevant to hydrothermal-magmatic-volcanic systems in order to illustrate the potential for subtle but potentially resolvable effects expressed in values of $\Delta^{33}S$ and $\Delta^{36}S$ associated with these processes. We apply a SO_2 disproportionation mass balance model based on previous work but newly constrained by our theoretical calculations to (hyper-)acid crater lakes associated with active volcanoes, and newly highlight the potential for the utility of multiple sulfur isotope analyses in volcanic gas monitoring and constraining sulfur cycling processes in such systems.

Keywords: sulfur isotopes, polysulfides, pyrite formation, disproportionation, acid crater lakes, hydrothermal

1. Introduction

Inorganic polysulfur compounds contain more than one sulfur atom and typically contain one or more sulfur-sulfur bonds. They commonly occur as anions dissolved in aqueous solutions. These include the aqueous polysulfides (S_x^{2-} and their protonated counterparts) and polysulfur radical anions ($S_x^{\cdot -}$) that contain relatively reduced sulfur (low oxidation state), and polythionates ($S_xO_6^{2-}$) and thiosulfate ($S_2O_3^{2-}$) that contain mixed-valence sulfur (low and high oxidation states).

The aqueous polysulfides can play a direct role in the formation of authigenic pyrite (FeS_2; e.g., Luther, 1991; Rickard & Luther, 2007). Authigenic pyrite is a ubiquitous component of marine sediments and sedimentary rocks that can begin forming in the water column and during the earliest stages of sediment diagenesis. Much of the reduced sulfur that is incorporated into pyrite is ultimately derived from dissimilatory sulfate reduction that produces H_2S/HS^- via anaerobic respiration. Pyrite preserved in sedimentary rocks is thus broadly viewed as a primary archive of the environmental sulfur and related elemental cycles, capturing a record that preserves isotopic signals of sulfur cycling processes at the time of their formation (e.g., Canfield, 2004; Johnston, 2011; Rickard, 2014). However, little is known about the potential isotope fractionations that may accompany pyrite formation processes from more primary sulfur sources in sedimentary environments. This may in part be due to the complexity of the aqueous sulfur speciation of compounds that are thought to directly participate in pyrite formation.

The molecular forms of sulfur and iron that participate in the process of pyrite precipitation and growth can vary depending on the environment and conditions, but a handful of relevant reactions have been identified based on experimental studies (Luther, 1991; Rickard, 1997; Rickard & Luther, 1997; Butler et al., 2004; Rickard & Luther, 2007):

$$HS^- + Fe^{2+} \rightleftharpoons FeS_{(aq)} + H^+ \quad (1)$$

$$HS^- + (x-1)S^0 \rightleftharpoons S_x^{2-} + H^+ \quad (2)$$

$$FeS_{(aq)} + S_x^{2-} \rightleftharpoons FeS_2 + S_{(x-1)}^{2-} \quad (3)$$

$$FeS_{(aq)} + H_2S \rightleftharpoons FeS_2 + H_2 \quad (4)$$

The S_x^{2-} represent the polysulfides of various chain-length ('x'; $x = 2 - 8$; Kamyshny et al., 2004, 2007) and their protonated forms HS_x^- and H_2S_x (Schwarzenbach & Fischer, 1960; Meyer et al., 1977), the S^0 generically refers to a form of zero valent sulfur (e.g., orthorhombic α-S, monoclinic β-S and γ-S, dissolved S_8 rings, etc.; Meyer, 1976; Boulegue, 1978), and $FeS_{(aq)}$ can refer to the molecular ferrous sulfide monomers in solution (e.g., the $FeS^0_{(aq)}$monomer species that may exist in a pH-dependent equilibrium with $FeSH^+$) and/or dissolved nano-particulate forms that have poorly constrained compositions and structures (Rickard & Morse, 2005; Rickard, 2006; Rickard & Luther, 2007). The reactions represented in equations 3 and 4 (the 'polysulfide' and 'hydrogen sulfide' mechanisms, respectively) are regarded as overall representations of the two experimentally documented mechanisms for pyrite nucleation/precipitation (Luther, 1991; Rickard, 1997), which combined with pyrite crystal growth mechanisms (Harmandas et al., 1998) represent the primary reactions thought to be responsible for 'pyrite formation' under conditions relevant to marine sedimentary environments (Rickard & Luther, 2007).

The isotopic composition of freshly precipitated/nucleated pyrite can be influenced not only by the isotopic composition of ambient $\sum H_2S_{(aq)}$ (e.g., sourced from dissimilatory sulfate reduction), but also the mass balance of exchange between aqueous sulfide and ambient elemental sulfur (potentially predominately sourced from the oxidative cycling of aqueous sulfide) that is facilitated by the polysulfides (Eq. 2). Aqueous sulfide and polysulfide compounds appear to achieve relatively rapid isotopic equilibrium at low temperatures (Fossing & Jørgensen, 1990). Thus, if the 'polysulfide mechanism' is in operation

the equilibrium isotope partitioning between aqueous polysulfide and sulfide may place first order controls on the isotopic composition of pyrite relative to ambient aqueous sulfide depending on the additional isotope fractionations that accompany the precipitation of pyrite. Although it is presently understood that the isotope fractionations associated with pyrite formation (e.g., relative to ambient $\sum H_2S_{(aq)}$) resulting from the mechanisms above must be relatively small (Wilkin & Barnes, 1996; Butler et al., 2004), there has been no attempt to quantify the fractionation factors associated with either pyrite formation processes or those among the precursor aqueous sulfur compounds that participate in pyrite precipitation and growth.

The role of analogous polysulfur radical anions ($S_x^{\cdot -}$) in natural sulfur cycling is actively being elucidated. Radical polysulfur anions have long been recognized to be responsible for the deep blue coloration of some sodalite group minerals (e.g., McLaughlan & Marshall, 1970) and some sulfur-rich aqueous fluids at elevated temperature (e.g., Giggenbach, 1971; Chivers & Elder, 2013, and references therein). Recent experimental work of sulfur-rich hydrothermal fluids has reinvigorated the study of the trisulfur radical anion ($S_3^{\cdot -}$; Pokrovski & Dubrovinsky, 2011; Jacquemet et al., 2014; Pokrovski & Dubessy, 2015; Schmidt & Seward, 2017). In particular, the trisulfur radical ion has been recently recognized as a potentially important ligand in the hydrothermal mobilization and transport of precious metals such as gold under certain redox/pH conditions (Pokrovski et al., 2015) and as having an intermediary role in thermochemical sulfate reduction (Truche et al., 2014). Additionally, the trisulfur radical anion has been observed to be a component of naturally-occurring aqueous fluid inclusions in minerals (quartz, fluorite, anhydrite) associated with thermally processed evaporites upon their re-heating in the laboratory (Barré et al., 2017). Polysulfur radical anions could play a role in facilitating isotope exchange between oxidized (i.e., sulfate) and reduced sulfur (i.e., sulfide) at elevated temperatures in hydrothermal fluids under some conditions (e.g., Pokrovski & Dubessy, 2015; Kokh et al., 2020) but such processes are not yet understood in detail. Few studies have directly constrained the isotopic fractionations among the polysul-

fur radicals and coexisting sulfur compounds such as aqueous sulfide and sulfate (i.e., limited to the theoretical calculations of Tossell, 2012). Such constraints are required to lay the groundwork for understanding the possible role these compounds may play in sulfur isotopic variability among naturally occurring phases that result from transformations related to these compounds.

In the present study, we use *Gaussian09* software (Frisch et al., 2013) and a 'supermolecular' explicit solvation water cluster model (encapsulation of solute in clusters containing 30-52 water molecules) to estimate equilibrium sulfur isotope fractionation factors for all three isotope ratios of sulfur ($^{33}S/^{32}S$, $^{34}S/^{32}S$, $^{36}S/^{32}S$) among numerous aqueous sulfur compounds. These include: (a) select polysulfides (S_x^{2-}, HS_x^-) and aqueous sulfide compounds (H_2S, HS^-, $FeS^0_{(aq)}$, $FeSH^+$) that are relevant to authigenic pyrite formation mechanisms, (b) aqueous polysulfur radical anions ($S_2^{\cdot-}$, $S_3^{\cdot-}$) and some of the coexisting sulfide and sulfate compounds/ion-pairs (e.g., H_2S, HS^-, $(Na^+HS^-)^0$, HSO_4^-, SO_4^{2-}, $(Na^+SO_4^{2-})^-$) relevant to some natural and experimental hydrothermal systems (Ohmoto & Lasaga, 1982; Pokrovski & Dubessy, 2015; Schmidt & Seward, 2017), and (c) select polythionates (trithionate, $S_3O_6^{2-}$; tetrathionate, $S_4O_6^{2-}$) that are also relevant to biological, aquatic, sedimentary and hydrothermal-magmatic systems (e.g., Takano, 1987; Zopfi et al., 2004; Leavitt et al., 2015; Findlay & Kamyshny, 2017). We additionally model a molecular S_8 ring in a 50 H_2O cluster to obtain estimates of the sulfur isotope partitioning behavior of dissolved elemental sulfur relevant to hydrothermal systems. S_8 is only sparingly soluble in water at 25℃ (e.g., 19±6 nM; Boulegue, 1978) but its solubility increases substantially with increasing temperature (e.g., Kamyshny, 2009). Most naturally-occurring and relevant forms of crystalline sulfur are also comprised of molecular S_8 (Meyer, 1976). The purpose of this study is to examine equilibrium sulfur isotope fractionations among predominately reduced sulfur compounds/moieties, and to provide constraints that may be useful to elucidating isotope partitioning in aqueous systems that exhibit complex molecular compositions.

2. Methods

2.1. Reduced Partition Function Ratio

Theoretical equilibrium isotope fractionation factors among molecular substances of interest can be computed utilizing computations of the reduced partition function ratios (RPFR) of their component isotopologues (Urey, 1947; Bigeleisen & Mayer, 1947):

$$RPFR = \prod_{i}^{l} \frac{u_i^* \times e^{-u_i^*/2} \times (1 - e^{-u_i})}{u_i \times e^{-u_i/2} \times (1 - e^{-u_i^*})} \quad (5)$$

where * denotes terms related to the isotopically substituted molecule and $u_i = \frac{hc\omega_i}{k_b T}$, where: k_b is the Boltzmann constant, h is the Planck constant, c is the speed of light, T is temperature, and ω_i is the wave number for harmonic vibrational mode i (note vibrational frequency $\nu_i = c\omega_i$) and the product is over all harmonic vibrational modes (number of modes equal to $l = 3a$–6 for a non-linear molecule and $l = 3a$–5 for a linear molecule, where a is the number of atoms in the molecule). This approach has been extensively reviewed elsewhere (Urey, 1947; Richet et al., 1977; Chacko et al., 2001; Liu et al., 2010). The primary variables needed to estimate RPFRs and, thus, fractionation factors are the harmonic vibrational frequencies (ν_i) of relevant isotopologues that can be readily obtained using modern quantum mechanics-based computational chemistry software packages.

2.2. Quantum Mechanical Software: Gaussian 09

We use *Gaussian09* software (Revision E.01; Frisch et al., 2013) for our electronic structure calculations. We implement the B3LYP/6-31+G(d,p) level of theory and basis set size to generate harmonic vibrational frequencies (unscaled) for computing RPFRs following our previous sulfur isotope study (Eldridge et al., 2016). As described in Eldridge et al. (2016), the B3LYP method is a hybrid HF/B-LYP theoretical approach that employs the Becke and Lee, Yang, Parr 3-parameter gradient-corrected correlational functional (Lee et al.,

1988; Becke, 1993; Foresman & Frisch, 1996) that includes electron correlation. The basis set is the double-zeta Pople basis set (6-31G) with diffuse functions added (+) to the non-hydrogen atoms that is often required for modeling anions, and polarization functions (p functions for all atoms, d functions for all non-hydrogen atoms) for additional flexibility in the computation of molecular orbitals. This approach is of relatively low/moderate computational complexity and accuracy that has been chosen for reasons of practicality given the relatively large molecular clusters modeled in this study. We use this same computational approach for calculations of the polysulfur radical ion species for the purpose of computing RPFRs following directly after Tossell (2012) (note: time-dependent methods for treating excited states such as TD-B3LYP and CIS have also been previously implemented for these species but only for the purpose of calculating UV-Visible spectra, which is beyond the scope of the present study; *cf.* Tossell, 2012). In conjunction with an explicit solvation model, this approach has been shown to be reasonably accurate for predicting equilibrium sulfur isotope effects among a number of aqueous sulfur compounds based on a comparison to available experimental constraints (Eldridge et al., 2016, 2018).

2.3. Explicit Solvation Model

Modeled sulfur compounds are encapsulated in clusters of water molecules (ranging 30-52 H_2O) to approximate the effect of aqueous solvation on molecular vibrations and RPFRs (e.g., Liu & Tossell, 2005; Rustad & Bylaska, 2007; Rustad et al., 2008; Zeebe, 2009; Li et al., 2009; Zeebe, 2010; Rustad et al., 2010; Li & Liu, 2011; Hill et al., 2014; Eldridge et al., 2016). The largest aqueous clusters for a given solute were constructed following an analogous 'manual' cluster building technique to our previous study (Eldridge et al., 2016). The manual aqueous cluster building technique differs from another common cluster generating technique that utilizes molecular dynamics simulations of solutes in water clusters to generate "snap shot" geometries to use as a starting point for optimization and frequency calculations for similar purposes (Rustad & Bylaska, 2007; Rustad et al., 2008, 2010; Hill et al., 2014). In short, our approach

involves the manual coordination of the sulfur solute with water molecules in a step-wise optimization procedure (typically 3-5 water molecules per step) until a maximum cluster size is achieved (ca. 45-52 H_2O in the present study). In general, the small cluster sizes generated during this step-wise procedure were not used for frequency calculations due in part to some instances of incomplete solvation coverage of the solute.

Several different clusters (up to 8 depending on the solute) of varying size (30 to 52 H_2O) were typically computed for each sulfur compound in order to assess the variability in RPFRs associated with water cluster size. Aqueous clusters of smaller size were primarily generated by the procedure of removing water molecules from the largest clusters generated for a given solute (ca. 45-52 H_2O) and subjecting the resulting clusters of smaller size to optimization and frequency calculations. This 'whittling-down' approach allows for much greater control on the solvation coverage of the solute in smaller clusters by selective water removal in order to avoid errant situations of incomplete solvation (i.e., migration of solute to the edge of a cluster), and also allows for the tracking of the same atomic sites of the solutes through different cluster sizes and optimizations. As we will demonstrate below, this approach led to different solvation environment around solutes based on observed differences in the number of water molecules that appear to be directly coordinated with atomic sites of the solute. A list of the computed sulfur solutes (polysulfide, polysulfur radical, polythionate, sulfide, elemental sulfur, and sulfate compounds) embedded in water clusters of various size is provided in Table 1 for reference.

2.4. Approach to Modeling the Polysulfides and their Structures

Thermodynamic data presently exists for polysulfides (S_x^{2-}) containing up to eight sulfur atoms (Kamyshny et al., 2004, 2007) but polysulfides with up to nine sulfur atoms have been observed experimentally (Gun et al., 2004). The pK_{a1} of polysulfides ($H_2S_x = HS_x^- + H^+$) decreases with increasing chain length from 5.0 for disulfide to 2.9 for octasulfide, and the pK_{a2} ($HS_x^- = S_x^{2-} + H^+$) decreases from 9.7 to 4.4 for the same species (Schwarzenbach & Fischer, 1960;

Meyer et al., 1977). Thus, under circum-neutral pH conditions the polysulfides with $x > 3$ predominantly exist in the form of S_x^{2-} and disulfide and trisulfide exist in the form of HS_x^-. For the purposes of the present study, the polysulfides of primary interest will be S_x^{2-} $(x = 2 - 8)$ and HS_x^- $(x = 2 - 3)$.

Multiple stereoisomers are possible for S_x^{2-} when $x \geq 4$ (Steudel, 2003; Rickard & Luther, 2007). For simplicity, the longer chain-length polysulfides $(x = 5 - 8)$ have each been modeled solely as helical structures that closely resemble all-trans stereoisomers (Steudel, 2003; Rickard & Luther, 2007). Additionally, we have not attempted to distinguish between the $d-$ and $l-$isomers of polysulfides ranging from $x = 4 - 8$ (Rickard & Luther, 2007), and similarly we do not make any attempt to distinguish between the stereoisomers of the protonated polysulfide, HS_3^-. These different stereoisomers result in different relative orientations of the component atoms but do not result in changes in bonding order with respect to a given sulfur atom. For simplicity, we also consider the aqueous ferrous sulfide species ($FeS_{(aq)}$) as the monomeric neutral diatomic $FeS^0_{(aq)}$ and its protonated counterpart $FeSH^+$ because the precise structures and compositions of $FeS_{(aq)}$ relevant to natural systems are complex and perhaps not well understood (Rickard & Morse, 2005; Rickard, 2006; Rickard & Luther, 2007; Haider et al., 2013).

2.5. Fractionation Factors

RPFRs corresponding to the isotopologues of a particular molecular substance can be conveniently related to isotope fractionation factors via β-values (Richet et al., 1977), represented in simplified and approximate form as:

$$\beta \approx \prod^{x} RPFR^{\frac{1}{x}} \tag{6}$$

Where x is the number of elemental sites in the molecule, and the product is over all singly-substituted isotopologues. In principle, the β-value represents a fractionation factor between a molecular substance of interest and an ideal monoatomic gaseous reference atom under the condition of equilibrium (Richet

et al., 1977). The exact β takes into account all isotopologues corresponding to a particular isotope substitution (i.e., ^{33}S or ^{34}S or ^{36}S) and their relative abundances including multiply substituted isotopologues to comprise a bulk isotopic composition of the molecular substance with respect to a particular isotope ratio. Eq. 6 approximates β by ignoring additional terms that relate to multiply substituted molecules that in practice have negligible influence on bulk isotopic compositions (e.g., Richet et al., 1977).

When elemental sites are not equivalent, more careful treatment may have to be taken in order to ensure accuracy. For the polysulfides and polysulfur radical anions in this study, we approximate β by assuming that the β-factor for the given S_x^{2-} (or HS_x^-) or $S_x^{\cdot -}$ is equivalent to the product of the RPFRs of x-number of individual singly substituted isotopologues raised to the power of x^{-1} (i.e., Eq. 6). This approximation includes the assumption that the singly substituted isotopologues of a given polysulfide chain (e.g., for S_3^{2-} or $S_3^{\cdot -}$: ^{34}S-^{32}S-^{32}S, ^{32}S-^{34}S-^{32}S, and ^{32}S-^{32}S-^{34}S) contribute in an equally proportional manner to the overall bulk isotopic composition of the polysulfide (i.e., are present in equal abundance), which is reasonable given what we will show to be the relatively small differences in RPFR between individual isotopologues of polysulfides and polysulfur radicals. We will illustrate in Section 3.3 the likely negligible impact of this approximation on our computations of β-factors for the polysulfides and polysulfur radical anions. For aqueous sulfur molecules containing only one sulfur atom (i.e., aqueous sulfide and sulfate compounds), $\beta \approx RPFR$ to a very good approximation that ignores only the contributions from multiply substituted isotopologues.

This treatment allows for straightforward computation of equilibrium fractionation factors (α) among compounds by taking the ratios of their β-factors (e.g., between compound A and compound B):

$$^{33}\alpha_{A-B} = \frac{^{33}R_A}{^{33}R_B} = \frac{^{33}\beta_A}{^{33}\beta_B} \quad (7)$$

$$^{34}\alpha_{A-B} = \frac{^{34}R_A}{^{34}R_B} = \frac{^{34}\beta_A}{^{34}\beta_B} \quad (8)$$

$$^{36}\alpha_{A-B} = \frac{^{36}R_A}{^{36}R_B} = \frac{^{36}\beta_A}{^{36}\beta_B} \quad (9)$$

Mass-dependent relationships can be computed from fractionation factors *via* the following relations:

$$^{33/34}\theta_{A-B} = \frac{ln(^{33}\alpha_{A-B})}{ln(^{34}\alpha_{A-B})} \quad (10)$$

$$^{36/34}\theta_{A-B} = \frac{ln(^{36}\alpha_{A-B})}{ln(^{34}\alpha_{A-B})} \quad (11)$$

We will generically refer to values of $^{33/34}\theta$ and $^{36/34}\theta$ as the "exponents of mass dependence" associated with particular equilibrium isotope exchange reactions. Similar relationships can be applied to exponents derived from β-factors for a particular compound (e.g., compound A):

$$^{33/34}\kappa_A = \frac{ln(^{33}\beta_A)}{ln(^{34}\beta_A)} \quad (12)$$

$$^{36/34}\kappa_A = \frac{ln(^{36}\beta_A)}{ln(^{34}\beta_A)} \quad (13)$$

where we follow the kappa-notation of Cao & Liu (2011). In the present study, polynomial fits to values of $^{33}\beta$ and $^{36}\beta$ as a function of temperature will be tabulated in terms of their corresponding $^{33/34}\kappa$ and $^{36/34}\kappa$ values to minimize spurious errors.

We can also define values of Δ^{33}S and Δ^{36}S in terms of fractionations between specific compounds:

$$\Delta^{33}S = \left(\frac{^{33}R_A}{^{33}R_B} - \left(\frac{^{34}R_A}{^{34}R_B}\right)^{0.515}\right) \times 1000 \quad (14)$$

$$\Delta^{36}S = \left(\frac{^{36}R_A}{^{36}R_B} - \left(\frac{^{34}R_A}{^{34}R_B}\right)^{1.90}\right) \times 1000 \quad (15)$$

Where Δ-values are in units of permil and the values of 0.515 and 1.90 are the conventional reference exponents. For equilibrium Δ-values between compounds the above isotope ratios can be replaced by the appropriate β-factors (*cf.* Eq. 7-9). Note that when values of Δ^{33}S and Δ^{36}S are reported in terms of a sample relative to a reference standard the isotope ratios of A in the above equations can be replaced by the isotope ratios of the sample and the isotope ratios for B can be replaced by the isotope ratios of the reference standard.

For aqueous sulfur molecules such as the polythionates ($S_xO_6^{2-}$) that contain sulfur atoms that have different oxidation states and therefore very different RPFRs, we will not use the concept of β to describe fractionation behavior. Instead, we will examine the isotope partitioning behavior of the unique sites within these molecules. The polythionates contain relatively reduced 'inner' sulfur atoms that we will schematically refer to as $^{*}\mathbf{S}_x(SO_3)_2^{2-}$ ($x = 1$ or 2 in this study, corresponding to tri- and tetrathionate) and the two equivalent 'sulfonate' sulfur atoms that we will schematically refer to as $S_x(^{*}\mathbf{S}O_3)_2^{2-}$ (in both instances, $^{*}\mathbf{S}$ refers to the atomic site of interest undergoing isotope substitution). The α-notation will be used to refer to fractionation factors between specific atomic sites within the polythionates and between these sites and other sulfur compounds.

2.6. General sources of uncertainty in the theoretical calculations

As summarized in our prior study (Eldridge et al., 2016), uncertainty in our theoretically estimated fractionation factors can arise from three primary sources: (1) errors arising from the harmonic and other approximations inherent to the RPFR as formulated in Eq. 5 (Bigeleisen & Mayer, 1947; Urey, 1947), (2) errors introduced by the choice of theoretical method and basis set size used to compute electronic potential energy surfaces to obtain harmonic vibrational frequencies, and (3) errors/variability arising from the water cluster geometry. We evaluated the relative sources of error introduced by (1) and (2) in our pre-

vious study (Eldridge et al., 2016) by performing exercises with calculations of model gaseous species. Gaseous species were chosen for these exercises because analogous computations involving solutes in water clusters ($\geq$ 30 H_2O) are not feasible due to the high computational demands associated with these calculations. The exercises related to points (1) and (2) in Eldridge et al. (2016) apply to the current study because we use the same theoretical method and basis set (B3LYP/6-31+G(d,p)).

Regarding (1) we evaluated the magnitude of the anharmonic corrections to the zero point energy (AnZPE; *cf.* Liu et al., 2010) on RPFR/β values for gaseous sulfur species computed at the B3LYP/6-31+G(d,p) level of theory and basis set (e.g., H_2S, SO_2, SO_3; Eldridge et al., 2016). We observed relative differences in RPFR/β values no greater than 1 ‰ at temperatures $\geq$ 25°C (Eldridge et al., 2016). Due to the low magnitudes of these corrections and the inability to apply appropriate anharmonic corrections to the large aqueous clusters investigated, all RPFR/β values reported in Eldridge et al. (2016) and the current study have been computed in the harmonic approximation. For further information/discussion regarding point (1) we refer the reader to Eldridge et al. (2016) (their Sections 3.5 and 5.1.1).

Regarding (2) we evaluated the relative magnitude of error introduced by theoretical method and basis set following approaches in previous studies (e.g., Li & Liu, 2011). Specifically, we calculated the harmonic vibrational frequencies of a handful of gaseous sulfur compounds (H_2S, S_2, SO, SO_2) using a high level theoretical method and large basis set (CCSD/aug-cc-pVTZ) and compared them to the harmonic vibrational frequencies obtained for the same molecules computed at the utilized theoretical method and basis set (B3LYP/6-31+G(d,p)). This exercise yielded a relatively small harmonic frequency scaling factor of 1.01-1.02 (Eldridge et al., 2016). Application of this scaling factor to calculations of solutes in water clusters resulted in differences in computed RPFR/β values that are dependent on the species and temperature considered but that amount to differences in $^{34}\alpha$ values no greater than 1-2‰ at temperatures $\geq$ 25°C (Eldridge et al., 2016). Additionally, we observed that the

harmonic vibrational frequencies of some gaseous molecules appear to scale differently than others between computational methods (e.g., SO_2 vs. H_2S, S_2, and SO; see Eldridge et al., 2016) meaning that harmonic scaling factors obtained are dependent on the model molecules chosen (similar to observations made in prior studies; e.g., Li & Liu, 2011). We raised related concerns that model gaseous compounds may not capture the full range of error introduced by theoretical method due to the greater complexity of aqueous species/anions in water clusters (Eldridge et al., 2016). Due to the small magnitude of these harmonic scaling corrections and the potential issues associated with this practice, we chose in Eldridge et al. (2016) and in the current study not to scale our harmonic frequencies. For further information/discussion regarding point (2) we again refer the reader to Eldridge et al. (2016) (their Sections 3.5 and 5.1.2).

Regarding (3) we evaluate the error/variability arising from the water cluster geometry for most of the investigated sulfur solutes by performing optimization and frequency calculations in water clusters of varying sizes (30-52 H_2O; Table 1). We estimate the uncertainty of any given computed quantity (e.g., geometric parameters, RPFRs, and β-factors) as the standard deviation of values derived from the different cluster sizes/conformations. We propagate these uncertainty estimates into derived quantities such as fractionation factors.

3. Results

3.1. Structures and Geometries

Examples of two-dimensional representations of optimized geometries of solute H_2O clusters are presented in Fig. 1-3 that are organized according to polysulfides, polysulfur radicals, and elemental sulfur (Fig. 1), sulfide compounds (Fig. 2), and sulfate and polythionate compounds (Fig. 3). The geometric parameters of the explicitly solvated sulfur solutes are summarized in Table 2, and represent mean values derived from the numerous water cluster configurations. Similar parameters for $S^{2-}_{x(g)}$ modeled as similar structures in vacuum

also computed at the B3LYP/6-31+G(d,p) level are listed for reference. A detailed description of the computed molecular geometries and their comparison to available theoretical and experimental data can be found in Appendix A.1.

3.2. Overview of RPFRs and β values

Table 3 contains the mean and standard deviation of the mean (1 s.d.) of RPFRs computed at 25°C for aqueous sulfide compounds ($H_2S{\bullet}nH_2O$, $HS^-{\bullet}nH_2O$, $FeS^0{\bullet}nH_2O$, $FeSH^+{\bullet}nH_2O$, $(Na^+HS^-)^0{\bullet}nH_2O$) and the component isotopologues of each polysulfide ($S_x^{2-}{\bullet}nH_2O$ and $HS_x^-{\bullet}nH_2O$) and polysulfur radicals ($S_x^{\cdot-}{\bullet}nH_2O$) based on the different water cluster size configurations. Table 3 additionally includes the mean number (range in parentheses) of water molecules that appear to be directly coordinated with each molecular sulfur atom in the clusters *via* an apparent intermolecular hydrogen bond (i.e., H-O-H$\cdots$S), which is generally observed to vary for a given sulfur atom in compounds contained within $n$$H_2O$ clusters of different size (n) in a non-systematic fashion.

The mean and standard deviation of the mean of β-factors derived from RPFRs for all heavy stable isotope substitution (^{33}S, ^{34}S, and ^{36}S) have been computed as a function of temperature and are provided in Table 4 in the form of coefficients based on polynomial fits to values of $^{34}\beta$, $^{33/34}\kappa$, and $^{36/34}\kappa$ over the equivalent of 0-5000°C in the form of $A/T^4 + B/T^3 + C/T^2 + D/T + E$ (T in K). The coefficients of polynomial fits to the mean $^{33/34}\kappa$ and $^{36/34}\kappa$ values are given rather than the corresponding $^{33}\beta$ and $^{36}\beta$ values in order to avoid spurious errors in the exponents that may arise from rounding errors in β values. Similar coefficients of polynomial fits to the analogous RPFR values of trithionate are given in Table 5.

We do not observe any systematic changes in values of ^{34}RPFRs and/or $^{34}\beta$ for each solute with cluster size over the range we have studied (ca. 30-52 H_2O). The variability in values of RPFR and/or β values arising from different cluster sizes appears to be relatively small. For example, the variability in values of ^{34}RPFR and/or $^{34}\beta$ for a given solute is on the order of $\leq$ 0.5 ‰ (1 s.d.) at 25°C (Table 3 and 4). The magnitude of this variability is comparable to the

variability that has been observed in previous computational studies of isotope partitioning behavior of numerous elements contained within anionic and other solutes modeled in water clusters of different size and geometric conformations, both for clusters that were built manually as in the present study (Li et al., 2009; Li & Liu, 2011) and for clusters generated from the subsequent optimization of "snap shots" from molecular dynamics simulations (Rustad et al., 2008, 2010; Hill et al., 2014). The slight variability in RPFRs and β values for explicitly solvated solutes can be viewed to arise from variability in the number of water molecules that appear to be coordinated with sulfur atoms via intermolecular hydrogen bonds that together contribute to the 'first solvation shell' (*cf.* Table 3), and the slight differences in the molecular geometry of sulfur solutes in the clusters of varying size that in some cases may be caused by the different direct interactions with water molecules in the clusters of varying size.

3.2.1. ^{34}RPFRs and $^{34}\beta$ values for Aqueous Polysulfide, Polysulfur Radical, and Sulfide Compounds

Mean values for ^{34}RPFRs and $^{34}\beta$ at 25°C from Table 3 are plotted in Fig. 4 for the explicitly solvated sulfide and polysulfide species (values for vacuum calculations of S_x^{2-} are also shown for reference). The singly substituted isotopologues of the polysulfide species (S_x^{2-}) exhibit slightly different RPFRs when x >2, but appear to follow similar patterns for both the explicitly solvated and vacuum calculations. The ^{34}RPFRs for S_x^{2-} isotopologues that correspond to the isotope substitution of the outer-most sulfur atoms are generally lower than the ^{34}RPFRs for isotopologues corresponding to isotope substitution of inner sulfur atoms (Fig. 4). The isotopologues that exhibit the highest ^{34}RPFRs correspond to isotope substitution of the inner sulfur atoms that are directly bonded to the outermost sulfur atoms (e.g., S-*S-S for S_3^{2-} and S-*S-S-S-S-S-S and its symmetrical equivalent for S_8^{2-}) (Fig. 4). For longer chain length S_x^{2-} (x = 5-8), the isotopologues corresponding to isotope substitution of the innermost sulfur atoms (e.g., S-S-*S-S-S for S_5^{2-}, and S-S-*S-S-S-S for S_6^{2-}) have intermediate ^{34}RPFR values. The magnitude of RPFRs corresponding to iso-

tope substitution at a symmetrically equivalent site (e.g., *S-S-S and S-S-*S for S_3^{2-}) are generally comparable for $S_x^{2-}\bullet nH_2O$, but do not appear to exhibit the perfectly symmetrical behavior in the water clusters that might be expected from the considerations of the vacuum calculations and ideal molecular symmetry.

The $^{34}\beta$ factors derived from ^{34}RPFRs for $S_x^{2-}\bullet nH_2O$ generally increase with increasing chain length ('x'), and the magnitude of this increase appears to diminish with increasing 'x' (Fig. 4). Similar behavior is observed in the vacuum calculations for S_x^{2-}. To a first order, the general increase in $^{34}\beta$ with increasing 'x' for S_x^{2-} can be described to arise from the proportionality between the $^{34}\beta$-factor and the number of ^{34}RPFR-contributing isotopologues that increases with 'x' (e.g., Equation 6). Such an increase in the number of singly substituted isotopologues with increasing chain-length can result in an increase in $^{34}\beta$ when the magnitudes of ^{34}RPFR of the component isotopologues generally increases with 'x' (as appears to be the case with the S_x^{2-} calculations in vacuum) or at least do not decrease with increasing 'x' (as appears to be the case with the $S_x^{2-}\bullet nH_2O$ calculations). The largest increase in $^{34}\beta$ with 'x' is between S_2^{2-} and S_3^{2-} (Fig. 4) and is the result of the contribution of the higher ^{34}RPFR of the centrally substituted isotopologue of S_3^{2-} (S-*S-S). With increasing 'x' ($x \geq 4$) the number of contributing inner substituted isotopologues increases, and due to their relatively higher ^{34}RPFR they appear to contribute to a relatively higher $^{34}\beta$. This effect appears to diminish among the longer chain length polysulfides (x = 5-8) due to the increasing contribution from isotopologues corresponding to inner-most sulfur atom substitution that have intermediary magnitude ^{34}RPFRs. Roughly speaking, $^{34}\beta$ values appear to approach the ^{34}RPFR of the innermost sulfur atoms with increasing 'x' for the longer chain-length polysulfides (x = 5-8).

The protonated polysulfide anions ($HS_x^-\bullet nH_2O$, x = 2 and 3) generally have larger magnitude $^{34}\beta$ than their unprotonated counterparts. This appears to arise from the generally higher ^{34}RPFRs of the component isotopologues of HS_2^- and HS_3^- relative to S_2^{2-} and S_3^{2-}, respectively, and especially from the higher

magnitude ^{34}RPFR of isotopologues that correspond to isotope substitution of the protonated sulfur atoms (Fig. 4, Table 3). Similar to $S_x^{2-}\bullet nH_2O$, the magnitude of $^{34}\beta$ for $HS_x^-\bullet nH_2O$ appears to increase slightly with increasing chain length over x = 2-3. The relative trends in RPFRs computed for isotopologues of polysulfides (S_x^{2-}, HS_x^-) that we have described at 25°C and are illustrated in Table 3 and Fig. 4 generally hold as a function of temperature. The only exception is for the HS_3^- species, which is predicted to have a crossover between its isotopologues (not shown). In this case, the isotopologue corresponding to isotope substitution of the H-S bonded site (S-S-*SH)- is predicted to exhibit a crossover in the RPFR with the isotopologue corresponding to isotope substitution of the central sulfur site (S-*S-SH)- in proximity to 135±20°C (not shown). This appears to be the only instance of an 'intramolecular isotopologue crossover' that we observe in our dataset.

The isotopologues of the explicitly solvated polysulfur radical anions ($S_2^{\cdot-}$ and $S_3^{\cdot-}$) exhibit similar relative patterns to the analogous polysulfide species (S_2^{2-} and S_3^{2-}) but have slightly larger magnitude ^{34}RPFRs and, thus, have higher $^{34}\beta$ values (Table 3). For example, the ^{34}RPFR values for isotope substitution of the outer sulfur atoms of $S_3^{\cdot-}$ are predicted to be 1.0098 ± 0.0003 at 25°C (*cf.* 1.0089 ± 0.0003 for S_3^{2-}) and ^{34}RPFR = 1.0165 ± 0.0003 for isotope substitution of the central sulfur atom (cf. ^{34}RPFR = 1.0134 ± 0.0002 for S_3^{2-}) (Table 3), which translates into a $^{34}\beta$ = 1.0120 ± 0.0002 for $S_3^{\cdot-}$ (*cf.* $^{34}\beta$ = 1.0104 ± 0.0002 for S_3^{2-}). The magnitude of $^{34}\beta$ increases with increasing chain length for the polysulfur radicals ($S_x^{\cdot-}$) over x = 2-3 that appears to arise from the contribution of the higher ^{34}RPFR of the centrally substituted isotopologue of $S_3^{\cdot-}$ (S-*S-S) similar to the analogous polysulfides. To a first order, the higher magnitude ^{34}RPFRs of the polysulfur radical anions may be a consequence of the different electronic structure and much shorter S-S bond lengths of the polysulfur radical species that may result in a 'tighter' bonding arrangement for sulfur in these compounds relative to the analogous polysulfide compounds.

For the aqueous sulfide species, the magnitude of $^{34}\beta$ (note for these species

^{34}RPFR $\approx$ $^{34}\beta$) increases with increasing coordination (due to either protonation or bonding with Fe) in a manner that is similar to our previous study (Eldridge et al., 2016). At 25°C, $H_2S\bullet nH_2O$ ($^{34}\beta = 1.0129\pm0.003$) > $HS^-\bullet nH_2O$ ($^{34}\beta = 1.0087\pm0.005$) > $S^{2-}\bullet nH_2O$ ($^{34}\beta = 1.0076$; $S^{2-}\bullet nH_2O$ from Eldridge et al. (2016)). Similar patterns are observed for the Fe-S molecular species where $FeSH^+\bullet nH_2O$ ($^{34}\beta = 1.0119\pm0.003$) > $FeS^0_{(aq)}\bullet nH_2O$ ($^{34}\beta = 1.0089\pm0.003$), where the latter is indistinguishable from the $^{34}\beta$ of $HS^-\bullet nH_2O$ at 25°C. The Fe atom in the $FeS^0_{(aq)}\bullet nH_2O$ species is coordinated with the oxygen atoms of three water molecules in all computed clusters (n = 31-50) that is consistent with previous molecular dynamics simulations of this species (Haider et al., 2013), whereas the Fe atom of $FeSH^+\bullet nH_2O$ is coordinated with four water molecules in all computed clusters (n = 34-50). The ion pair $(Na^+HS^-)^0\bullet nH_2O$ is computed to have β-values that are indistinguishable from those of $HS^-\bullet nH_2O$ at all temperatures and therefore will not be individually described or discussed in any further detail.

3.2.2. Relative error introduced by the approximation of β for polysulfur compounds

In this study, we approximate β values ($^{33}\beta$ or $^{34}\beta$ or $^{36}\beta$) for the computation of fractionation factors among polysulfides and polysulfur radicals by assuming that the bulk equilibrium isotopic composition of a given 'x'-chain length polysulfur compound (i.e., S_x^-, S_x^{2-}, HS_x^-) can be represented by the RPFRs of singly substituted 'x'-number of isotopologues present in equal relative abundance (Section 2.5). In this approximate form, it is expected that this assumption (equal abundance of major singly-substituted isotopologues) would introduce more error into β than the other common assumption in the computation of β that multiply substituted isotopologues (e.g., ^{34}S-^{34}S-^{32}S, ^{34}S-^{34}S-^{34}S for S_3^{2-}) represent a negligible contribution (Richet et al., 1977). As an example, we will consider the impact of the assumption of equal abundance on the computation of $^{34}\beta$ for the trisulfur polysulfide, S_3^{2-}, which is chosen as exemplary because the unique sulfur atoms of S_3^{2-} ('outer' and 'central') ex-

hibit a range in RPFR values that is comparable to the range exhibited in other polysulfides of longer chain length (Fig. 4). At 25°C, the RPFRs computed for the three major ^{34}S-based isotopologues of S_3^{2-} are 1.0088 ± 0.0002 (^{34}S-^{32}S-^{32}S), 1.0134 ± 0.0002 (^{32}S-^{34}S-^{32}S), and 1.0090 ± 0.0003 (^{32}S-^{32}S-^{34}S), where the isotopologues with outer atom isotope substitution are predicted to have the same RPFR within the estimated uncertainty (based on numerous cluster conformations) as is expected by molecular symmetry and the equivalence of bonding environment. These RPFR values imply that the relative fractional abundances of these isotopologues corresponds to: 0.3328 ± 0.0001 and 0.3329 ± 0.0001 for the outer substituted isotopologues, and 0.3348 ± 0.0001 for the centrally-substituted isotopologue. Taking these relative abundances into consideration would yield a $^{34}\beta = 1.0104 \pm 0.0002$, which is indistinguishable from the value of $^{34}\beta = 1.0104 \pm 0.0002$ where equal abundance (i.e., 1/3) of these major isotopologues is assumed (Table 3). Similar computations of other polysulfides yield similar results. The similar exercise with the trisulfur radical anion $S_3^{\cdot-}$ that is computed to exhibit a slightly larger range in RFPR between the 'outer' and 'central' sulfur atoms (Table 3) also yields essentially identical values for β (i.e., $^{34}\beta = 1.0120 \pm 0.0002$ at 25°C for both approaches). We thus conclude that our approximate form of β for the polysulfur compounds ($S_x^{\cdot-}$, S_x^{2-}, HS_x^-) is not likely to introduce any significant error into our estimations of fractionation factors involving these compounds.

3.2.3. Aqueous Polythionates

Trithionate ($S_3O_6^{2-}$, or $S(SO_3)_2^{2-}$) contains three sulfur atoms but only two unique atomic sulfur sites: two equivalent sulfur atoms in sulfonate groups ($S(^*SO_3)_2^{2-}$) that are bound to a unique and central sulfur atom ($^*S(SO_3)_2^{2-}$). Tetrathionate ($S_4O_6^{2-}$, or $S_2(SO_3)_2^{2-}$) is similar in that it also contains two equivalent sulfonate groups ($S_2(^*SO_3)_2^{2-}$) connected via two central sulfur atoms that are equivalent to each other ($^*S_2(SO_3)_2^{2-}$). The somewhat analogous thiosulfate dianion ($S_2O_3^{2-}$, or $S(SO_3)^{2-}$) contains sulfur in two different oxidation states where the formal charge on the outer sulfur atom is consistent with a -1

oxidation state and the sulfonate sulfur is consistent with a +5 oxidation state (Vairavamurthy et al., 1993), but a comparable experimental study for the polythionates has not been conducted to our knowledge. Similar to the thiosulfate dianion, the RPFRs for the two unique sulfur sites in polythionate are very different. For example, trithionate: ^{34}RPFR = 1.0142±0.0002 for $^{*}S(SO_3)_2^{2-}$ and ^{34}RPFR = 1.0708±0.0005 to 1.0714±0.0002 for $S(^{*}SO_3)_2^{2-}$ at 25℃ (equivalent for the 'sulfonate' sulfur atoms within the estimated uncertainty based on cluster size/geometry). Values of RPFRs for the two analogously unique atomic sites in tetrathionate (corresponding to $^{*}S_2(SO_3)_2^{2-}$ and $S_2(^{*}SO_3)_2^{2-}$) are computed to be essentially indistinguishable from those of trithionate at all temperature values (e.g., at 25℃ the ^{34}RPFR for $^{*}S_2(SO_3)_2^{2-}$ is 1.0140±0.0002 to 1.0150±0.0002 for the two central sulfur atoms, and ^{34}RPFR for $S_2(^{*}SO_3)_2^{2-}$ is 1.0714±0.0001 to 1.0704±0.0002 for the two sulfonate sulfur atoms), and thus for the remainder of this manuscript we will describe fractionation factors involving the polythionates in generic terms of $^{*}S_x(SO_3)_2^{2-}$ and $S_x(^{*}SO_3)_2^{2-}$ where x = 1 and 2. Compared to thiosulfate, the reduced sulfur atoms ($^{*}S_x(SO_3)_2^{2-}$ vs. $^{*}S(SO_3)^{2-}$) and the sulfonate sulfur atoms ($S_x(^{*}SO_3)_2^{2-}$ vs. $S(^{*}SO_3)^{2-}$) in the polythionates are predicted to exhibit slightly larger RPFR values but are nevertheless relatively similar (*cf.* at 25℃ the ^{34}RPFR = 1.0116 for $^{*}S(SO_3)^{2-}$, and ^{34}RPFR = 1.0675 for $S(^{*}SO_3)^{2-}$; Eldridge et al., 2016).

3.2.4. Aqueous Sulfate

The aqueous sulfate compounds and ion-pairs modeled herein all exhibit very similar β-values. The magnitude of $^{34}\beta$ appears to follow the relationship of $HSO_4^-\bullet nH_2O$ ($^{34}\beta = 1.0800\pm0.0002$) > $(Na^+SO_4^{2-})^-\bullet nH_2O$ ($^{34}\beta = 1.0795$) ≈ $(Mg^{2+}SO_4^{2-})^0\bullet nH_2O$ (1.0794±0.0001) ≥ $SO_4^{2-}\bullet nH_2O$ (1.0792±0.0002) (all $^{34}\beta$-values at 25℃). Interestingly, $^{34}\beta$-values for HSO_4^- and SO_4^{2-} appear to exhibit the opposite relationship than values theoretically predicted for the analogous $(HO)SO_2^-$ (HO-bonded isomer of HSO_3^-) and SO_3^{2-} (Eldridge et al., 2016), i.e., β-HSO_4^- > β-SO_4^{2-} *vs.* β-SO_3^{2-} > β-$(HO)SO_2^-$, but nevertheless are very similar in magnitude to each other. Ion-pairing of the sulfate dianion with Na^+ and

Mg^{2+} appears to have a similar and essentially negligible predicted effect on isotope partitioning of sulfur despite the observation that the Mg^{2+} appears to more strongly affect the bonding environment of the SO_4^{2-} dianion (Table 2). These results are consistent with the general expectation that aqueous speciation that does not directly affect the bonding environment of the element of interest (i.e., no changes in redox state and/or bonding-order of the sulfur atom) will not greatly affect isotope partitioning behavior.

3.3. β-values as a function of temperature: Proclivity for crossovers among reduced S compounds

The $^{34}\beta$ values for all aqueous sulfur compounds computed herein are plotted as a function of inverse temperature (T^{-2}) in Fig. 5A-E where it can be readily observed that numerous crossovers are predicted among these compounds. For example: (1) the HS^- species is predicted to exhibit crossovers with S_2^{2-} (Fig. 5A) and $FeS_{(aq)}$ (Fig. 5C) at ambient temperature (roughly 0-100℃) and numerous longer chain-length S_x^{2-} at higher temperatures (roughly 100-500℃; Fig. 5A), (2) the protonated polysulfide HS_2^- exhibits a crossover with higher order polysulfides (e.g., S_8^{2-}) at ambient temperatures (roughly 0-100℃; Fig. 5A), (3) the $FeSH^+$ species exhibits a crossover with S_8^{2-} and HS_3^- at ambient temperature, (4) crossovers are predicted among $S_x^{\cdot-}$ (x =2-3) and HS^-/H_2S (Fig. 5B), and (5) the more reduced sulfur atoms in the polythionates, $^*S_x(SO_3)_2^{2-}$, are predicted to exhibit crossovers with H_2S in rough proximity to 75℃ (Fig. 5D). Many of the compounds that exhibit similar β-values at 25℃ plotted in Fig. 4 are exhibiting crossovers at or near this temperature (the exception being S_2^{2-} and $FeS_{(aq)}$ that exhibit similar magnitude β values at 25℃ but do not crossover).

Crossovers in β or RPFR values among aqueous sulfur compounds that contain relatively reduced sulfur atoms arise because these compounds/atoms exhibit similar magnitude β/RPFR values but have different temperature dependencies. In particular, the temperature dependence of β or RPFR values associated with compounds having S-S and/or Fe-S bonds (i.e., contributions

from mostly lower magnitude stretching frequencies) result in more-linear relationships for β-values as a function of T^{-2}, whereas compounds having H-S bonds (i.e., contributions from high magnitude stretching vibrational frequencies) typically exhibit stronger curvature as a function of T^{-2} (Fig. 5A-D), and this difference in temperature dependence leads to crossover behavior. This also appears to be the explanation for the 'intramolecular crossover' that is predicted for the HS_3^- species (not shown).

3.4. Mass Dependence of RPFRs and β values

The exponents $^{33/34}\kappa$ and $^{36/34}\kappa$ that quantify the relationships of mass dependence among β factors are plotted as a function of temperature in Fig. 6A-B for all compounds computed in this study (for trithionate, similar values of $\ln(^{33}\text{RPFR})/\ln(^{34}\text{RPFR})$ and $\ln(^{36}\text{RPFR})/\ln(^{34}\text{RPFR})$ are plotted for the distinct sulfur sites). At the high temperature limit (i.e., as T^{-2} approaches '0'), we obtain mean values for all explicitly solvated sulfur compounds in this study of $^{33/34}\kappa = 0.51587 \pm 0.00006$ and $^{36/34}\kappa = 1.8904 \pm 0.0001$ (1 s.d.; Table 4), which are consistent with the expected values of 0.51588 and 1.8904 from the mass differences among the isotopic sulfur atoms (Matsuhisa et al., 1978). The values of $^{33/34}\kappa$ and $^{36/34}\kappa$ for the relatively reduced sulfur compounds/moieties examined in the present study (sulfide, S_x^{2-}, $S_x^{\cdot-}$, and $^*S_x(SO_3)_2^{2-}$) do not exhibit a strong temperature dependence compared to aqueous sulfur-oxygen anions containing sulfur in higher oxidation states that exhibit larger β/RPFR values (e.g., SO_2^{2-}, SO_3^{2-}, SO_4^{2-}; Fig. 6A-B), which is similar to the observations made in our previous theoretical calculations (Eldridge et al., 2016). Values for $^{33/34}\kappa$ and $^{36/34}\kappa$ for the aqueous sulfate species exhibit the largest variations with temperature and are essentially indistinguishable from each other. Values of $\ln(^{33}\text{RPFR})/\ln(^{34}\text{RPFR})$ and $\ln(^{36}\text{RPFR})/\ln(^{34}\text{RPFR})$ as a function of temperature for the unique sulfur sites in the polythionates ($^*S_x(SO_3)_2^{2-}$ and $S_x(^*SO_3)_2^{2-}$) are predicted to be essentially identical to the analogous sulfur sites in thiosulfate: $^*S(SO_3)^{2-}$ and $S(^*SO_3)^{2-}$, respectively (Eldridge et al., 2016).

4. Discussion

4.1. Fractionation factors (α) between compounds

4.1.1. Aqueous sulfide compounds

Our prediction for the H_2S/HS^- fractionation factor as a function of $1/T^2$ is shown in Fig. 7 alongside other direct and indirect experimental estimates and previous theoretical calculations. The predicted fractionation factor between aqueous H_2S and HS^- is $1000\times\ln(^{34}\alpha) = 4.2 \pm 0.6$ ‰ at 25°C (1 s.d.). Few direct experimental data exist for equilibrium fractionation factors among aqueous sulfide compounds (Fig. 7), and those that do exist correspond to ambient laboratory temperature conditions (20-22°C). The most recent experimental determination (Sim et al., 2019) yields $1000\times\ln(^{34}\alpha) = 3.1 \pm 0.2$ ‰ at 20.6±0.5°C. This is within error of our earlier theoretical estimate at their experimental temperature utilizing singular 30 H_2O clusters (3.1 ‰; Eldridge et al., 2016) but slightly lower than our current estimate utilizing the mean values of multiple cluster conformations (4.2±0.6‰, 1 s.d.). We note that our present theoretical estimate is still within error of Sim et al. (2019) at the 2 s.d. level, and is likely to better capture the error associated with the calculations due to the usage of multiple cluster sizes and conformations. Both studies (Eldridge et al., 2016; Sim et al., 2019) reviewed the earlier experiments in detail (Fry et al., 1986; Geßler & Gehlen, 1986) and highlight potential experimental issues. Despite potential issues with experimental design, the direct experimental determinations from Geßler & Gehlen (1986) appear to be within the estimated error of the theoretical calculations.

The indirect estimate of the H_2S/HS^- fractionation factor that is based on the arithmetic analysis of experimentally estimated fractionation factors among $ZnS/S_{(g)}$, $H_2S/S_{(g)}$, and ZnS/HS^- from Ohmoto & Rye (1979) is generally lower than any other estimates (Fig. 7), and is within error of $1000\times\ln(^{34}\alpha) = 0$ ‰ (no fractionation) at the lowest temperature (50°C: 1.2 ± 1.4 ‰, 1σ; Ohmoto & Rye, 1979). The temperature dependence of our theoretical $1000\times\ln(^{34}\alpha)$ value for H_2S/HS^- exhibits pronounced curvature in $1/T^2$ space that is not reflected

in Ohmoto & Rye (1979). The estimates of Ohmoto & Rye (1979) might be affected by the propagation of uncertainties/errors from numerous experimental datasets and/or possible assertions made regarding the temperature dependence over the experimental temperature range (i.e., linear in $1000\times\ln(^{34}\alpha)$ *vs.* $1/T^2$ space).

Previous theoretical estimates for the H_2S/HS^- fractionation factor (Sakai, 1968; Tossell, 2012; Otake et al., 2008; Eldridge et al., 2016) exhibit variability that arises from the different approaches taken (Fig. 7). Our recent calculations utilizing computations of single $H_2S\bullet 30H_2O$ and $HS^- \bullet 30H_2O$ clusters yield a comparable but slightly lower value of $1000\times\ln(^{34}\alpha) = 3.3$ ‰ at 25°C (not shown; Eldridge et al., 2016). Earlier calculations (Otake et al., 2008; Tossell, 2012) suggest a larger fractionation factor of $1000\times\ln(^{34}\alpha) = 6.2$-$6.6$ ‰ at 25°C (Fig. 7). In addition to differences in theoretical model and basis set, these two studies (Otake et al., 2008; Tossell, 2012) utilized an implicit solvation model (IEF-PCM and/or PCM) that approximates the effect of solvation by encasing the solute in a cavity of specified dielectric constant that is solvent- and compositional-/condition-specific, and their implementation of these models for the H_2S and HS^- compounds yield very similar fractionation factors to those obtained from calculations in vacuum without any solvation model applied (e.g., $1000\times\ln(^{34}\alpha) = 6.8$ ‰ at 25°C from modeling these compounds in vacuum) (Otake et al., 2008). These values are comparable to vacuum calculations at the B3LYP/6-31+G(d,p) level of $1000\times\ln(^{34}\alpha) = 6.8$ ‰ at 25°C from our own calculations (not shown). In general, implicit solvation models such as IEF-PCM may be regarded as less effective in approximating the effects of solvation in the computation of RPFRs than the explicit or 'supramolecular water cluster' solvation models that can account for water-solute interactions in a more direct manner. The calculations of Sakai (1968) assumed the RPFR for $H_2S_{(aq)}$ can be approximated by the RPFR for $H_2S_{(g)}$ and were performed using older spectroscopic data, but nevertheless appear to yield similar magnitude fractionation factors to those of the present study and Geßler & Gehlen (1986) at ambient temperature but exhibit a slightly different temperature dependence.

Predictions for fractionation factors among discreet aqueous ferrous iron sulfide species and aqueous sulfide species are presented as a function of $1/T^2$ in Fig. 8. The predicted fractionation factor for $FeS^0_{(aq)}/HS^-$ is $1000\times\ln(^{34}\alpha)$ = 0.1 ± 0.6‰ at 25°C, and its negligible magnitude is due to a crossover in proximity to this temperature (Fig. 8). The predicted fractionation factor for $FeSH^+/H_2S$ is $1000\times\ln(^{34}\alpha)$ = -1.0 ± 0.4‰ at 25°C. The predicted equilibrium fractionation factor associated with $FeSH^+/FeS_{aq}$ is $1000\times\ln(^{34}\alpha)$ = 3.0 ± 0.4 ‰ and is comparable to the somewhat analogous H_2S/HS^- fractionation factor. To our knowledge, there are no other estimates of these fractionation factors in the literature for comparison.

Recent experimental studies (Syverson et al., 2013, 2015) revised the experimental value for the equilibrium fractionation factor between $FeS_{2(pyrite)}/H_2S$ under hydrothermal conditions obtaining a value of $1000\times\ln(^{34}\alpha)$ = -1.9 ± 0.8 ‰ (1 s.d.) at 350°C, which is in contrast in direction to previous estimates of ca. $1000\times\ln(^{34}\alpha)$ = 1.0 ‰ at 350°C that is from the assessment of Ohmoto & Rye (1979) based on earlier experimental data. The direction of the newly revised $FeS_{2(pyrite)}/H_2S$ fractionation factor from Syverson et al. (2015) is consistent with the direction of our predicted fractionation factors between the discreet aqueous ferrous sulfide species ($FeSH^+$, $FeS_{(aq)}$) and H_2S at comparable temperatures (Fig. 8). We additionally note that the direction of the predicted fractionation factor between $FeS_{(aq)}/H_2S$ at elevated temperature (e.g., $1000\times\ln(^{34}\alpha)$ = -2.4±0.1 ‰ at 350°C) is opposite from that of FeS(pyrrhotite)/H_2S (i.e., $1000\times\ln(^{34}\alpha)$ = 0.3 ‰ at 350°C) that is also compiled in Ohmoto & Rye (1979) that is based on earlier experimental data (Kajiwara & Krouse, 1971). Our estimates of homogeneous equilibrium isotope fractionations among modeled aqueous solutes are not directly comparable to the experimental heterogeneous equilibrium isotope fractionations between crystalline phases and aqueous solutes, and the factors that influence the magnitude and direction of isotope partitioning between crystalline and molecular ferrous iron sulfides are expected to be different due to differences in bonding environment. However, our computational results and the recent experimentation of Syverson et al. (2013, 2015)

may be potentially suggestive that equilibrium fractionation factors for certain ferrous sulfide solutes/phases relative to H_2S may exhibit different directions and/or exhibit a different temperature dependence than previously understood (i.e., Ohmoto & Rye, 1979). Further experimental work is clearly needed for a more complete assessment.

4.1.2. Aqueous Sulfide and Polysulfide Compounds

The equilibrium isotopic compositions of the polysulfides (S_x^{2-} and HS_x^-) are predicted to be within the range of the equilibrium isotopic compositions of H_2S and HS^- at 25°C (Fig. 4), and therefore fractionations among aqueous sulfide and polysulfides are expected to be relatively small. The fractionation factors between S_x^{2-}/HS^- are predicted to generally increase with increasing 'x' from $1000\times\ln(^{34}\alpha)$ = -0.1± 0.7‰ for S_2^{2-}/HS^- to $1000\times\ln(^{34}\alpha)$ = 2.9 ± 0.5‰ for S_8^{2-}/HS^- (1 s.d.). The negligible fractionation factor between S_2^{2-}/HS^- at 25°C is due to a predicted crossover in proximity to this temperature, which is illustrated in Fig. 9. The fractionation factors between HS_x^-/HS^- are predicted to be $1000\times\ln(^{34}\alpha)$ = 2.9 ± 0.5‰ for HS_2^-/HS^- and $1000\times\ln(^{34}\alpha)$ = 3.5 ± 0.6‰ for HS_3^-/HS^- (25°C, 1 s.d.). The predicted fractionation factors between S_x^{2-}/H_2S are in the opposite direction relative to S_x^{2-}/HS^-. Thus, they exhibit an opposing trend with respect to magnitude and 'x' relative to S_x^{2-}/HS^- and yield fractionation factors that range between $1000\times\ln(^{34}\alpha)$ = -4.3 ± 0.5 ‰ for S_2^{2-}/H_2S and $1000\times\ln(^{34}\alpha)$ = -1.2 ± 0.3 ‰ for S_8^{2-}/H_2S at 25°C (i.e., the magnitude of the fractionation factor decreases with increasing 'x').

The temperature dependence of fractionation factors among aqueous sulfide and polysulfide compounds exhibit interesting behavior due to the predicted proclivity for crossovers among these compounds (Fig. 9). In the current dataset, crossovers in fractionation factors corresponding to a specific isotope ratio occur at specific temperatures (the crossover temperature, T_c) and lead to apparent inverse temperature dependence above the T_c whereby the fractionation factor increases in magnitude with increasing temperature until a relative maximum in magnitude is reached. At temperatures above the relative maximum, the

fractionation factor decreases in magnitude with increasing temperature until approaching nil fractionation (i.e., $\alpha = 1$, or 0 ‰) at the high-temperature limit. Fractionation factors computed among aqueous sulfur compounds that exhibit crossovers over the temperature ranges studied (T $\geq$ 0°C) or that appear to exhibit crossovers below 0°C have the characteristics of this type of temperature dependence. This type of temperature dependence associated with a crossover appears to have been previously described (e.g., Stern et al., 1968). Examples of these types of crossovers among aqueous sulfide/polysulfide compounds include S_x^{2-}/ HS^- (x = 2-8, where T_c may increase with 'x'; Fig. 9) and $FeS_{(aq)}/HS^-$ (Fig. 8). Examples of fractionation factors that appear to exhibit crossovers below 0°C include $FeSH^+/H_2S$ (Fig. 8) and S_x^{2-}/H_2S (x = 3-8) (Fig. 9). Fractionation factors that appear to exhibit crossovers below 0°C appear to generally have larger magnitude relative maximum fractionation factors at $T > T_c$ (e.g., 2-3 ‰ for S_x^{2-}/H_2S x = 3-8) than those exhibiting crossovers $\geq$ 0°C (e.g., ca. $<$ 1 ‰ for S_x^{2-}/HS^- x = 2-8, and FeS_{aq}/HS^-).

Fig. 10A contains calculations of the experimentally constrained distribution (in terms of concentration, μM) of aqueous polysulfide and sulfide compounds in a model S^0-saturated aqueous solution (pure water, total aqueous sulfide concentration = 100μM; Kamyshny et al., 2004, 2007). Fig. 10A reveals that the major polysulfide species under these conditions are HS_2^- and S_x^{2-} (x = 3-8), and the bulk of the aqueous sulfur mass balance can be accounted for by considering only these species and the major aqueous sulfide compounds (H_2S and HS^-). In terms of molecular concentration, HS_2^- dominates polysulfide speciation at lower pH (ca. 6-8.5) and S_x^{2-} dominate polysulfide speciation above a pH of about 8.5 and follow a relative distribution of $S_5^{2-} > S_4^{2-} > S_6^{2-} > S_3^{2-} > S_7^{2-} > S_8^{2-} > S_2^{2-}$. We note that even though the polysulfides stay below 10μM under these model conditions (where total dissolved sulfur = 100μM) they dominate sulfur mass balance under high pH conditions (pH $\geq \approx$ 9.5) because of their high sulfur content per molecule. For example, at pH = 11 the sulfur compound in highest concentration, pentasulfide (S_5^{2-}), has a molecular concentration of only 7.8 μM under these modeled conditions but

comprises nearly 40% of the total dissolved sulfur content.

In Fig. 10B we combine the relative distributions of the polysulfides as computed in Fig. 10A with our theoretical calculations to compute a bulk aqueous polysulfide/sulfide isotope fractionation factor as a function of pH. In terms of bulk fractionation factors, the isotopic compositions of total polysulfides relative to aqueous sulfide species are predicted to be relatively constant above a pH of about 8 (i.e., $1000\times\ln(^{34}\alpha) = 2.2 \pm 0.5‰$ at 25°C). This is due largely to the similarity in the predicted equilibrium isotopic compositions of the dominant polysulfides (i.e., x = 4-6; cf. Fig. 4) and their constant relative distribution under these conditions, and the constancy of aqueous sulfide speciation under these conditions (i.e., principally HS^- above a pH≈8-8.5). The predicted reversal in the direction of the bulk polysulfide/sulfide fractionation factor around pH = 6.5-7 in Fig. 10B is due principally to the shift in the dominant sulfide species (HS^- vs. H_2S; pK_d is 6.98 at 25°C and low ionic strength; Hershey et al., 1988) and the relative direction of fractionation factors between the polysulfides and the two principle sulfide species (cf. Fig. 4). The speciation of polysulfides varies as a function of temperature and ionic strength, but the general relationships that we illustrate in Fig. 10B are predicted to change only subtly as a function of ionic strength (up to μ = 0.7 mol/kg at 25°C) and temperature over 5-75°C. Thus, despite their complex speciation in aqueous solution the polysulfides are predicted to closely track the isotopic composition of aqueous sulfide at equilibrium under fairly wide ranges of environmental conditions.

Amrani et al. (2006) is the only experimental study that we are aware of that reports the isotopic composition of polysulfide compounds of specific chain length isolated from aqueous solutions. They report the isotopic compositions (in terms of $\delta^{34}S$) of the methylated derivatives of polysulfides (i.e., $H_3C\text{-}S_x\text{-}CH_3$) of chain length x = 4-7 that were generated by the rapid derivatization reaction of methyl triflate and precursor aqueous polysulfides. They observed that the isotopic compositions of polysulfides in terms of $\delta^{34}S$ increase with increasing chain length 'x'. The increase in $\delta^{34}S$ with increasing 'x' is consistent with our theoretical calculations that predict a general increasing trend in

the compound specific fractionation factors (β) with increasing 'x' (Fig. 4). If we make the assumption that the isotopic composition of the sulfur extracted from the methylated polysulfanes represents the equilibrium isotopic compositions of the precursor aqueous polysulfides, then the data of Amrani et al. (2006) imply an equilibrium fractionation factor between S_7^{2-}/S_4^{2-} on the order of $1000\times\ln(^{34}\alpha) = 3.2 \pm 0.7$ ‰ at 25°C (1 s.d. from the duplicate experiments reported, based on data digitally extracted from their figures). This estimate based on experimental data is larger than the estimate based on our theoretical calculations of $1000\times\ln(^{34}\alpha) = 0.7 \pm 0.2$ ‰ for S_7^{2-}/S_4^{2-} at 25°C. This slight disagreement may suggest that uncertainty remains in the exact values of the fractionation factors among polysulfides of differing chain-length.

Despite the possible uncertainties in the exact values of fractionation factors among the polysulfides of different chain-length, the calculations provide detailed insight into the isotope partitioning behavior of polysulfides. The calculations newly reveal the relative patterns in values of RPFRs for singly substituted polysulfides at different atomic sites (Table 3, Fig. 4) and thus provide a more detailed explanation for earlier experimental observations (Amrani et al., 2006). The calculations illustrate that the general increase in $^{34}\beta$ with increasing 'x' for S_x^{2-} can be described to arise from the proportionality between the $^{34}\beta$-factor and the number of ^{34}RPFR-contributing isotopologues that increases with 'x' (Section 3.2.1). The ^{34}RPFR values that correspond to isotope substitution of the outer sulfur atoms (exhibiting the lowest RPFR values of each polysulfide isotopologue) have comparable values for all polysulfides (e.g., mean $^{34}\text{RPFR} = 1.0090\pm0.0003$ for S_x^{2-} at 25°C, x = 2-8), and similarly the ^{34}RPFR values that correspond to isotope substitution of the interior sulfur atom that is immediately bonded to the outer sulfur atom (exhibiting the highest RPFR values of polysulfide isotopologues) have comparable ^{34}RPFR values for all pertinent polysulfides (e.g., mean $^{34}\text{RPFR} = 1.0132 \pm 0.0005$ for S_x^{2-} at 25°C, x = 3-8). Thus, the calculations predict some uniformity in the isotope partitioning behavior among comparable isotopologues of polysulfides irrespective of chain length. At 25°C, it is interesting to note that these values are predicted to be

indistinguishable from the ^{34}RPFR values of HS^- (^{34}RPFR = 1.0087 ± 0.0005 at 25°C) and H_2S (^{34}RPFR = 1.0129 ± 0.0003 at 25°C), respectively, which is actually the result of predicted crossovers in values of RPFRs among the sulfide compounds and these particular isotopologues of polysulfides at approximate ambient temperature. Thus, the calculations reveal many underlying details and complexities of the isotope partitioning behavior of the polysulfides relative to aqueous sulfide compounds that may not be expressed at the bulk level (e.g., Fig. 10).

One of two primary mechanisms that have been identified for pyrite precipitation from precursor aqueous sulfur compounds involves the polysulfides ('polysulfide mechanism'; e.g., Luther, 1991; Butler et al., 2004; Rickard & Luther, 2007). In the 'polysulfide mechanism', it has been proposed that pyrite precipitation proceeds *via* the nucleophilic bimolecular reaction between a polysulfide and a ferrous sulfide complex (either the discreet molecular species in solution as we have computed in the present study, or nano-particulate $FeS_{(aq)}$ phases), whereby the two sulfur atoms that eventually become the disulfide in pyrite (Tossell, 1983) are derived entirely from polysulfide (Luther, 1991). Using pentasulfide (S_5^{2-}) and the $FeSH^+$ species as the example reactants, this mechanism can be schematically represented as (*cf.* Luther, 1991; Chadwell et al., 1999):

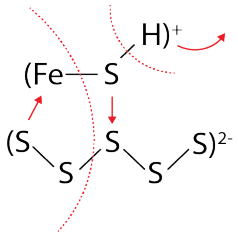

(16)

The dashed red curves indicate where bonds are to be broken and the straight arrows indicate where new bonds are to be formed based on this type of mechanism (note that the positions of the charges are not deliberate and merely represent overall molecular charge). The overall reaction corresponding to this schematic mechanism is given by:

$$FeSH^+ + S_5^{2-} \rightarrow FeS_2 + S_4^{2-} + H^+ \quad (17)$$

This type of mechanism suggests that the two sulfur atoms in polysulfide that are expected to have the highest and lowest RPFR values under equilibrium conditions (*cf.* Fig. 4) are those that are incorporated into pyrite, which our calculations predict have nearly uniform RPFR values for polysulfides irrespective of polysulfide chain-length (Fig. 4). Although the kinetic isotope effects that may be associated with pyrite precipitation/nucleation are unknown, this mechanism alongside our calculations may indicate that any apparent isotope fractionations that accompany the formation of pyrite from precursor compounds *via* a 'polysulfide mechanism' (e.g., apparent fractionations relative to ambient aqueous sulfide) are likely to be relatively small and potentially relatively uniform with respect to the specific polysulfides that may be involved.

We note that the mechanism expressed in Eq. 16-17 is only one simple example of many potential reactions that an aqueous ferrous iron species can undergo with polysulfide to form an initial nucleation of pyrite. The specific form of the 'polysulfide mechanism' that may occur or dominate in any given environment will likely depend on the activities of the various ferrous iron and polysulfide species and therefore solution conditions. It may also be noted that a heterogenous reaction involving aqueous polysulfide and a 'solid' FeS phase is possible and has been proposed to follow an analogous mechanism (e.g., Luther, 1991).

4.1.3. Aqueous Sulfide and Polysulfur Radical Compounds

Fractionation factors among polysulfur radicals ($S_x^{\cdot -}$, x = 2-3) and H_2S/HS^- are presented in Fig. 11 as a function of $1/T^2$. Fractionation factors among $S_2^{\cdot -}/HS^-$ and $S_3^{\cdot -}/HS^-$ are predicted to exhibit crossovers at elevated temperature around 175±70°C and 455±125°C, respectively, which lead to very small fractionation factors at high-temperature (i.e., $1000\times\ln(^{34}\alpha) \leq$ 0.7‰ at T $\geq$ 200°C). Fractionation factors among $S_2^{\cdot -}/H_2S$ and $S_3^{\cdot -}/H_2S$ each appear to ex-

hibit a temperature dependence that is characteristic of a crossover occuring below 0°C. The type of temperature dependence associated with crossovers (or apparent crossovers) for these fractionation factors is the same as that described above for aqueous polysulfide/sulfide. Recent *in situ* Raman spectroscopic investigations of sulfur-rich aqueous fluids contained in fused silica capillaries and hydrothermal diamond anvil cells have documented that the $S_3^{\cdot-}$ (and possibly $S_2^{\cdot-}$) exists as a nominally stable component in equilibrium with aqueous sulfide and sulfate compounds in appreciable amounts at least over the temperature range of ca. 200-500°C under particular pH and redox conditions (Pokrovski & Dubrovinsky, 2011; Pokrovski & Dubessy, 2015; Schmidt & Seward, 2017). Over this temperature range, the fractionation factor between $S_3^{\cdot-}/H_2S$ is predicted to range between $1000\times\ln(^{34}\alpha)$ = -1.9±0.2 ‰ at 200°C (near its predicted relative maximum in magnitude) to -1.3±0.1 ‰ at 500°C. The fractionation factor between $S_2^{\cdot-}/H_2S$ is predicted to be slightly larger in magnitude and for comparison ranges between $1000\times\ln(^{34}\alpha)$ = -2.6±0.2 ‰ at 200°C to -1.6±0.1 ‰ at 500°C. The polysulfur radicals may thus lead to subtle shifts in the sulfur isotope composition of aqueous sulfide (and sulfate) species depending on mass balance under conditions where they coexist in isotopic equilibrium. For reference, the magnitude and direction of the equilibrium fractionations that are predicted between the polysulfur radicals and H_2S at these elevated temperatures are comparable to those between pyrite and aqueous H_2S at 350°C obtained from Syverson et al. (2015) (Fig. 8).

4.1.4. Aqueous Sulfide and Sulfate Compounds

Fractionation factors among aqueous sulfate and select sulfide compounds are presented in Fig. 12 as a function of $1/T^2$ encompassing the temperature range of 200-400°C where experimental constraints presently exist for comparison. From 200 to 400°C, the predicted SO_4^{2-}/H_2S fractionation factor ranges between $1000\times\ln(^{34}\alpha)$ = 28.3 ± 0.2 ‰ and 14.5 ± 0.1‰, respectively, and is essentially identical to our previous estimates utilizing $30H_2O$ clusters (Eldridge et al., 2016). The computed fractionation factor between HSO_4^- and

H_2S is similar in magnitude but is predicted to be slightly larger and ranges from $1000\times\ln(^{34}\alpha) = 29.0 \pm 0.2$ ‰ to 15.0 ± 0.1‰ over 200 to 400°C, respectively. The fractionation factors between the two computed sulfate ion pairs, $(Na^+SO_4^{2-})^-$ and $(Mg^{2+}SO_4^{2-})^0$, and H_2S are indistinguishable from one another over all temperature values and have intermediary values between the SO_4^{2-}/H_2S and HSO_4^-/H_2S. Thus, the predicted fractionation factors between all computed sulfate species and H_2S are all very similar. Also shown in Fig. 12 is the fractionation factor between $HSO_4^-/S_3^{\cdot-}$ that ranges between 30.8 ± 0.1 ‰ and 16.5 ± 0.1 from 200 to 400°C, respectively (i.e., slightly larger than fractionations among aqueous sulfate/sulfide species).

Previous experimental determinations of equilibrium sulfur isotope fractionations between aqueous sulfate and sulfide species are in agreement with our theoretical predictions at the level of ≤1 ‰ (Fig. 12). The compilation of Ohmoto & Lasaga (1982) that incorporates numerous experimental datasets over 200-400°C yields fractionation factors between aqueous sulfate and sulfide of $1000\times\ln(^{34}\alpha) = 29.4 \pm 0.5$ ‰ at 200°C and 14.8 ± 0.5 ‰ at 400°C based on their $1000\times\ln(^{34}\alpha)$ vs. $1/T^2$ linear fit to selected experimental data. The largest difference between Ohmoto & Lasaga (1982) and the SO_4^{2-}/H_2S calculations presented here and in our previous study (Eldridge et al., 2016) is ≈1 ‰ at 200°C (Fig. 12). Under the experimental conditions of most experiments that are included in the compilation of Ohmoto & Lasaga (1982) the aqueous speciation of sulfate may largely be in the form of HSO_4^- due to the low *in situ* pH of experimental fluids that is necessary to facilitate feasible equilibration times due to higher rates of isotope exchange under acidic conditions. The computed HSO_4^-/H_2S fractionation factor in Fig. 12 is in agreement with the experimental compilation of Ohmoto & Lasaga (1982) at the level of ≤0.46 ‰ over 200-400°C (see residual plot in Fig. 12), which is within the error reported by Ohmoto & Lasaga (1982). The slight divergence between our HSO_4^-/H_2S estimate and Ohmoto & Lasaga (1982) at 200°C (≤0.5 ‰) could reflect a true difference in the temperature dependence (e.g., arising from inadequacies in the theoretical calculations), or could reflect (a) the paucity of experimental

data at 200°C (e.g., 1 data point taken from Robinson (1973) corresponding to $1000\times\ln(^{34}\alpha_{HSO_4^-/H_2S}) = 28.9$ ‰) and/or (b) the assumption of Ohmoto & Lasaga (1982) that the temperature dependence of the fractionation factor is linear over 200-400°C in $1000\times\ln(^{34}\alpha)$ *vs.* $1/T^2$ space (*cf.* the theoretical calculations that all exhibit subtle curvature in this space over 200-400°C; Fig. 12). Syverson et al. (2015) recently obtained a fractionation factor between aqueous sulfate/sulfide of $1000\times\ln(^{34}\alpha) = 17.5 \pm 0.6$ ‰ at 350°C (1 s.d., duplicate equilibrated experiments) judged to be at equilibrium based on constraints from complimentary Δ^{33}S measurements. The experiments of Syverson et al. (2015) were also performed under low pH conditions where HSO_4^- likely dominates the aqueous sulfate speciation. Their value is indistinguishable from our computed estimate of the HSO_4^-/H_2S fractionation factor at 350°C of $1000\times\ln(^{34}\alpha) = 17.3 \pm 0.1$ ‰ (Fig. 12). Overall, the theoretical calculations presented here appear to reproduce established experimental observations of the aqueous sulfate/sulfide fractionation factor within the estimated errors of the approaches.

At 25°C, equilibrium fractionations between select aqueous sulfate and sulfide compounds are predicted to be $1000\times\ln(^{34}\alpha) = 63.3 \pm 0.4$ ‰ for SO_4^{2-}/H_2S, 64.1 ± 0.4 ‰ for HSO_4^-/H_2S, and 67.5 ± 0.6 ‰ for SO_4^{2-}/HS^-. It is notable that our theoretical calculation of the $1000\times\ln(^{34}\alpha)$ corresponding to the SO_4^{2-}/H_2S fractionation factor presented here and in Eldridge et al. (2016) is lower than previous theoretical estimates at 25°C by as much as ≈ 9 ‰ (e.g., those of Farquhar et al., 2003; Ono et al., 2007). We further note that these previous theoretical estimates (Farquhar et al., 2003; Ono et al., 2007) are systematically higher than our theoretical calculations at higher temperatures as well (e.g., by ≥ 2 ‰ over 200-400°C) and, thus, do not agree as well with experimental constraints. It is our judgement that the estimates of the aqueous sulfate/sulfide fractionation factors at lower temperatures derived from our calculations (i.e., the current study and Eldridge et al., 2016) are likely to be among the best estimates available to date for low temperature applications (e.g., in models of microbial metabolism such as dissimilatory sulfate reduction) due to the apparent agreement with established experimental constraints at higher

temperatures (Fig. 12). However, we emphasize that no experimental data exist to our knowledge that directly constrain the aqueous sulfate/sulfide equilibrium fractionation factor at temperatures < 200℃ and thus the verification of any theoretical estimates at lower temperatures (either previously published or presented here) is not possible at this time.

From the analysis above, it can be inferred that the predicted equilibrium sulfur isotope fractionation among coexisting aqueous sulfate species is small in magnitude. For example, at 25℃ the estimated fractionation factor between the direct magnesium sulfate ion pair $(Mg^{2+}SO_4^{2-})^0$ and SO_4^{2-} is $1000\times\ln(^{34}\alpha)$ = 0.25 ± 0.18 ‰ (similar for the direct sodium ion pair), and for HSO_4^- and SO_4^{2-} we estimate a value of $1000\times\ln(^{34}\alpha)$ = 0.75 ± 0.22 ‰. Thus, sulfate speciation in natural waters such as those of high ionic strength (e.g., seawater and naturally occurring brines) that could involve substantial formation of ion-pairs, and those containing high acidity (e.g., natural acid lakes or drainage) appears unlikely to have a significant effect on sulfur isotope partitioning.

4.1.5. Polythionates

Pertinent fractionation factors involving the unique atomic sites in the polythionates computed in this study ($S_3O_6^{2-}$ and $S_4O_6^{2-}$, or $S_x(SO_3)_2^{2-}$ where x = 1 or 2) are plotted in Fig. 13 as a function of $1/T^2$ alongside analogous fractionation factors involving thiosulfate ($S_2O_3^{2-}$ or $S(SO_3)^{2-}$) from Eldridge et al. (2016) for reference. The 'intramolecular' fractionation factor for polythionate that represents the difference in equilibrium isotopic composition between the unique sulfur sites within the molecule (i.e., the equivalent 'sulfonate' groups, $S_x(^*\mathbf{S}O_3)_2^{2-}$, and the central 'sulfanyl' atoms, $^*\mathbf{S}_x(SO_3)_2^{2-}$) is predicted to be $1000\times\ln(^{34}\alpha) = 54.4 \pm 0.8$ ‰ at 25℃. This is comparable to our earlier predictions of the 'intramolecular' fractionation factor for thiosulfate: $1000\times\ln(^{34}\alpha)$ ≈ 53.8 ‰ at 25℃ (Eldridge et al., 2016). The predicted fractionation factor between the 'sulfonate' groups in trithionate and $H_2S_{(aq)}$ is predicted to be $1000\times\ln(^{34}\alpha) = 55.8 \pm 0.6$ ‰ at 25℃. This is also comparable to the analogous values for thiosulfate but perhaps slightly larger in magnitude: $1000\times\ln(^{34}\alpha)$

= 52.5 ± 0.3 ‰ at 25°C (Eldridge et al., 2016). The fractionation factors for the 'sulfanyl' sulfur atoms in trithionate and thiosulfate relative to H_2S are much smaller in magnitude and exhibit complex behavior as a function of temperature due to crossovers. For example, at 25°C the fractionation factors for the 'sulfanyl' sulfur atoms in the computed polythionates and thiosulfate relative to H_2S are predicted to be similar in magnitude but opposite in direction: $1000\times\ln(^{34}\alpha)$ = 1.4 ± 0.7 ‰ for 'sulfanyl' in polythionate relative H_2S, and $1000\times\ln(^{34}\alpha)$ = -1.3 ± 0.3 ‰ for 'sulfanyl' in thiosulfate relative to H_2S. However, above approximately 75°C the fractionation factors between the 'sulfanyl' groups in both trithionate and thiosulfate are both predicted to be in the same direction relative to H_2S (Fig. 13) and agree with the direction of the experimental constraints for thiosulfate (Uyama et al., 1985; Chu et al., 2004).

4.1.6. Elemental Sulfur and Sulfate/Sulfide

Data from hydrothermal experiments have been used previously to estimate an equilibrium fractionation factor between elemental sulfur (generically S^0) and aqueous sulfide and sulfate (Robinson, 1973; Kusakabe et al., 2000). These data are plotted in Fig. 14 alongside our corresponding theoretical estimates. The combined experimental data of Robinson (1973) and Kusakabe et al. (2000) yield an estimate of the fractionation factor between S^0 and sulfate (HSO_4^-) of $1000\times\ln(^{34}\alpha)$ = 30.2 to 19.3 ‰ (±0.29, 1 s.d.) over a temperature range of 200-230°C that is comparable to our theoretical calculations (Fig. 14A). The data of Robinson (1973) can be used to estimate a fractionation factor between S^0 and H_2S that yields values that range between $1000\times\ln(^{34}\alpha_{S^0/H_2S})$ = -1.2 and -2.3 (±0.28) ‰ over 200-320°C that are essentially temperature-invariant (mean over 200-320°C: $1000\times\ln(^{34}\alpha_{S^0/H_2S})$ = -1.7 ± 0.4 ‰, 1 s.d.). Over this same temperature range, our theoretical calculations predict an essentially temperature-invariant fractionation factor of about $1000\times\ln(^{34}\alpha_{S_{8(aq)}/H_2S})$ = -1.6 ± 0.1 ‰ that corresponds to the maximum predicted magnitude of this fractionation factor ($T \geq 0$°C) that arises over this temperature range due to crossover behavior at lower temperature (Fig. 14B). In short, our theoretical

calculations appear to capture the broad behavior of isotope partitioning exhibited experimentally in the S^0-H_2S-HSO_4^- system.

4.2. Mass Dependence of Equilibrium Isotope Exchange at Crossovers

The crossovers in equilibrium fractionation factors among aqueous sulfide, polysulfur radical, and polysulfide compounds result in unusual exponents of mass-dependence ($^{33/34}\theta$, $^{36/34}\theta$) in proximity to the crossover temperatures. These effects have been previously described for theoretical isotopic exchange between exemplary gaseous sulfur molecules (Deines, 2003; Otake et al., 2008). Using the $S_{2(g)}/H_2S_{(g)}$ example, Deines (2003) recognized that exponents describing mass dependence (e.g., $^{33/34}\theta$) asymptotically approach values from $+\infty$ to $-\infty$ near temperature values that approach the crossover. In Fig. 15, we illustrate the effect of crossovers on values of $^{33/34}\theta$ and $\Delta^{33}S$ for numerous equilibrium isotope exchange reactions that have been theoretically computed in our study among aqueous sulfur compounds. The calculations of the $^{33/34}\theta$ reveal the expected asymptotic behavior in proximity to the T_c (Fig. 15A-C). Below the T_c, values for $^{33/34}\theta$ typically approach values of $-\infty$ with increasing temperature (Fig. 15A-C). Above the T_c, $^{33/34}\theta$ drop precipitously from $+\infty$ with increasing T until eventually approaching $\approx$0.5156 at the high-temperature limit. Despite these infinitely large shifts in values of $^{33/34}\theta$ at crossovers, these unusual exponents do not result in any notable deviations in values of $\Delta^{33}S$ arising from equilibrium isotope exchange as shown in the accompanying Fig. 15D-F that is due principally to the very small values of fractionation factors (α) in proximity to the T_c. We note that analogous relationships and conclusions can be drawn for computations of $^{36/34}\theta$ and $\Delta^{36}S$ values that are not illustrated here for reasons of economy.

Deines (2003) suggested that the unusual exponents of mass dependence in proximity to crossover temperatures for isotope exchange reactions could be amplified by subsequent Rayleigh processes to potentially generate compounds that have isotopic compositions exhibiting anomalous $^{33/34}\theta$ and/or $\Delta^{33}S$ values. This hypothesis can be examined in further detail using our theoretical frac-

tionation factors computed near crossovers. We perform an exercise where we compute the isotopic composition of a product that is generated via a Rayleigh process in a closed system that involves a reactant that has an isotopic composition that corresponds to a crossover. For the purposes of this example, we use S_2^{2-} as the reactant and consider its composition relative to HS^- where a crossover is predicted in rough proximity to ambient temperature (≈16℃; *cf.* Fig. 9). The product of their reaction could hypothetically be anything that could irreversibly react with S_2^{2-}, but we point out that this example could be made relevant to a simplified polysulfide pyrite precipitation mechanism (e.g., Rickard & Luther, 2007):

$$Fe^{2+} + S_2^{2-} = FeS_2 \tag{18}$$

According to the hypothesis implied by Deines (2003), in this example the isotopic composition of the product (i.e., pyrite) may obtain an anomalous isotopic composition (e.g., $\Delta^{33}S \neq 0$) relative to ambient HS^- if precipitation occurs via S_2^{2-} in proximity to the T_c.

We have run through a handful of scenarios where we compute the product of a closed-system Rayleigh process (e.g., in this example 'pyrite') involving S_2^{2-} where its initial composition is constrained as being in equilibrium with HS- at 16℃ (the approximate T_c), which corresponds to a composition of $\delta^{33}S = 0.0 \pm 0.4$ ‰, $\delta^{34}S = 0.0 \pm 0.7$ ‰, and $^{33/34}\theta = 1.936$ (i.e., extremely anomalous relative to the reference exponent of 0.515) where all compositions are referenced to HS^- (e.g., $\delta^{34}S = {}^{34}R/{}^{34}R_{HS^-}$ - 1, where $^{34}R = {}^{34}S/{}^{32}S$). We compute Rayleigh distillation scenarios in terms of the isotopic composition of the accumulated product relative to HS^- utilizing different assumptions of the value of the isotope effect associated with the unidirectional process (e.g., the isotope effect associated with FeS_2 precipitation in this simplified example). We assume for the purposes of the calculation that the isotope fractionations accompanying the Rayleigh process (e.g., unidirectional precipitation) are ≤ 20 ‰ (where 20 ‰ could be considered unrealistically large for this type of process) and ad-

ditionally assume that the process conforms to the conventions of a 'normal' isotope effect (i.e., products isotopically depleted relative to reactants). We additionally assume that the isotope effects associated with the unidirectional process conform to the reference exponent (i.e., 0.515), which is necessary in order to examine the effect of the initial crossover composition on the composition of the pooled product.

Our calculations reveal that the unusual exponents associated with crossovers do not lead to substantial $\Delta^{33}S$ effects in terms of the isotopic composition of a product resulting from a closed-system Rayleigh process. The maximum deviations occur for the largest assumed isotope effect for the Rayleigh process (-20 ‰) and approach a maximum of $\Delta^{33}S = 0.02$ ‰ (note that typical quoted external precision of $\Delta^{33}S$ based on SF_6-IRMS is on the order of 0.01 ‰, 1 s.d.). We note that nearly identical results are obtained in this computation regardless of the assumed initial $^{33/34}\theta$ of the reactant (in this case S_2^{2-}). This suggests that the choice of initial composition in proximity to the crossover is not important and that any amplification of unusual exponents associated with crossovers via a closed-system Rayleigh process is likely insignificant. The evolution of the $\Delta^{33}S$ of the residual reactant over the full extent of the Rayleigh process is also not sensitive to values of $^{33/34}\theta$. In general, Rayleigh processes can lead to significant $\Delta^{33}S$ effects in the residual reactant but only when very small amounts of residual reactant remain (note: this will be illustrated in the following section in the context of modeled disproportionation reactions). These effects occur irrespective of crossovers and/or the initial isotopic compositions of reactants. Thus, it is difficult to imagine how crossovers may lead to any notable anomalous sulfur isotopic compositions among naturally occurring phases/compounds either as a result of equilibrium (Fig. 15) or subsequent Rayleigh distillation.

The more interesting aspect of crossover behavior in sulfur isotope systematics from our perspective is how crossovers lead to non-intuitive temperature dependencies of fractionation factors (cf. Fig. 8, 9, 11, 13, 14). Depending on the temperature at which they occur, crossovers can enable small but still relatively significant equilibrium isotope fractionations among compounds with respect to

a singular isotope ratio at relatively high temperature, despite instances where fractionation factors exhibit generally small to negligible fractionation factors at low temperature (e.g., for $S_3^{\cdot-}/H_2S$, $1000\times\ln(^{34}\alpha)$ = -0.4 ± 0.5 ‰ at 0°C but -1.9 ± 0.2 ‰ at 200°C; Fig. 11).

4.3. Example Applications: Model Disproportionation Reactions

4.3.1. General Framework & First-Order Implementation Using Theoretical Equilibrium Isotope Effects

Sulfur compounds of intermediate oxidation state (i.e., S^{OS} where -2 < OS < +6; e.g., SO_2, S_8) and mixed-valence (e.g., $S_2O_3^{2-}$; OS = -1 and +5) (Vairavamurthy et al., 1993) can undergo hydrolytic disproportionation reactions at elevated temperatures to form sulfur compounds of both higher and lower valence (e.g., SO_4^{2-} and H_2S, or SO_4^{2-} and S^0). Examples of hydrolytic disproportionation reactions include:

$$S_2O_3^{2-} + H_2O \rightarrow H_2S + SO_4^{2-} \quad (19)$$

$$3S^0 + 2H_2O \rightarrow 2H_2S + SO_{2(aq)} \quad (20)$$

$$4S^0 + 4H_2O \rightarrow 3H_2S + HSO_4^- + H^+ \quad (21)$$

$$4SO_{2(aq)} + 4H_2O \rightarrow 3HSO_4^- + H_2S + 3H^+ \quad (22)$$

$$3SO_{2(aq)} + 2H_2O \rightarrow 2HSO_4^- + S^0 + 2H^+ \quad (23)$$

These reactions, especially those involving thiosulfate and elemental sulfur as the principle reactants, have long been exploited for experimental hydrothermal sulfur isotope partitioning studies (e.g., Thode et al., 1971; Robinson, 1973; Ohmoto & Lasaga, 1982; Uyama et al., 1985; Kusakabe et al., 2000; Syverson et al., 2015) and *in situ* spectroscopic thermodynamic/speciation studies (e.g., Pokrovski & Dubessy, 2015; Schmidt & Seward, 2017). Such investigations led to the discovery of the apparent stability of the $S_3^{\cdot-}$ radical ion under hydrothermal conditions following (e.g., Pokrovski & Dubrovinsky, 2011; Pokrovski & Dubessy, 2015):

$$S_3^{\cdot -} + 2.5H_2O + 0.75O_2 \rightleftharpoons SO_4^{2-} + 2H_2S + H^+ \tag{24}$$

The decomposition of the $S_3^{\cdot -}$ radical ion (e.g., upon the cooling of a fluid) presumably follows a reaction similar to the forward progress of Eq. 24 that resembles hydrolytic disproportionation but as written also involves explicit oxidation.

Hydrolytic disproportionation reactions such as those represented in Eq. 19-24 can be modeled in a simple way as branching reactions following the generalized network:

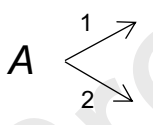

(25)

Here, some sulfur compound of intermediate or mixed oxidation state, A, undergoes a unidirectional reaction to compounds B and C. Reaction 1 and reaction 2 are associated with their respective kinetic isotope effects, ${}^i\alpha_1 \equiv {}^ik_1/{}^{32}k_1$ and ${}^i\alpha_2 \equiv {}^ik_1/{}^{32}k_2$ (where i = 33, 34, or 36; NOTE: the symbol α is used here to represent a kinetic isotope effect (format: ${}^i\alpha_{rxn}$) for the sake of simplicity and should not be confused with other uses of α in this study). The general analytical solutions for the compositions (given as isotope ratios ${}^iR = {}^iS/{}^{32}S$) for sulfur phases A, B, and C in a closed system are given by (derivations provided in the Appendix A.2):

$${}^iR_{A,t} = {}^iR_{A,0} \times f^{(b\times{}^i\alpha_1+(1-b)\times{}^i\alpha_2-1)} \tag{26}$$

$${}^iR_{B,t} = \frac{{}^i\alpha_1 \times {}^iR_{A,0} \times \left(1 - f \times f^{(b\times{}^i\alpha_1+(1-b)\times{}^i\alpha_2-1)}\right)}{(1-f)\times(b\times{}^i\alpha_1+(1-b)\times{}^i\alpha_2)} \tag{27}$$

$$ {}^{i}R_{C,t} = \frac{{}^{i}\alpha_2 \times {}^{i}R_{A,0} \times \left(1 - f \times f^{(b \times {}^{i}\alpha_1 + (1-b) \times {}^{i}\alpha_2 - 1)}\right)}{(1-f) \times (b \times {}^{i}\alpha_1 + (1-b) \times {}^{i}\alpha_2)} \quad (28) $$

The variable $b = \frac{[B]}{[B]+[C]}$ is the product branching ratio that can be related to the reaction stoichiometries of the various disproportionation reactions (e.g., Eq. 19-24) and f is the fraction of the reactant remaining at any given time point in the reaction ($[A]_t/[A]_0$; see Appendix A.2 for further details). At present, Eq. 26-28 cannot be solved completely and/or directly for most disproportionation reactions (e.g., Eq.19-24) because the overall kinetic isotope effects associated with these reactions are not presently constrained to our knowledge (especially for all three sulfur isotope ratios).

An initial glimpse of the potential multiple sulfur isotope fractionation behavior associated with a variety of disproportionation reactions can be obtained by substituting equilibrium isotope effects for the kinetic isotope effects required by Eq. 26-28 constrained by a combination of our calculations from the present study and our previous study (Eldridge et al., 2016). Substituting equilibrium isotope effects for kinetic isotope effects for the purpose of this exercise is equivalent to assuming that the true kinetic isotope effects associated with these reactions are of comparable magnitude (and exhibit similar mass laws, ${}^{33/34}\theta$ and ${}^{36/34}\theta$) and temperature dependence to the equilibrium isotope effects among the considered species, which are recognized as important limitations. Solutions to models applying this simplifying substitution corresponding to an example each of SO_2, S^0, and S_3^- are provided in Fig. 16. The purpose of this exercise is to illustrate the subtle shifts in the $\Delta^{33}S$ and $\Delta^{36}S$ compositions of the reactants and products of disproportionation-type processes that arise from mass balance ('mass conservation effects'; e.g., Farquhar et al., 2007), which to-date have not been systematically constrained by experiments. The true kinetic isotope effects and corresponding 'mass laws' (${}^{33/34}\theta$ and ${}^{36/34}\theta$) and their temperature dependence associated with disproportionation reactions in Eq. 19-24 are currently unconstrained by either theory or experiments, and so the full range of $\Delta^{33}S$ and $\Delta^{36}S$ variations associated with these reactions are not yet known.

Given these limitations to understanding the multiple sulfur isotope behavior associated with hydrolytic disproportionation reactions, we explore in the following section a natural example that utilizes a simple mass balance approach and our new theoretical calculations to investigate how disproportionation reactions may manifest in measurable shifts in $\Delta^{33}S$ and $\Delta^{36}S$ compositions of naturally occurring compounds that may reflect the properties and dynamics of an example natural system.

4.3.2. Natural Example Based on Mass Balance Modeling: Volcanic (hyper-) acid crater Lakes

Hydrolytic disproportionation reactions can contribute to sulfur-cycling in magmatic-hydrothermal systems. A primary example we will highlight here are (hyper-) acid crater lakes associated with active arc volcanoes (e.g., see overview/reviews in Kusakabe et al., 2000; Marini et al., 2011; Delmelle & Bernard, 2015). Such lakes are often typified by low pH (e.g., pH = -0.6 to 4.9), high concentrations of dissolved sulfate (e.g., $[SO_4^{2-}]$ = 0.6-0.8 mol/kg), and in some cases are characterized by elemental sulfur in the forms of floating cinders thought in some cases to be derived from molten pools of sulfur at the lake bottom (e.g., Delmelle et al., 2000; Kusakabe et al., 2000; Delmelle & Bernard, 2015, and references therein). The $\delta^{34}S$ values of dissolved sulfate ($\delta^{34}S = ({}^{34}R_{sample}/{}^{34}R_{VCDT}$ - 1)×1000) in many (hyper-)acid crater lakes have been observed to be relatively high (e.g., $\delta^{34}S$ values as high as 20-25 ‰ reported relative to CDT in their study; Kusakabe et al., 2000) and in such cases exhibit relatively large fractionations relative to ambient/associated elemental sulfur: $1000 \times ln\left({}^{34}R_{HSO_4^-}/{}^{34}R_{S^0}\right)$ up to ≈ 30 ‰ (Kusakabe et al., 2000). Such compositions (and fractionations) in (hyper-)acid crater lakes cannot be explained by oxidation processes because in such a case the $\delta^{34}S$ values of reduced and oxidized sulfur species would be expected to more closely track each other. These compositions are instead generally explained by much of the sulfate originating from hydrolytic SO_2 disproportionation (e.g., Rye et al., 1992; Taran et al., 1996; Delmelle et al., 2000; Kusakabe et al., 2000; Marini et al.,

2011; Delmelle & Bernard, 2015).

Informed by their experimental investigations of SO_2 disproportionation in the laboratory, Kusakabe et al. (2000) provided a mass balance model based on the hydrolytic disproportionation of SO_2 to elemental sulfur and sulfate following Eq. 23 to account for the sulfur isotope compositions of (hyper-)acid crater lake dissolved sulfate assuming that all sulfate originates from SO_2 disproportionation. Kusakabe et al. (2000) based their model on Taran et al. (1996) where a similar model was presented for Eq. 22 (i.e., where H_2S and HSO_4^- are assumed to be the products). We additionally note that a comparable model was also recently presented in Marini et al. (2011) where additional sulfide oxidation processes are included, which we will omit for simplicity here. We reproduce here a complete version of the model presented by Kusakabe et al. (2000) in terms of isotope ratios (${}^iR = {}^iS/{}^{32}S$, where i = 33, 34, or 36) for both disproportionation products of Eq. 23 (derivation provided in Appendix A.3):

$$ {}^iR_{HSO_4^-} = \frac{{}^iR_T \times (r+1)}{r \times {}^i\alpha_{H_2S/HSO_4^-} + (1/3) \times {}^i\alpha_{S^0/HSO_4^-} + (2/3)} \tag{29} $$

$$ {}^iR_{S^0} = \frac{{}^iR_T \times (r+1)}{r \times {}^i\alpha_{H_2S/S^0} + (2/3) \times {}^i\alpha_{HSO_4^-/S^0} + (1/3)} \tag{30} $$

Where r is the molar H_2S/SO_2 ratio of the source gas ultimately fed from the magmatic system, ${}^iR_T$ corresponds to the bulk isotope ratio of the gaseous sulfur (assumed to be comprised solely of H_2S + SO_2), and the α's are the temperature dependent equilibrium fractionation factors between the designated species (following the convention of ${}^i\alpha_{A/B} = {}^iR_A/{}^iR_B$). The factors of 1/3 and 2/3 arise from the stoichiometry of the assumed SO_2 disproportionation reaction (Eq. 23). A key assumption of this model is that all species are isotopically equilibrated at the temperature of disproportionation.

Kusakabe et al. (2000) solved a simplified version of Eq. 29 for $\delta^{34}S$ (see Appendix A.3) using the experimental equilibrium ${}^{34}\alpha_{sulfide/sulfate}$ from Ohmoto & Lasaga (1982) and the experimental equilibrium ${}^{34}\alpha_{S^0/HSO_4^-}$ derived from

their experimental data and Robinson (1973). They illustrated that dissolved sulfate (and perhaps elemental sulfur) associated with many (hyper-)acid crater lakes near the summits of active arc volcanoes exhibit $\delta^{34}S$ compositions that are broadly consistent with this type of mass balance model. Because of the agreement between our theoretical calculations and these experimental studies (Fig. 12 and 14) our solutions to these equations utilizing our theoretical fractionation factors yields essentially identical results to Kusakabe et al. (2000) with respect to $\delta^{34}S$. The advantage of using our theoretical calculations in the present exercise is that (*i*) we do not need to extrapolate experimental fractionation factors into temperature ranges that are not constrained by experiment, and (*ii*) we can directly solve these equations for $\delta^{33}S$ and $\delta^{36}S$ (and, thus, $\Delta^{33}S$ and $\Delta^{36}S$) using direct constraints for the minor isotope equilibrium fractionation factors from our theoretical calculations without having to make assumptions about the equilibrium mass laws.

In Fig. 17, we present solutions of Eq. 29 and 30 in terms of $\delta^{34}S$, $\Delta^{33}S$, and $\Delta^{36}S$ utilizing our theoretical fractionation factors as the principle constraints. For the purpose of this exercise, we follow Kusakabe et al. (2000) and assume $\delta^{34}S_T = +5$ ‰ (from Ueda & Sakai, 1984; Taylor, 1986) and we compute compositions over ranges of $r = H_2S/SO_2 = 0.1$-10 and over temperatures of 150-400℃. We further assume that $\Delta^{33}S_T = 0$ ‰ and $\Delta^{36}S_T = 0$ ‰ corresponding to $\delta^{33}S_T = +2.57$ ‰ and $\delta^{36}S_T = +9.52$ ‰. The resulting compositional fields presented in Fig. 17 for sulfate and elemental sulfur in multiple sulfur isotope space as a function of temperature and r result from the underlying mass balance of varying contributions of SO_2 disproportionation. As such, the shifts in $\Delta^{33}S$ and $\Delta^{36}S$ can be described as 'mass conservation effects' (e.g., Farquhar et al., 2007).

In Fig. 17, we also run through a related exercise undertaken by Kusakabe et al. (2000) where we use the empirical $\delta^{34}S$-based fractionation between HSO_4^- and S^0 from a handful of (hyper-)acid crater lake localities as a thermometer to constrain the temperature of SO_2 disproportionation such that $r = H_2S/SO_2$ may be constrained. Localities include: Yugama (Japan), Kawah

Ijen (East Java, Indonesia), Keli Mutu (East Nusa Tenggara, Indonesia), Mount Ruapehu (New Zealand), and Maly Semiachik (Kamchatka Peninsula, Russia) (all δ^{34}S data are taken from Kusakabe et al. (2000) and further details can be found there and references therein). This exercise is identical to the exercise conducted by Kusakabe et al. (2000) in their Fig. 11 only here we newly have the additional capability of computing model output Δ^{33}S and Δ^{36}S values for these localities. In Fig. 17 we predict subtle but potentially resolvable shifts in Δ^{33}S and Δ^{36}S values for these localities within the simple model framework of Eq. 29 - 30 that, again, arise from mass conservation effects. We emphasize that the Δ^{33}S and Δ^{36}S compositions of sulfur species from these crater lake localities have not been determined to the best of our knowledge. A prediction from this simple model is that dissolved sulfate should exhibit higher Δ^{33}S relative to the bulk sulfur isotope composition of the magmatic-hydrothermal sulfur source (up to 0.04-0.05 ‰ higher) and lower Δ^{36}S values (as much as 0.4 ‰ lower) depending on values of r and the temperature of disproportionation. Similar but more subtle relationships are also predicted in values of Δ^{33}S and Δ^{36}S between dissolved sulfate and associated/ambient elemental sulfur assuming that SO_2 disproportionation at higher temperatures alone is responsible for their origin in (hyper-)acid crater lakes (Fig. 17). We recognize that the sulfur isotope compositions of elemental sulfur and sulfate in these environments are not necessarily so tightly coupled and that other processes associated with the sourcing and cycling of these species in the lakes would complicate this simple prediction. To first order, the multiple sulfur isotope analyses (Δ^{33}S and Δ^{36}S in addition to δ^{34}S) could provide additional constraints on the sources and cycling of sulfur in these systems.

The simple model presented in Fig. 17 highlights the potential sensitivity of Δ^{33}S and Δ^{36}S values of (hyper-)acid crater lake dissolved sulfate to underlying hydrothermal-magmatic properties and processes that may serve as additional parameters for monitoring volcanic gases and sulfur cycling processes in these systems. Values of r are complex and depend on aspects of magma exsolution (i.e., magma sources, degassing dynamics, and vapor/melt partition

coefficients that are a function of temperature, pressure, and redox-properties of the magmatic system; e.g., Oppenheimer et al., 2011) and other (secondary) processes occurring during gas transport through conduits to the surface (e.g., wall rock interactions; Giggenbach, 1987; Christenson & Tassi, 2015; Delmelle & Bernard, 2015, and references therein). Dramatic decreases in r have been inferred to be correlated with eruptive events using either dissolved polythionate concentrations in (hyper-)acid crater lakes (e.g., Takano, 1987, see Delmelle & Bernard (2015) for detailed summary and potential complications of this proxy) or $\delta^{34}S_{HSO_4^-}$ as described in the context of the model presented above (e.g., Ohsawa et al., 1993; Kusakabe et al., 2000). Using an unparalleled dataset from Yugama Lake (Japan) beginning with the work of Sakai (1957), Ohsawa et al. (1993) and Kusakabe et al. (2000) illustrated how dramatic shifts in $\delta^{34}S_{HSO_4^-}$ (up to ≈10 ‰ overall) can be associated with eruptive events that were interpreted to reflect enhanced SO_2 fluxes to the system (and thus decreasing r) during eruptions. Interestingly, Kusakabe et al. (2000) illustrated that pre-eruption values of $\delta^{34}S_{HSO_4^-}$ appear to be largely recovered in Yugama Lake following eruption activity. Based on the simple model framework presented here (Fig. 17), we would predict subtle shifts in $\Delta^{33}S$ (ca. 0.01 ‰) and $\Delta^{36}S$ (ca. 0.1 ‰) corresponding to these observed shifts in $\delta^{34}S_{HSO_4^-}$ during those eruptive events at Yugama Lake (Kusakabe et al., 2000), which approach the current analytical precision of the measurements but may nevertheless allow further tracking capabilities under some circumstances. We propose that multiple sulfur isotope analyses ($\delta^{34}S$ and the precise measurement of $\Delta^{33}S$ and $\Delta^{36}S$) of sulfur phases in (hyper-)acid crater lakes, in addition to detailed characterization of the concentrations and perhaps isotope compositions of other minor sulfur species (polythionates, polysulfides, thiosulfate, sulfite, etc.; *cf.* Delmelle & Bernard, 2015), may allow further testing of such models and reveal even more detail of the complexities of the fascinating aqueous sulfur chemistry and dynamics of (hyper-)acid crater lakes and its relation to volcanic eruptions in future work.

5. Summary and Conclusion

We present theoretical estimates of RPFRs (and/or site-averaged β-factors) for aqueous polysulfur compounds (S_x^{2-}, x = 2-8; HS_x^-, x = 2,3; $S_x^{\cdot -}$, x = 2, 3; and $S_x(SO_3)_2^{2-}$, x = 3, 4; S_8) and associated aqueous sulfate (HSO_4^-, SO_4^{2-}, and select Na^+- and Mg^{2+}-ion pairs) and sulfide compounds (H_2S, HS^-, select aqueous Fe^{2+}-complexes and Na^+-ion pairs). We utililize the B3LYP/6-31+G(d,p) level of theory and basis set in conjunction with an explicit solvation model whereby solutes are modeled in water clusters of generally varying size in the range of 30-52 water molecules. We do not observe any systematic deviation in molecular geometries, mean water coordination number, or RPFR/β values associated with water cluster size, and therefore estimate an uncertainty in these values based on the variability that we observe among different cluster sizes and conformations. The typical variability associated with cluster size is relatively small and on the order of $\leq$ 0.5 ‰ (1 s.d.) in estimates of ^{34}RPFR/$^{34}\beta$ values at 25°C that generally keep estimated uncertainties in values of $^{34}\alpha$ < 1 ‰ (1 s.d.). It is important to emphasize that these uncertainty estimates do not take into consideration any systematic errors due to inadequacies in the utilized B3LYP/6-31+G(d,p) theoretical method and basis set, which are difficult to determine. Instead, we emphasize comparing our theoretically calculated fractionation factors to available experimental determinations and find generally good agreement within the estimated errors of the approaches. For example, our calculations agree with experimental dterminations of the HSO_4^-/H_2S fractionation factor within $\leq$ 0.5 ‰ over the experimental temperature range of 200-400°C. Because we utilize the same approach to computing RPFRs (and/or β-factors) to our previous study (Eldridge et al., 2016) these two datasets can be viewed as one larger dataset aiming to constrain the equilibrium isotope fractionations among many aqueous sulfur compounds for applications to natural and experimental systems.

Our calculations reveal a propensity for crossover behavior among reduced polysulfur and sulfide compounds/moieties, where fractionation factors switch

in direction at specific temperatures and thereby exhibit non-intuitive temperature dependences. Numerous crossovers are predicted among aqueous sulfide, polysulfide, polysulfur radical compounds, in addition to the central reduced atomic sites in select polythionates. The calculations likely do not precisely constrain the values of crossover temperatures for any of the fractionation factors computed (i.e., estimated uncertainties are on the order of several 10's of ℃), but nevertheless reveal important and hitherto unrecognized fractionation relationships among the computed compounds. We document the expected so-called 'non-canonical' exponents of mass dependence associated with equilibrium isotope exchange that occur in close proximity to crossover temperatures that asymptotically approach values of $+\infty$ and $-\infty$, but illustrate that it is highly unlikely that these unusual exponents result in any significant deviations in the isotopic compositions of naturally occurring compounds as a result of either equilibrium isotope exchange or Rayleigh distillation occurring in close proximity to the crossover temperature.

We highlight two primary applications to natural systems in this study that are both poorly constrained by experiment and may represent new opportunities for future research: (*i*) low-temperature authigenic pyrite formation, and (*ii*) hydrolytic disproportionation reactions extended to a natural example of (hyper-)acid crater lakes associated with active volcanoes. We provide some explanation for why pyrite formation may be associated with relatively small isotope fractionation with respect to precursor aqueous sulfur compounds in the framework of established mechanisms (e.g., the polysulfide mechanism), but emphasize that the isotope fractionations in terms of fractionation factors associated with pyrite formation are yet to be experimentally constrained. Additionally, we highlight the potential utility of multiple sulfur isotope analysis (i.e., measurements of $\delta^{34}S$, $\Delta^{33}S$, and $\Delta^{36}S$) in monitoring volcanic gas output in active volcanoes using a model approach based primarily on the seminal work of Kusakabe et al. (2000). We illustrate that values of $\delta^{34}S$, $\Delta^{33}S$, and $\Delta^{36}S$ of dissolved HSO_4^- may all be sensitive to the amount of magmatic SO_2 supplied to (hyper-)acid crater lakes associated with active volcanoes (parameterized as

$r = H_2S/SO_2$), and identify such measurements as targets for future study.

6. Acknowledgements

This work was primarily supported by a Carnegie Postdoctoral Fellowship (Geophysical Laboratory; 2016-2018) awarded to D.L. Eldridge that is gratefully acknowledged. J. Farquhar acknowledges support for computational resources (computer and *Gaussian09* license) by the National Science Foundation (NSF grant 1361945). We thank Bjørn Mysen, Doug Rumble, and George Cody for valuable comments on earlier drafts of this manuscript. We additionally thank Weifu Guo for illuminating discussions throughout the undertaking of this study. We are thankful to the late Jack Tossell for early mentorship in aqueous cluster electronic structure calculations and credit his 2012 publication (Tossell, 2012) for partly spurring our interest in pursuing calculations of aqueous polysulfur compounds in further detail. We thank Ruth Blake (Yale) for editorial handling, and Drew Syverson (Yale) and two anonymous reviewers for comments and suggestions that greatly improved the presentation in this manuscript.

Figure Captions

Figure 1: Example two-dimensional ball-and-stick representations of the optimized aqueous polysulfide and polysulfur radical compounds: (A) disulfide, $S_2^{2-}\bullet 30H_2O$, (B) trisulfide, $S_3^{2-}\bullet 34H_2O$, (C) tetrasulfide, $S_4^{2-}\bullet 38H_2O$, (D) pentasulfide, $S_5^{2-}\bullet 42H_2O$, (E) hexasulfide, $S_6^{2-}\bullet 42H_2O$, (F) heptasulfide, $S_7^{2-}\bullet 50H_2O$, (G) octasulfide, $S_8^{2-}\bullet 50H_2O$, (H) hydrogen disulfide, $HS_2^-\bullet 34H_2O$, (I) hydrogen trisulfide, $HS_3^-\bullet 34H_2O$, (J) trisulfur radical, $S_3^{\cdot -}\bullet 50H_2O$, (K) disulfur radical, $S_2^{\cdot -}\bullet 50H_2O$, (L) elemental sulfur, $S_8\bullet 50H_2O$. The general color scheme for atoms follows red = oxygen, gray = hydrogen, and yellow-orange = sulfur, but different colors were chosen for the trisulfur radical (sulfur = blue) and disulfur radical (sulfur = yellow) to visually distinguish these compounds from the analogous polysulfides.

Figure 2: Example two-dimensional ball-and-stick representations of the optimized aqueous sulfide compounds: (A) hydrogen sulfide, $H_2S\bullet 45H_2O$, (B) bisulfide, $HS^-\bullet 45H_2O$, (C) ferrous sulfide monomer, $FeS^0\bullet 50H_2O$, (D) ferrous bisulfide, $FeSH^+\bullet 50H_2O$, (E) sodium bisulfide ion-pair, $(Na^+HS^-)^0\bullet 45H_2O$. The general color scheme for atoms follows: red = oxygen, gray = hydrogen, yellow-orange = sulfur, purple = iron, and orange = sodium.

Figure 3: Example two-dimensional ball-and-stick representations of the optimized aqueous sulfate compounds and polythionates: (A) sulfate, $SO_4^{2-}\bullet 44H_2O$, (B) bisulfate, $HSO_4^-\bullet 44H_2O$, (C) sodium sulfate ion-pair, $(Na^+\ SO_4^{2-})^-\bullet 43H_2O$, (D) magnesium sulfate ion-pair, $(Mg^{2+}SO_4^{2-})^0\bullet 43H_2O$, (E) trithionate, $S_3O_6^{2-}\bullet 52H_2O$, (F) tetrathionate, $S_4O_6^{2-}\bullet 42H_2O$. The general color scheme for atoms follows: red = oxygen, gray = hydrogen, yellow-orange = sulfur, orange = sodium, black = magnesium.

Figure 4: Computed ^{34}RPFRs and $^{34}\beta$ values for aqueous sulfide and polysulfide compounds at 25℃. Larger symbols indicate $^{34}\beta$ values (square = aqueous sulfide compounds, diamond = polysulfide compounds). Smaller circles with connecting lines indicate ^{34}RPFR values for singly-substituted polysulfides, and are plotted in a schematic fashion that imitates molecular structure. Calculations of ^{34}RPFRs and $^{34}\beta$ values for polysulfides modeled as similar structures in vacuum (in red) are shown for reference.

Figure 5: Computed $^{34}\beta$ values (and/or ^{34}RPFR) plotted as a function of $1/T^2$. All plots (A)-(E) contain computations of aqueous sulfide (H_2S, HS^-, S^{2-}; solid black curves) for reference. (A) aqueous polysulfide compounds (yellow-orange = S_x^{2-}, gray = HS_x^-) and elemental sulfur (orange = S_8), (B) aqueous polysulfur radical anions (blue), (C) ferrous sulfide compounds (purple), (D) the central reduced 'sulfanyl' sulfur ^{34}RPFR for trithionate (dark green) and the outer reduced 'sulfanyl' sulfur for thiosulfate for reference (light green, from Eldridge et al., 2016), (E) aqueous sulfate species (all; red) and the 'sulfonate' sulfur for trithionate (dark green), alongside calculations of the 'sulfonate' sulfur of thiosulfate (light green), sulfoxylate (SO_2^{2-}; gray), and sulfite (SO_3^{2-}; gray) from Eldridge et al. (2016) for reference.

Figure 6: Exponents quantifying 'mass-dependence' of β values (and/or RPFRs) for all compounds computed in this study as a function of $1/T^2$. Color scheme and labeling follows after Fig. 5 except where noted. (A) $^{33/34}\kappa$ values (or similar $\ln(^{33}\text{RPFR})/\ln(^{34}\text{RPFR})$ values), and (B) $^{36/34}\kappa$ values (or similar $\ln(^{36}\text{RPFR})/\ln(^{34}\text{RPFR})$ values).

Figure 7: Compilation of different estimates (theoretical, direct experimental, and indirect experimental) of the equilibrium fractionation factor between aqueous H_2S and HS^- as a function of $1/T^2$. The results of the current study are presented as the black curve where the shaded bounds reflect the error estimate (1 s.d.) based on the propagation of estimated errors on the aqueous sulfide calculations from numerous cluster sizes. See main text for descriptions of the different estimates from the literature (Section 4.1.1).

Figure 8: Estimated equilibrium fractionation factors among the ferrous sulfide compounds and HS^- or H_2S as a function of $1/T^2$. The shaded bounds represent the error estimates (1 s.d.) based on the propagation of estimated errors on the various aqueous sulfide calculations from numerous cluster sizes. The recent experimental estimate of the pyrite(FeS_2)/$H_2S_{(aq)}$ fractionation factor of Syverson et al. (2015) is shown for reference.

Figure 9: Estimated equilibrium fractionation factors among select aqueous polysulfide and sulfide compounds as a function of $1/T^2$. The shaded bounds represent the error estimate (1 s.d.) based on the propagation of estimated errors on polysulfide and sulfide calculations from numerous cluster sizes.

Figure 10: (A) Equilibrium distribution of aqueous sulfide and polysulfide compounds at 25°C based on the experimental data of Kamyshny et al. (2004, 2007) in a S^0-saturated system containing a total aqueous sulfur concentration of 100μM. The inset plot has the same labelling as the bounding plot and is focused on a smaller concentration range to illustrate the polysulfide distributions in greater detail. Other polysulfides (e.g., S_2^{2-} and HS_x^- where $x > 2$) are in too low of concentration to be seen on this plot. (B) Computed bulk equilibrium fractionation factor between total aqueous polysulfide and sulfide as a function of pH under the same conditions illustrated in panel (A). The bounding dashed curves in panel (B) represent the error estimate (1 s.d.) based on the propagation of estimated errors on polysulfide and sulfide calculations from numerous cluster sizes.

Figure 11: Estimated equilibrium fractionation factors among aqueous polysulfur radicals and sulfide compounds as a function of $1/T^2$. The shaded bounds represent the error estimate (1 s.d.) based on the propagation of estimated errors on polysulfur radical and sulfide calculations from numerous cluster sizes.

Figure 12: Comparison of our theoretical equilibrium fractionation factors among various aqueous sulfate species and aqueous H_2S (and $HSO_4^-/S_3^{\cdot-}$ for comparison) and experimental determinations (Ohmoto & Lasaga, 1982; Syverson et al., 2015) as a function of $1/T^2$. The residual plot shows the difference between the experimental studies and our theoretical HSO_4^-/H_2S fractionation factor (experiment - theory), which is likely the most comparable to the experimental studies. See text for further explanation.

Figure 13: Theoretical estimates of equilibrium fractionation factors involving the two sulfur moieties in polythionate ($S_3O_6^{2-}$ and $S_4O_6^{2-}$; green curves) alongside analogous fractionation factors for thiosulfate (thiosulfate experimental data are from Uyama et al. (1985) and Chu et al. (2004) and theoretical calculations are from Eldridge et al. (2016)). (A) The 'intramolecular' fractionation factor between the two different sulfur moieties in polythionate (green curves) compared to the analogous fractionation factor predicted for thiosulfate. (B) Fractionation factors between the sulfonate moieties in polythionate ($S_x(^*\mathbf{S}O_3)_2^{2-}$ where $x = 2$ or 3 corresponding to $S_3O_6^{2-}$ and $S_4O_6^{2-}$, respectively) and H_2S (green curves). The analogous fractionation factor for thiosulfate ($S(^*\mathbf{S}O_3)/H_2S$) is shown for reference. (C) Fractionation factors between the reduced moieties in polythionate ($^*\mathbf{S}_x(SO_3)_2^{2-}$ where $x = 2$ or 3 corresponding to $S_3O_6^{2-}$ and $S_4O_6^{2-}$, respectively) and H_2S (green curves). The analogous fractionation factor for thiosulfate ($^*\mathbf{S}(SO_3)/H_2S$) is shown for reference. The shaded bounds on the theory curves are the error estimate (1 s.d.) based on the propagated error estimates of the polythionate and H_2S calculations from numerous cluster sizes.

Figure 14: Comparison of theoretical (orange curves) and experimental (orange squares) fractionation factors between elemental sulfur (S^0 or S_8) and (A) sulfate (HSO_4^-) and (B) sulfide (H_2S). Experimental data are from the studies of Robinson (1973) and Kusakabe et al. (2000). Panel (A) also includes the theoretical HSO_4^-/H_2S fractionation factor (grey dashed curve) for reference. The shaded bounds on the theory curve in panel (B) represent the error estimate (1 s.d.) based on the propagated error estimates of the aqueous H_2S calculations from numerous cluster sizes.

Figure 15: Quantities relating to the 'mass dependence' of equilibrium isotope exchange ($^{33/34}\theta$ and Δ^{33}S values) among various aqueous sulfur compounds that exhibit crossovers: (A)-(C) $^{33/34}\theta$ exponent associated with the equilibrium fractionation between select aqueous polysulfide, polysulfur radical, and sulfide compounds. The vertical dashed lines indicate the temperature of the crossover (T_c) for each exchange reaction (note all computed S_x^{2-}/HS^- exhibit crossovers where T_c increases with 'x'). (D)-(F) The corresponding Δ^{33}S values for equilibrium fractionation among the compounds represented in panels (A)-(C).

Figure 16: Solutions to a simple closed-system disproportionation model (Eq. 26-28) using equilibrium fractionation factors constrained here (rather than kinetic isotope effects that are currently unconstrained) in terms of δ^{34}S *vs.* Δ^{33}S (A, C, E) or Δ^{36}S (B, D, F) for: (A)-(B) SO_2 to HSO_4^- and H_2S (Eq. 22); (C)-(D) elemental sulfur to SO_4^{2-} and H_2S (Eq. 21); (E)-(F) $S_3^{\cdot-}$ to SO_4^{2-} and H_2S (Eq. 24).

Figure 17: Δ^{33}S and Δ^{36}S *vs.* δ^{34}S values for elemental sulfur and sulfate generated from the quantitative disproportionation of sulfur dioxide as a function of temperature and r (the molar H_2S/SO_2 ratio of the magmatic source) from the mass balance model described in the text (Eq. 29 - 30) that is based on Kusakabe et al. (2000) and constrained by the theoretical calculations of the current study. For illustrative purposes we also plot model-generated composition predictions (based on the same mass balance model) of sulfate and elemental sulfur in select (hyper-)acid crater lakes associated with active volcanoes based on the δ^{34}S data and assumptions of Kusakabe et al. (2000) (see text for further explanation). Note that the Δ^{33}S and Δ^{36}S compositions of sulfur phases from these crater lake localities have not been determined to the best of our knowledge.

Appendix A.

Appendix A.1. Geometries

Mean geometric parameters for aqueous sulfur compounds modeled herein can be found in Table 2. The direct coordination of polysulfide anions with water molecules in supermolecular clusters ($\geq$ 30 H_2O) affects the resulting polysulfide geometries relative to vacuum, but exhibit similar patterns to computations in vacuum. The mean sulfur-sulfur bond lengths (R(S-S)) for the explicitly solvated polysulfides ($S_x^{2-}\bullet nH_2O$) range from 2.167±0.008 Å ($x = 2$)

to 2.099±0.015 Å ($x = 8$) and are generally lower than those obtained from S_x^{2-} having similar structures modeled in vacuum. For both the explicitly solvated (S_x^{2-}•nH_2O) and vacuum computations of S_x^{2-} ($x = 2 - 8$), the mean R(S-S) appears to generally decrease with increasing chain-length 'x' (Table 2). The R(S-S) of HS_2^-•nH_2O is 2.124 ± 0.003 Å and is shorter than the R(S-S) of its unprotonated counterpart S_2^{2-}•nH_2O. The R(S-S) for HS_3^-•nH_2O differs for the protonated (2.120 ± 0.003 Å) and unprotonated (2.085 ± 0.003Å) outer sulfur atoms. The mean ∠(S-S-S) bond angle for all S_x^{2-}•nH_2O of 110.0 ± 0.9° is comparable between the different polysulfides (S_x^{2-}•nH_2O, $x = 3 - 8$; i.e., does not appear to vary systematically with 'x') and is generally lower than the value for the vacuum calculations (mean vacuum: 114.7 ± 1.2°). The mean ∠(S-S-S) for HS_3^-•nH_2O (109.8 ± 0.4°) is comparable to its unprotonated counterpart S_3^{2-}•nH_2O (111.1 ± 1.0°) (Table 2). The mean dihedral angle ∠(S-S-S-S) of 87 ± 7° is comparable among the pertinent S_x^{2-}•nH_2O ($x = 4 - 8$) and is also comparable to the value of 89± 4° from the calculations in vacuum (i.e., close to ≈90°).

The polysulfur radicals ($S_x^{\bullet-}$, $x = 2, 3$) modeled in water clusters exhibit different geometries than the analogous polysulfides in water clusters (S_x^{2-}, $x = 2, 3$). The mean sulfur-sulfur bond lengths R(S-S) for the explicitly solvated polysulfur radicals $S_2^{\bullet-}$•nH_2O (2.032±0.001 Å) and $S_3^{\bullet-}$•nH_2O (2.031±0.011 Å) are computed to be significantly shorter than the polysulfides (S_x^{2-}•nH_2O). The ∠(S-S-S) for the trisulfur radical $S_3^{\bullet-}$•nH_2O (114.3 ± 1.1°) is computed to be larger than the value for S_3^{2-}•nH_2O and the other S_x^{2-}•nH_2O. The geometric parameters for the trisulfur radical $S_3^{\bullet-}$ are comparable to previous theoretical studies that obtain S-S bond lengths of 1.99-2.04 Å and ∠(S-S-S) = 113.4°-116.1° (Koch et al., 1995; Chen et al., 2001; Tossell, 2012) based on numerous theoretical methods with and without different solvation models applied.

The geometric parameters for the modeled aqueous sulfide species appear to compare well to the available experimental data. The R(H-S) for the aqueous sulfide species H_2S•nH_2O (1.347±0.002 Å) and HS^-•nH_2O (1.349 ± 0.002 Å) are similar to one another and to the experimental value for $H_2S_{(g)}$ of 1.352 Å

(Cook et al., 1975). The R(H-S) for the $FeSH^+$ species of 1.349 Å is indistinguishable from $HS^-\bullet nH_2O$, and the R(H-S) for the $(Na^+HS^-)^0\bullet nH_2O$ ion-pair is also very similar (1.345±0.003 Å). The computed ∠(H-S-H) for $H_2S\bullet nH_2O$ is 92.9 ± 0.5° and is similar to the experimental value for $H_2S_{(g)}$ of 92.13° (Cook et al., 1975). The R(Fe-S) for $FeSH^+\bullet nH_2O$ (2.27±0.02 Å) is significantly larger than the value for $FeS_{(aq)}\bullet nH_2O$ (2.140±0.004 Å). The values for R(Fe-S) are consistent with a covalent bond between the iron and sulfur atoms and are similar to (or shorter than) the R(Fe-S) for ferrous sulfide/polysulfide minerals mackinawite (2.256 Å; Rickard & Luther, 2007) and pyrite (2.266 Å; Wu et al., 2004). The ∠(H-S-Fe) bond angle for $FeSH^+\bullet nH_2O$ is computed to be 103.7±0.9°. The ∠(H-S-Na) for $(Na^+HS^-)^0\bullet nH_2O$ is more variable and ranges between 75-105°C (mean = 95±11°) and the R(S-Na) is computed to be 2.76 ± 0.02 Å.

The geometric parameters for the modeled aqueous sulfate species are similar to each other and to the available experimental data. The R(S-O) for all sulfate species is similar and ranges between 1.49±0.01 Å ($HSO_4^-\bullet nH_2O$) to 1.52±0.01 Å ($SO_4^{2-}\bullet nH_2O$ and $(Na^+SO_4^{2-})^-\bullet nH_2O$). These values compare well to experimental constraints for SO_4^{2-} (1.495±0.006Å; Vchirawongkwin et al., 2007). The calculations predict that protonation of an oxygen atom in $HSO_4^-\bullet nH_2O$ causes an extension of the S-OH bond (i.e., R(S-OH) = 1.596 ± 0.002 Å) relative to the other S-O bonds associated with unprotonated oxygen atoms that is analogous to our previous computations of the HO-bonded isomer of aqueous bisulfite, $(HO)SO_2^-$, from Eldridge et al. (2016). Direct ion-pairing with Mg^{2+} also appears to cause a slight extension of the S-O bond associated with the oxygen atom that is directly coordinated with the Mg^{2+} cation (R(S-O(Mg)) = 1.547±0.001 Å), but ion-pairing with Na^+ does not appear to have this effect (R(S-O(Na)) = 1.496 Å). The ∠(O-S-O) bond angles for all aqueous sulfate species corresponds to 109.5° and is indistinguishable from expectations of tetrahedral molecules where the central atom is four-fold bonded with atoms of the same element (i.e., $\cos^{-1}(-1/3) \approx 109.47°$).

The geometric parameters for the computed aqueous polythionates do not

appear to have experimental counterparts in the literature but compare well to those of trithionate salts such as $K_2S_3O_6$ (Zachariasen, 1934). The computed R(S-S) for trithionate ($S_3O_6^{2-}\bullet nH_2O$) of 2.17±0.02 Å is similar to the value for $K_2S_3O_6$ of 2.15Å (Zachariasen (1934)). Additionally, the R(S-O) for $S_3O_6^{2-}\bullet nH_2O$ of 1.49±0.01 Å is similar to the value for $K_2S_3O_6$ of 1.50 Å (Zachariasen, 1934). The ∠(S-S-S) for $S_3O_6^{2-}\bullet nH_2O$ of 104.2 ± 1.3° is also comparable to the value of 103.1° for $K_2S_3O_6$ (Zachariasen, 1934). Geometric parameters for tetrathionate ($S_4O_6^{2-}\bullet nH_2O$) are similar to analogous parameters in trithionate, except the central S-S bond in tetrathionate is computed to be significantly shorter (2.036 ± 0.003 Å) than S-S bonds corresponding to sulfonate groups ('S-S(O_3)' = 2.20±0.02 Å; Table 2). The sulfur dihedral in tetrathionate is computed to be 104.0 ± 2.9°.

The S_8 ring that we compute in a water cluster has a mean R(S-S) = 2.10 ± 0.01 Å, which is slightly longer than S-S bond lengths in S_8 rings comprising crystalline forms of elemental sulfur (2.06 Å) (Meyer, 1976). Our aqueous S_8 ring exhibits a mean ∠(S-S-S) = 108.7 ± 1.1° and a mean dihedral angle of 97.8 ± 3.3° (Table 2), which compare well to S_8 rings in crystalline forms of sulfur (108.0±0.7° and 98.3°, respectively)(Meyer, 1976).

Appendix A.2. General Hydrolytic Disproportionation Model in a Closed System

The overall, generalized reaction network describing the hydrolytic disproportionation of some sulfur-bearing compound, A, into two sulfur-bearing products, B and C, can be given in a simple form by:

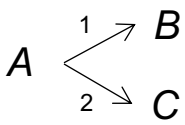

(A.1)

The exact sulfur isotope mass balance corresponding to Eq. A.1 is given by:

$$[A]_0 \times {}^i\chi_{A,0} = [A]_t \times {}^i\chi_{A,t} + [B]_t \times {}^i\chi_{B,t} + [C]_t \times {}^i\chi_{C,t} \tag{A.2}$$

Where ${}^i\chi = {}^i\mathrm{S}/({}^{32}\mathrm{S} + {}^{33}\mathrm{S} + {}^{34}\mathrm{S} + {}^{36}\mathrm{S})$ (i = 33, 34, or 36) and is the mole or atom fraction of a given minor sulfur isotope. The subscripts 0 and t indicate quantities at the initial time point ($t = 0$) and at some arbitrary time point of reaction t, respectively. In strict terms, the relationship between ${}^i\chi$ and ${}^iR$ (${}^iR = {}^i\mathrm{S}/{}^{32}\mathrm{S}$) is:

$${}^i\chi = \frac{{}^iR}{1 + {}^{33}R + {}^{34}R + {}^{36}R} \tag{A.3}$$

For simplicity, we make the approximation that ${}^i\chi \approx {}^iR$ transforming the exact mass balance of Eq. A.2 into an approximate form:

$$[A]_0 \times {}^iR_{A,0} = [A]_t \times {}^iR_{A,t} + [B]_t \times {}^iR_{B,t} + [C]_t \times {}^iR_{C,t} \tag{A.4}$$

We define two terms: the fraction of reactant remaining, f, and a product branching ratio, b:

$$f = \frac{[A]_t}{[A]_0} \tag{A.5}$$

$$b = \frac{[B]_t}{[B]_t + [C]_t} = \frac{k_1}{k_1 + k_2} \tag{A.6}$$

The branching ratio, b, can be related to the reaction stoichiometry of a given sulfur disproportionation reaction. In the simple framework of this model, k_1 and k_2 are first order rate constants associated with the reaction of $A \xrightarrow{1} B$ and $A \xrightarrow{2} C$, respectively. Substituting Eq. A.5 and A.6 into Eq. A.4 yields:

$${}^iR_{A,0} = f \times {}^iR_{A,t} + (1 - f) \times (b \times {}^iR_{B,t} + (1 - b) \times {}^iR_{C,t}) \tag{A.7}$$

Eq. A.7 is the generalized mass balance relationship that will be the basis for modeling disproportionation reactions herein.

Next, we derive the equation describing the evolution of the isotopic composition of the reactant using a simple kinetic approach. From Eq. A.1, we have:

$$-\frac{d[^{32}A]}{dt} = [^{32}A] \times (^{32}k_1 + {}^{32}k_2) \tag{A.8}$$

$$-\frac{d[^{i}A]}{dt} = [^{i}A] \times (^{i}k_1 + {}^{i}k_2) \tag{A.9}$$

Where $[^{32}A]$ is the ^{32}S-bearing isotopologue of compound A and the $[^{i}A]$ is the ^{i}S-bearing isotopologue of compound A (again where i = 33, 34, or 36). Accordingly, the rate constants (k) are also now written in terms of these specific isotopic molecules. Taking the ratio of Eq. A.9 to Eq. A.8 followed by rearrangement yields:

$$\left(\frac{1}{[^{i}A]}\right) d[^{i}A] = \left(\frac{^{i}k_1 + {}^{i}k_2}{^{32}k_1 + {}^{32}k_2}\right) \times \left(\frac{1}{[^{32}A]}\right) d[^{32}A] \tag{A.10}$$

Integrating both sides (bounds: 0, t) yields:

$$ln\left(\frac{[^{i}A]_t}{[^{i}A]_0}\right) = \left(\frac{^{i}k_1 + {}^{i}k_2}{^{32}k_1 + {}^{32}k_2}\right) \times ln\left(\frac{[^{32}A]_t}{[^{32}A]_0}\right) \tag{A.11}$$

For simplicity, we will use α to symbolize a kinetic isotope effect (i.e., $^{i}\alpha_{rxn} = {}^{i}k_{rxn}/{}^{32}k_{rxn}$) but we note that a ratio of forward rate constants should not be confused with other uses of α in this study. For this problem, we also apply an approximate form of the product branching ratio ($b \approx \frac{^{32}k_1}{^{32}k_1 + {}^{32}k_2}$). Taking this definition of a kinetic isotope effect and the approximate b into account, it is easily shown that:

$$\frac{^{i}k_1 + {}^{i}k_2}{^{32}k_1 + {}^{32}k_2} = b \times {}^{i}\alpha_1 + (1-b) \times {}^{i}\alpha_2 \tag{A.12}$$

Making this substitution and subtracting $ln\left(\frac{[^{32}A]_t}{[^{32}A]_0}\right)$ from each side of Eq. A.11 followed by rearrangment yields:

$$\left(\frac{[^{i}A]}{[^{32}A]}\right)_t = \left(\frac{[^{i}A]}{[^{32}A]}\right)_0 \times \left(\frac{[^{32}A]_t}{[^{32}A]_0}\right)^{(b\times {}^{i}\alpha_1+(1-b)\times {}^{i}\alpha_2-1)} \tag{A.13}$$

Where again the ${}^{i}\alpha$ terms in this case are fractionation factors corresponding to kinetic isotope effects (i.e., ${}^{i}\alpha_1 \equiv {}^{i}k_1/{}^{32}k_1$, ${}^{i}\alpha_2 \equiv {}^{i}k_2/{}^{32}k_2$).

In Eq. A.13, it is clear that the term $\frac{[^{32}A]_t}{[^{32}A]_0}$ is equivalent to $\frac{[^{32}S]_{A,t}}{[^{32}S]_{A,0}}$ regardless of what compound A may represent. However, it is notable that the terms $\left(\frac{[^{i}A]}{[^{32}A]}\right)_0$ and $\left(\frac{[^{i}A]}{[^{32}A]}\right)_t$ represent the ratio of isotopic molecules of A at time 0 and t, respectively, rather than sulfur isotope ratios corresponding to A. To relate these ratios of isotopic molecules to sulfur isotope ratios, we will assume a random distribution of isotopes among the singly substituted molecules of A (i.e., ${}^{i}A$) and will further assume that sulfur isotope substitution in A does not affect its symmetry. Under these assumptions, $\frac{[^{i}A]}{[^{32}A]} \approx \left(\frac{[^{i}S]}{[^{32}S]}\right)_A = {}^{i}R_A$. Eq. A.13 can thus be re-written as:

$${}^{i}R_{A,t} = {}^{i}R_{A,0} \times \left(\frac{[^{32}S]_{A,t}}{[^{32}S]_{A,0}}\right)^{(b\times {}^{i}\alpha_1+(1-b)\times {}^{i}\alpha_2-1)} \tag{A.14}$$

For our purposes, we make the additional approximation:

$$\frac{[^{32}S]_{A,t}}{[^{32}S]_{A,0}} = f \times \left(\frac{1+{}^{33}R_{A,0}+{}^{34}R_{A,0}+{}^{36}R_{A,0}}{1+{}^{33}R_{A,t}+{}^{34}R_{A,t}+{}^{36}R_{A,t}}\right) \approx f \tag{A.15}$$

Applying this approximation yields a familiar form of the Rayleigh equation:

$${}^{i}R_{A,t} = {}^{i}R_{A,0} \times f^{(b\times {}^{i}\alpha_1+(1-b)\times {}^{i}\alpha_2-1)} \tag{A.16}$$

Thus, the evolution of the sulfur isotope composition of a sulfur intermediate undergoing hydrolytic disproprotionation in a closed system under the simple framework of Eq. A.1 follows Rayleigh distillation dictated by a composite

fractionation factor $(b \times {}^{i}\alpha_1 + (1-b) \times {}^{i}\alpha_2)$ that is a function of the branching ratio to the products (in this case, related to overall reaction stoichiometry) and the two kinetic isotope effects corresponding to the formation of the two disproportionation products.

The substitution of Eq. A.16 into Eq. A.7 while also recognizing that ${}^{i}R_{B,t}/{}^{i}R_{C,t} = {}^{i}\alpha_1/{}^{i}\alpha_2$ yields the following relationships that describe the evolution of the disproportionation products, B and C, as a function of f, ${}^{i}R_{A,0}$, and other reaction-specific quantities (i.e., b, ${}^{i}\alpha_1$, and ${}^{i}\alpha_2$):

$$ {}^{i}R_{B,t} = \frac{{}^{i}\alpha_1 \times {}^{i}R_{A,0} \times \left(1 - f \times f^{(b\times{}^{i}\alpha_1 + (1-b)\times{}^{i}\alpha_2 - 1)}\right)}{(1-f) \times (b \times {}^{i}\alpha_1 + (1-b) \times {}^{i}\alpha_2)} \tag{A.17} $$

$$ {}^{i}R_{C,t} = \frac{{}^{i}\alpha_2 \times {}^{i}R_{A,0} \times \left(1 - f \times f^{(b\times{}^{i}\alpha_1 + (1-b)\times{}^{i}\alpha_2 - 1)}\right)}{(1-f) \times (b \times {}^{i}\alpha_1 + (1-b) \times {}^{i}\alpha_2)} \tag{A.18} $$

Appendix A.3. Derivation of the (hyper-)acid crater Lake Mass Balance Model (SO_2-disproportionation)

Equations 29 and 30 in the main text (solutions in Fig. 17) are based on a mass balance model presented by Kusakabe et al. (2000) (developed from Taran et al., 1996) that predicts the compositions of sulfate (HSO_4^-) and elemental sulfur produced by the hydrolytic disproportionation of SO_2 corresponding to an initial (or magmatic) $r = H_2S/SO_2$ molar ratio and total magmatic/volatile sulfur isotope composition (${}^{34}R_T$ or $\delta^{34}S_T$) as a function of the temperature at which disproportionation of SO_2 occurs in the subsurface hydrothermal-magmatic system. We illustrate the derivation of these equations here in full and in terms of isotope ratios (${}^{i}R$) and fractionation factors (${}^{i}\alpha$).

We begin with the assumption that the total source of sulfur in the (hyper-)acid crater lake system is given by magmatic H_2S and SO_2 having a bulk sulfur isotope composition (given as isotope ratio) of ${}^{i}R_T$ (i = 33, 34, or 36):

$$ S_{TOTAL} = [H_2S] + [SO_2] \tag{A.19} $$

$$^{i}R_T = f_{H_2S} \times^{i} R_{H_2S} + f_{SO_2} \times^{i} R_{SO_2} \tag{A.20}$$

Equation A.19 could instead be written in terms of partial pressures or fugacities but we forego such description here. The mass balance of Eq. A.20 contains the same approximation as Eq. A.4 (i.e., $^{i}\chi \approx {}^{i}R$). The f-terms in Eq. A.20 represent mole fractions of each phase and are given by:

$$f_{H_2S} = \frac{[H_2S]}{[S_T]} = \frac{r}{r+1} \tag{A.21}$$

$$f_{SO_2} = \frac{[SO_2]}{[S_T]} = \frac{1}{r+1} \tag{A.22}$$

Where $r = [\mathrm{H_2S}]/[\mathrm{SO_2}]$ and represents the molar ratio of hydrogen sulfide to sulfur dioxide. We next assume that SO_2 undergoes quantitative disproportionation to form S^0 and HSO_4^- following the stoichiometry of Eq. 23 in the main text, which corresponds to the mass balance given by ($^{i}\chi \approx {}^{i}R$ applied once again):

$$^{i}R_{SO_2} = \frac{1}{3} \times {}^{i}R_{S^0} + \frac{2}{3} \times {}^{i}R_{HSO_4^-} \tag{A.23}$$

Substituting Eq. A.21-A.22 and A.23 into Eq. A.20 yields:

$$^{i}R_T = \frac{r}{r+1} \times {}^{i}R_{H_2S} + \frac{1}{r+1} \times \left(\frac{1}{3} \times {}^{i}R_{S^0} + \frac{2}{3} \times {}^{i}R_{HSO_4^-}\right) \tag{A.24}$$

Finally, if we assume that H_2S, HSO_4^-, and S^0 isotopically equilibrate at the temperature of SO_2 disproportionation we can substitute equilibrium fractionation factors for isotope ratios (*via*, for example, $^{i}\alpha_{H_2S/HSO_4^-} = {}^{i}R_{H_2S}/{}^{i}R_{HSO_4^-}$ & $^{i}\alpha_{S^0/HSO_4^-} = {}^{i}R_{S^0}/{}^{i}R_{HSO_4^-}$, etc.) to obtain the final expressions:

$$^{i}R_{HSO_4^-} = \frac{^{i}R_T \times (r+1)}{r \times {}^{i}\alpha_{H_2S/HSO_4^-} + \frac{1}{3} \times {}^{i}\alpha_{S^0/HSO_4^-} + \frac{2}{3}} \tag{A.25}$$

$$^{i}R_{S^0} = \frac{^{i}R_T \times (r+1)}{r \times {}^{i}\alpha_{H_2S/S^0} + \frac{2}{3} \times {}^{i}\alpha_{HSO_4^-/S^0} + \frac{1}{3}} \tag{A.26}$$

$$^{i}R_{H_2S} = \frac{^{i}R_T \times (r+1)}{r + \frac{1}{3} \times {}^{i}\alpha_{S^0/H_2S} + \frac{2}{3} \times {}^{i}\alpha_{HSO_4^-/H_2S}} \quad \text{(A.27)}$$

The solutions to Eq. A.25 and A.26 over the specified r and T values are what is represented in Fig. 17 in the main text.

We note that Kusakabe et al. (2000) derived their version of this model in terms of δ^{34}S values (rather than isotope ratios) and the equivalent of $^{34}\epsilon$ values (rather than values of $^{34}\alpha$, where $^{34}\epsilon \equiv {}^{34}\alpha$ - 1 in units of ‰). If the same approach is followed above but mass balance and fractionation factors are cast in these terms instead to derive the equivalent of Eq. A.25 the following is obtained:

$$\delta^{i}S_{HSO_4^-} = \frac{\delta^{i}S_T + \left(\frac{r}{r+1}\right) \times {}^{i}\epsilon_{HSO_4^-/H_2S} + \frac{1}{3} \times \left(\frac{1}{r+1}\right) \times {}^{i}\epsilon_{HSO_4^-/S^0}}{{}^{i}\alpha_{H_2S/HSO_4^-} \times \left(\frac{r}{r+1}\right) \times \left(\frac{1}{3} \times {}^{i}\alpha_{S^0/HSO_4^-} + \frac{2}{3}\right) \times \left(\frac{1}{r+1}\right)} \quad \text{(A.28)}$$

The numerator of Eq. A.28 is identical to Kusakabe et al. (2000)'s Eq. 11 (i = 34), indicating that Kusakabe et al. (2000) (and by extension Taran et al., 1996; Marini et al., 2011, in analogous models) omit the denominator terms in Eq. A.28 in their expressions. This approximation taken by these previous studies (Taran et al., 1996; Kusakabe et al., 2000; Marini et al., 2011) appears to impart minimal errors into computations of δ^{i}S values but does lead to spurious errors in the computation of Δ^{33}S and Δ^{36}S values and, thus, is avoided here.

References

Amrani, A., Kamyshny, A., Lev, O., & Aizenshtat, Z. (2006). Sulfur Stable Isotope Distribution of Polysulfide Anions in an $(NH_4)_2S_n$ Aqueous Solution. *Inorganic Chemistry*, *45*, 1427–1429. doi:10.1021/ic051748r.

Barré, G., Truche, L., Bazarkina, E. F., Michels, R., & Dubessy, J. (2017). First evidence of the trisulfur radical ion $S_3^{\cdot-}$ and other sulfur polymers in natural fluid inclusions. *Chemical Geology*, *462*, 1–14. doi:10.1016/j.chemgeo.2017.03.027.

Becke, A. D. (1993). Density-functional thermochemistry. III. The role of exact exchange. *The Journal of Chemical Physics*, *98*, 5648–5652. doi:10.1063/1.464913.

Bigeleisen, J., & Mayer, M. G. (1947). Calculation of Equilibrium Constants for Isotopic Exchange Reactions. *The Journal of Chemical Physics*, *15*, 261–267. doi:10.1063/1.1746492. arXiv:arXiv:1011.1669v3.

Boulegue, J. (1978). Solubility of Elemental Sulfur in Water at 298 K. *Phosphorus and Sulfur and the Related Elements*, *5*, 127–128. doi:10.1080/03086647808069875.

Butler, I. B., Böttcher, M. E., Rickard, D., & Oldroyd, A. (2004). Sulfur isotope partitioning during experimental formation of pyrite via the polysulfide and hydrogen sulfide pathways: implications for the interpretation of sedimentary and hydrothermal pyrite isotope records. *Earth and Planetary Science Letters*, *228*, 495–509. doi:10.1016/j.epsl.2004.10.005.

Canfield, D. E. (2004). The evolution of the Earth surface sulfur reservoir. *American Journal of Science*, *304*, 839–861. doi:10.2475/ajs.304.10.839.

Cao, X., & Liu, Y. (2011). Equilibrium mass-dependent fractionation relationships for triple oxygen isotopes. *Geochimica et Cosmochimica Acta*, *75*, 7435–7445. doi:10.1016/j.gca.2011.09.048.

Chacko, T., Cole, D. R., & Horita, J. (2001). Equilibrium Oxygen, Hydrogen and Carbon Isotope Fractionation Factors Applicable to Geologic Systems. *Reviews in Mineralogy and Geochemistry*, *43*, 1–81. doi:10.2138/gsrmg.43.1.1.

Chadwell, S. J., Rickard, D., & Luther, G. W. (1999). Electrochemical Evidence for Pentasulfide Complexes with Mn^{2+}, Fe^{2+}, Co^{2+}, Ni^{2+}, Cu^{2+} and Zn^{2+}. *Aquatic Geochemistry*, *5*, 29–57. doi:10.1023/A:1009611719625.

Chen, M., Liu, M., Zheng, L., Zhang, Q., & Au, C. (2001). A density functional study for the isomers of anionic sulfur clusters S_n^- (n=3–20). *Chemical Physics Letters*, *350*, 119–127. doi:10.1016/S0009-2614(01)01289-1.

Chivers, T., & Elder, P. J. W. (2013). Ubiquitous trisulfur radical anion: fundamentals and applications in materials science, electrochemistry, analytical chemistry and geochemistry. *Chemical Society Reviews*, *42*, 5996–6005. doi:10.1039/c3cs60119f.

Christenson, B., & Tassi, F. (2015). Gases in Volcanic Lake Environments. In D. Rouwet, B. Christenson, F. Tassi, & J. Vandemeulebrouck (Eds.), *Volcanic Lakes* (pp. 125–153). Berlin, Heidelberg: Springer Berlin Heidelberg. doi:10.1007/978-3-642-36833-2_5.

Chu, X., Ohmoto, H., & Cole, D. R. (2004). Kinetics of sulfur isotope exchange between aqueous sulfide and thiosulfate involving intra- and intermolecular reactions at hydrothermal conditions. *Chemical Geology*, *211*, 217–235. doi:10.1016/j.chemgeo.2004.06.013.

Cook, R. L., De Lucia, F. C., & Helminger, P. (1975). Molecular force field and structure of hydrogen sulfide: recent microwave results. *Journal of Molecular Structure*, *28*, 237–246. doi:10.1016/0022-2860(75)80094-9.

Deines, P. (2003). A note on intra-elemental isotope effects and the interpretation of non-mass-dependent isotope variations. *Chemical Geology*, *199*, 179–182. doi:10.1016/S0009-2541(03)00076-7.

Delmelle, P., & Bernard, A. (2015). The Remarkable Chemistry of Sulfur in Hyper-Acid Crater Lakes: A Scientific Tribute to Bokuichiro Takano and Minoru Kusakabe. In D. Rouwet, B. Christenson, F. Tassi, & J. Vandemeulebrouck (Eds.), *Volcanic Lakes* (pp. 239–259). Berlin, Heidelberg: Springer Berlin Heidelberg. doi:10.1007/978-3-642-36833-2_10.

Delmelle, P., Bernard, A., Kusakabe, M., Fischer, T. P., & Takano, B. (2000). Geochemistry of the magmatic-hydrothermal system of Kawah Ijen volcano,

East Java, Indonesia. *Journal of Volcanology and Geothermal Research*, *97*, 31–53. doi:10.1016/S0377-0273(99)00158-4.

Eldridge, D., Guo, W., & Farquhar, J. (2016). Theoretical estimates of equilibrium sulfur isotope effects in aqueous sulfur systems: Highlighting the role of isomers in the sulfite and sulfoxylate systems. *Geochimica et Cosmochimica Acta*, *195*, 171–200. doi:10.1016/j.gca.2016.09.021.

Eldridge, D. L., Mysen, B. O., & Cody, G. D. (2018). Experimental estimation of the bisulfite isomer quotient as a function of temperature: Implications for sulfur isotope fractionations in aqueous sulfite solutions. *Geochimica et Cosmochimica Acta*, *220*, 309–328. doi:10.1016/j.gca.2017.10.005.

Farquhar, J., Johnston, D. T., & Wing, B. A. (2007). Implications of conservation of mass effects on mass-dependent isotope fractionations: Influence of network structure on sulfur isotope phase space of dissimilatory sulfate reduction. *Geochimica et Cosmochimica Acta*, *71*, 5862–5875. doi:10.1016/j.gca.2007.08.028.

Farquhar, J., Johnston, D. T., Wing, B. A., Habicht, K. S., Canfield, D. E., Airieau, S., & Thiemens, M. H. (2003). Multiple sulphur isotopic interpretations of biosynthetic pathways: implications for biological signatures in the sulphur isotope record. *Geobiology*, *1*, 27–36. doi:10.1046/j.1472-4669.2003.00007.x.

Findlay, A. J., & Kamyshny, A. (2017). Turnover rates of intermediate sulfur species (S_x^{2-}, S^0, $S_2O_3^{2-}$, $S_4O_6^{2-}$-, SO_3^{2-}) in anoxic freshwater and sediments. *Frontiers in Microbiology*, *8*, 1–15. doi:10.3389/fmicb.2017.02551.

Foresman, J. B., & Frisch, Æ. (1996). *Exploring chemistry with electronic structure methods: a guide to using Gaussian*. (2nd ed.). Wallingford, CT: Gaussian, Inc.

Fossing, H., & Jørgensen, B. B. (1990). Isotope exchange reactions with radi-

olabeled sulfur compounds in anoxic seawater. *Biogeochemistry*, *9*, 223–245. doi:10.1007/BF00000600.

Frisch, M. J., Trucks, G., Schlegel, H. B., Scuseria, G. E., Robb, M. A., Cheeseman, J. R., Scalmani, G., Barone, V., Mennucci, B., Petersson, G. A., Nakatsuji, H., Caricato, M., Li, X., Hratchian, H. P., Izmaylov, A. F., Bloino, J., Zheng, G., Sonnenberg, J. L., Frisch, M. J., Trucks, G. W., Schlegel, H. B., Scuseria, G. E., Robb, M. A., Cheeseman, J. R., Scalmani, G., Barone, V., Mennucci, B., Petersson, G. A., Nakatsuji, H., Caricato, M., Li, X., Hratchian, H. P., Izmaylov, A. F., Bloino, J., Zheng, G., Sonnenberg, J. L., Hada, M., Ehara, M., Toyota, K., Fukuda, R., Hasegawa, J., Ishida, M., Nakajima, T., Honda, Y., Kitao, O., Nakai, H., Vreven, T., Montgomery, J. A., J., Peralta, J. E., Ogliaro, F., Bearpark, M., Heyd, J. J., Brothers, E., Kudin, K. N., Staroverov, V. N., Kobayashi, R., Normand, J., Raghavachari, K., Rendell, A., Burant, J. C., Iyengar, S. S., Tomasi, J., Cossi, M., Rega, N., Millam, J. M., Klene, M., Knox, J. E., Cross, J. B., Bakken, V., Adamo, C., Jaramillo, J., Gomperts, R., Stratmann, R. E., Yazyev, O., Austin, A. J., Cammi, R., Pomelli, C., Ochterski, J. W., Martin, R. L., Morokuma, K., Zakrzewski, V. G., Voth, G. A., Salvador, P., Dannenberg, J. J., Dapprich, S., Daniels, A. D., Farkas, Ö., Foresman, J. B., Ortiz, J. V., Cioslowski, J., & Fox, D. J. (2013). *Gaussian 09, Revision E.01*. Gaussian, Inc.: Wallingford, CT.

Fry, B., Gest, H., & Hayes, J. (1986). Sulfur isotope effects associated with protonation of HS^- and volatilization of H_2S. *Chemical Geology: Isotope Geoscience section*, *58*, 253–258. doi:10.1016/0168-9622(86)90014-X.

Geßler, R., & Gehlen, K. v. (1986). Investigation of sulfur isotope fractionation between H_2S gas and aqueous solutions. *Fresenius' Zeitschrift für Analytische Chemie*, *324*, 130–136. doi:10.1007/BF00473353.

Giggenbach, W. (1971). Blue solutions of sulfur in water at elevated temperatures. *Inorganic Chemistry*, *10*, 1306–1308. doi:10.1021/ic50100a043.

Giggenbach, W. (1987). Redox processes governing the chemistry of fumarolic

gas discharges from White Island, New Zealand. *Applied Geochemistry*, *2*, 143–161. doi:10.1016/0883-2927(87)90030-8.

Gun, J., Modestov, A. D., Kamyshny, A., Ryzkov, D., Gitis, V., Goifman, A., Lev, O., Hultsch, V., Grischek, T., & Worch, E. (2004). Electrospray Ionization Mass Spectrometric Analysis of Aqueous Polysulfide Solutions. *Microchimica Acta*, *146*, 229–237. doi:10.1007/s00604-004-0179-5.

Haider, S., Di Tommaso, D., & de Leeuw, N. H. (2013). Density functional theory simulations of the structure, stability and dynamics of iron sulphide clusters in water. *Physical Chemistry Chemical Physics*, *15*, 4310–4319. doi:10.1039/c3cp43560a.

Harmandas, N. G., Navarro Fernandez, E., & Koutsoukos, P. G. (1998). Crystal Growth of Pyrite in Aqueous Solutions. Inhibition by Organophosphorus Compounds. *Langmuir*, *14*, 1250–1255. doi:10.1021/la970354c.

Hershey, J. P., Plese, T., & Millero, F. J. (1988). The pK_1^* for the dissociation of H_2S in various ionic media. *Geochimica et Cosmochimica Acta*, *52*, 2047–2051.

Hill, P. S., Tripati, A. K., & Schauble, E. A. (2014). Theoretical constraints on the effects of pH, salinity, and temperature on clumped isotope signatures of dissolved inorganic carbon species and precipitating carbonate minerals. *Geochimica et Cosmochimica Acta*, *125*, 610–652. doi:10.1016/j.gca.2013.06.018.

Jacquemet, N., Guillaume, D., Zwick, A., & Pokrovski, G. S. (2014). In situ Raman spectroscopy identification of the S_3^- ion in S-rich hydrothermal fluids from synthetic fluid inclusions. *American Mineralogist*, *99*, 1109–1118. doi:10.2138/am.2014.4524.

Johnston, D. T. (2011). Multiple sulfur isotopes and the evolution of Earth's surface sulfur cycle. *Earth-Science Reviews*, *106*, 161–183. doi:10.1016/j.earscirev.2011.02.003.

Kajiwara, Y., & Krouse, H. R. (1971). Sulfur Isotope Partitioning in Metallic Sulfide Systems. *Canadian Journal of Earth Sciences*, *8*, 1397–1408. doi:10.1139/e71-129.

Kamyshny, A. (2009). Solubility of cyclooctasulfur in pure water and sea water at different temperatures. *Geochimica et Cosmochimica Acta*, *73*, 6022–6028. doi:10.1016/j.gca.2009.07.003.

Kamyshny, A., Goifman, A., Gun, J., Rizkov, D., & Lev, O. (2004). Equilibrium Distribution of Polysulfide Ions in Aqueous Solutions at 25 °C: A New Approach for the Study of Polysulfides' Equilibria. *Environmental Science & Technology*, *38*, 6633–6644. doi:10.1021/es049514e.

Kamyshny, A., Gun, J., Rizkov, D., Voitsekovski, T., & Lev, O. (2007). Equilibrium distribution of polysulfide ions in aqueous solutions at different temperatures by rapid single phase derivatization. *Environmental science & technology*, *41*, 2395–2400.

Koch, W., Natterer, J., & Heinemann, C. (1995). Quantum chemical study on the equilibrium geometries of S_3 and S_3^-, The electron affinity of S_3 and the low lying electronic states of S_3^-. *The Journal of Chemical Physics*, *102*, 6159–6167. doi:10.1063/1.469350.

Kokh, M. A., Assayag, N., Mounic, S., Cartigny, P., Gurenko, A., & Pokrovski, G. S. (2020). Multiple sulfur isotope fractionation in hydrothermal systems in the presence of radical ions and molecular sulfur. *Geochimica et Cosmochimica Acta*, *285*, 100–128. doi:10.1016/j.gca.2020.06.016.

Kusakabe, M., Komoda, Y., Takano, B., & Abiko, T. (2000). Sulfur isotopic effects in the disproportionation reaction of sulfur dioxide in hydrothermal fluids: Implications for the $\delta^{34}S$ variations of dissolved bisulfate and elemental sulfur from active crater lakes. *Journal of Volcanology and Geothermal Research*, *97*, 287–307. doi:10.1016/S0377-0273(99)00161-4.

Leavitt, W. D., Bradley, A. S., Santos, A. A., Pereira, I. A. C., & Johnston, D. T. (2015). Sulfur Isotope Effects of Dissimilatory Sulfite Reductase. *Frontiers in Microbiology*, *6*, 1–20. doi:10.3389/fmicb.2015.01392.

Lee, C., Yang, W., & Parr, R. G. (1988). Development of the Colle-Salvetti correlation-energy formula into a functional of the electron density. *Physical Review B*, *37*, 785–789. doi:10.1103/PhysRevB.37.785.

Li, X., & Liu, Y. (2011). Equilibrium Se isotope fractionation parameters: A first-principles study. *Earth and Planetary Science Letters*, *304*, 113–120. doi:10.1016/j.epsl.2011.01.022.

Li, X., Zhao, H., Tang, M., & Liu, Y. (2009). Theoretical prediction for several important equilibrium Ge isotope fractionation factors and geological implications. *Earth and Planetary Science Letters*, *287*, 1–11. doi:10.1016/j.epsl.2009.07.027.

Liu, Q., Tossell, J. A., & Liu, Y. (2010). On the proper use of the Bigeleisen–Mayer equation and corrections to it in the calculation of isotopic fractionation equilibrium constants. *Geochimica et Cosmochimica Acta*, *74*, 6965–6983. doi:10.1016/j.gca.2010.09.014.

Liu, Y., & Tossell, J. A. (2005). Ab initio molecular orbital calculations for boron isotope fractionations on boric acids and borates. *Geochimica et Cosmochimica Acta*, *69*, 3995–4006. doi:10.1016/j.gca.2005.04.009.

Luther, G. W. (1991). Pyrite synthesis via polysulfide compounds. *Geochimica et Cosmochimica Acta*, *55*, 2839–2849. doi:10.1016/0016-7037(91)90449-F.

Marini, L., Moretti, R., & Accornero, M. (2011). Sulfur Isotopes in Magmatic-Hydrothermal Systems, Melts, and Magmas. *Reviews in Mineralogy and Geochemistry*, *73*, 423–492. doi:10.2138/rmg.2011.73.14.

Matsuhisa, Y., Goldsmith, J. R., & Clayton, R. N. (1978). Mechanisms of hydrothermal crystallization of quartz at 250°C and 15 kbar. *Geochimica et Cosmochimica Acta*, *42*, 173–182. doi:10.1016/0016-7037(78)90130-8.

McLaughlan, S. D., & Marshall, D. J. (1970). Paramagnetic resonance of sulfur radicals in synthetic sodalites. *The Journal of Physical Chemistry*, *74*, 1359–1363. doi:10.1021/j100701a035.

Meyer, B. (1976). Elemental Sulfur. *Chemical Reviews*, *76*, 367–388. doi:10.1021/cr60301a003.

Meyer, B., Peter, L., & Spitzer, K. (1977). Trends in the Charge Distribution in Sulfanes, Sulfanesulfonic Acids, Sulfanedisulfonic Acids, and Sulfurous Acid. *Inorganic Chemistry*, *16*, 27–33. doi:10.1021/ic50167a007.

Ohmoto, H., & Lasaga, A. C. (1982). Kinetics of reactions between aqueous sulfates and sulfides in hydrothermal systems. *Geochimica et Cosmochimica Acta*, *46*, 1727–1745. doi:10.1016/0016-7037(82)90113-2.

Ohmoto, H., & Rye, R. O. (1979). Isotopes of Sulfur and Carbon. In H. L. Barnes (Ed.), *Geochemistry of Hydrothermal Ore Deposits* chapter 10. (pp. 509–567). John Wiley & Sons. (2nd ed.).

Ohsawa, S., Takano, B., Kusakabe, M., & Watanuki, K. (1993). Variation in Volcanic Activity of Kusatsu-Shirane Volcano as Inferred from δ^{34}S in Sulfate from the Yugama Crater Lake. *Bulletin of the Volcanological Society of Japan*, *38*, 95–99. doi:10.18940/kazan.38.3_95.

Ono, S., Shanks, W. C., Rouxel, O. J., & Rumble, D. (2007). S-33 constraints on the seawater sulfate contribution in modern seafloor hydrothermal vent sulfides. *Geochimica et Cosmochimica Acta*, *71*, 1170–1182. doi:10.1016/j.gca.2006.11.017.

Oppenheimer, C., Scaillet, B., & Martin, R. S. (2011). Sulfur Degassing From Volcanoes: Source Conditions, Surveillance, Plume Chemistry and Earth

System Impacts. *Reviews in Mineralogy and Geochemistry*, *73*, 363–421. doi:10.2138/rmg.2011.73.13.

Otake, T., Lasaga, A. C., & Ohmoto, H. (2008). Ab initio calculations for equilibrium fractionations in multiple sulfur isotope systems. *Chemical Geology*, *249*, 357–376. doi:10.1016/j.chemgeo.2008.01.020.

Pokrovski, G. S., & Dubessy, J. (2015). Stability and abundance of the trisulfur radical ion. *Earth and Planetary Science Letters*, *411*, 298–309. doi:10.1016/j.epsl.2014.11.035.

Pokrovski, G. S., & Dubrovinsky, L. S. (2011). The S_3^- Ion Is Stable in Geological Fluids at Elevated Temperatures and Pressures. *Science*, *331*, 1052–1054. doi:10.1126/science.1199911.

Pokrovski, G. S., Kokh, M. A., Guillaume, D., Borisova, A. Y., Gisquet, P., Hazemann, J. L., Lahera, E., Del Net, W., Proux, O., Testemale, D., Haigis, V., Jonchière, R., Seitsonen, A. P., Ferlat, G., Vuilleumier, R., Saitta, A. M., Boiron, M. C., & Dubessy, J. (2015). Sulfur radical species form gold deposits on Earth. *Proceedings of the National Academy of Sciences*, *112*, 13484–13489. doi:10.1073/pnas.1506378112.

Richet, P., Bottinga, Y., & Javoy, M. (1977). A review of hydrogen, carbon, nitrogen, oxygen, sulphur, and chlorine stable isotope fractionation among gaseous molecules. *Annual Review of Earth and Planetary Sciences*, *5*, 65–110.

Rickard, D. (1997). Kinetics of pyrite formation by the H_2S oxidation of iron (II) monosulfide in aqueous solutions between 25 and 125°C: The rate equation. *Geochimica et Cosmochimica Acta*, *61*, 115–134. doi:10.1016/S0016-7037(96)00321-3.

Rickard, D. (2006). Metal Sulfide Complexes and Clusters. *Reviews in Mineralogy and Geochemistry*, *61*, 421–504. doi:10.2138/rmg.2006.61.8.

Rickard, D. (2014). The Sedimentary Sulfur System: Biogeochemistry and Evolution through Geologic Time. In *Treatise on Geochemistry* (pp. 267–326). Elsevier. (2nd ed.). doi:10.1016/B978-0-08-095975-7.00710-5.

Rickard, D., & Luther, G. W. (1997). Kinetics of pyrite formation by the H_2S oxidation of iron (II) monosulfide in aqueous solutions between 25 and 125°C: The mechanism. *Geochimica et Cosmochimica Acta*, *61*, 135–147. doi:10.1016/S0016-7037(96)00322-5.

Rickard, D., & Luther, G. W. (2007). Chemistry of Iron Sulfides. *Chemical Reviews*, *107*, 514–562. doi:10.1021/cr0503658.

Rickard, D., & Morse, J. W. (2005). Acid volatile sulfide (AVS). *Marine Chemistry*, *97*, 141–197. doi:10.1016/j.marchem.2005.08.004.

Robinson, B. W. (1973). Sulphur isotope equilibrium during sulphur hydrolysis at high temperatures. *Earth and Planetary Science Letters*, *18*, 443–450. doi:10.1016/0012-821X(73)90101-5.

Rustad, J. R., & Bylaska, E. J. (2007). Ab Initio Calculation of Isotopic Fractionation in $B(OH)_3$(aq) and BOH_4^-(aq). *Journal of the American Chemical Society*, *129*, 2222–2223. doi:10.1021/ja0683335.

Rustad, J. R., Bylaska, E. J., Jackson, V. E., & Dixon, D. A. (2010). Calculation of boron-isotope fractionation between $B(OH)_3$(aq) and BOH_4^-(aq). *Geochimica et Cosmochimica Acta*, *74*, 2843–2850. doi:10.1016/j.gca.2010.02.032.

Rustad, J. R., Nelmes, S. L., Jackson, V. E., & Dixon, D. A. (2008). Quantum-Chemical Calculations of Carbon-Isotope Fractionation in CO_2(g), Aqueous Carbonate Species, and Carbonate Minerals. *The Journal of Physical Chemistry A*, *112*, 542–555. doi:10.1021/jp076103m.

Rye, R. O., Bethke, P. M., & Wasserman, M. D. (1992). The stable isotope geochemistry of acid sulfate alteration. *Economic Geology*, *87*, 225–262. doi:10.2113/gsecongeo.87.2.225.

Sakai, H. (1957). Fractionation of sulphur isotopes in nature. *Geochimica et Cosmochimica Acta*, *12*, 150–169. doi:10.1016/0016-7037(57)90025-X.

Sakai, H. (1968). Isotopic properties of sulfur compounds in hydrothermal processes. *GEOCHEMICAL JOURNAL*, *2*, 29–49. doi:10.2343/geochemj.2.29.

Schmidt, C., & Seward, T. M. (2017). Raman spectroscopic quantification of sulfur species in aqueous fluids: Ratios of relative molar scattering factors of Raman bands of H_2S, HS^-, SO_2, HSO_4^-, SO_4^{2-}, $S_2O_3^{2-}$, S_3^- and H_2O at ambient conditions and information on changes with pressure and temperature. *Chemical Geology*, *467*, 64–75. doi:10.1016/j.chemgeo.2017.07.022.

Schwarzenbach, G., & Fischer, A. (1960). Die Acidität der Sulfane und die Zusammensetzung wässeriger Polysulfidlösungen. *Helvetica Chimica Acta*, *43*, 1365–1390. doi:10.1002/hlca.19600430521.

Sim, M. S., Sessions, A. L., Orphan, V. J., & Adkins, J. F. (2019). Precise determination of equilibrium sulfur isotope effects during volatilization and deprotonation of dissolved H_2S. *Geochimica et Cosmochimica Acta*, *248*, 242–251. doi:10.1016/j.gca.2019.01.016.

Stern, M. J., Spindel, W., & Monse, E. U. (1968). Temperature Dependences of Isotope Effects. *The Journal of Chemical Physics*, *48*, 2908–2919. doi:10.1063/1.1669550.

Steudel, R. (2003). Inorganic Polysulfides S_n^{2-} and Radical Anions $S_n^{\cdot-}$. In *Elemental Sulfur and Sulfur-Rich Compounds II* (pp. 127–152). doi:10.1007/b13183.

Syverson, D. D., Borrok, D. M., & Seyfried, W. E. (2013). Experimental determination of equilibrium Fe isotopic fractionation between pyrite and dissolved Fe under hydrothermal conditions. *Geochimica et Cosmochimica Acta*, *122*, 170–183. doi:10.1016/j.gca.2013.08.027.

Syverson, D. D., Ono, S., Shanks, W. C., & Seyfried, W. E. (2015). Multiple sulfur isotope fractionation and mass transfer processes during pyrite precipita-

tion and recrystallization: An experimental study at 300 and 350°C. *Geochimica et Cosmochimica Acta*, *165*, 418–434. doi:10.1016/j.gca.2015.06.022.

Takano, B. (1987). Correlation of volcanic activity with sulfur oxyanion speciation in a crater lake. *Science*, *235*, 1633–1635. doi:10.1126/science.235.4796.1633.

Taran, Y. A., Znamenskiy, V. S., & Yurova, L. M. (1996). Geochemical model of the hydrothermal systems of Baranskiy volcano, Iturup, Kuril Islands. *Volcanology & Seismology*, *17*, 471–496.

Taylor, B. E. (1986). Magmatic volatiles: isotopic variation of C, H, and S. *Reviews in Mineralogy and Geochemistry*, *16*, 185–225.

Thode, H. G., Cragg, C. B., Hulston, J. R., & Rees, C. E. (1971). Sulphur isotope exchange between sulphur dioxide and hydrogen sulphide. *Geochimica et Cosmochimica Acta*, *35*, 35–45. doi:10.1016/0016-7037(71)90102-5.

Tossell, J. A. (1983). A qualitative molecular orbital study of the stability of polyanions in mineral structures. *Physics and Chemistry of Minerals*, *9*, 115–123. doi:10.1007/BF00308367.

Tossell, J. A. (2012). Calculation of the properties of the S_3^- radical anion and its complexes with Cu^+ in aqueous solution. *Geochimica et Cosmochimica Acta*, *95*, 79–92. doi:10.1016/j.gca.2012.07.020.

Truche, L., Bazarkina, E. F., Barré, G., Thomassot, E., Berger, G., Dubessy, J., & Robert, P. (2014). The role of S_3^- ion in thermochemical sulphate reduction: Geological and geochemical implications. *Earth and Planetary Science Letters*, *396*, 190–200. doi:10.1016/j.epsl.2014.04.018.

Ueda, A., & Sakai, H. (1984). Sulfur isotope study of Quaternary volcanic rocks from the Japanese Islands Arc. *Geochimica et Cosmochimica Acta*, *48*, 1837–1848. doi:10.1016/0016-7037(84)90037-1.

Urey, H. C. (1947). The thermodynamic properties of isotopic substances. *Journal of the Chemical Society*, (pp. 562–581). doi:10.1039/jr9470000562.

Uyama, F., Chiba, H., Kusakabe, M., & Sakai, H. (1985). Sulfur isotope exchange reactions in the aqueous system: thiosulfate-sulfide-sulfate at hydrothermal temperature. *Geochemical Journal*, *19*, 301–315.

Vairavamurthy, A., Manowitz, B., Luther, G. W., & Jeon, Y. (1993). Oxidation-State of Sulfur in Thiosulfate and Implications for Anaerobic Energy-Metabolism. *Geochimica Et Cosmochimica Acta*, *57*, 1619–1623. doi:10.1016/0016-7037(93)90304-F.

Vchirawongkwin, V., Rode, B. M., & Persson, I. (2007). Structure and Dynamics of Sulfate Ion in Aqueous SolutionAn ab initio QMCF MD Simulation and Large Angle X-ray Scattering Study. *The Journal of Physical Chemistry B*, *111*, 4150–4155. doi:10.1021/jp0702402.

Wilkin, R., & Barnes, H. (1996). Pyrite formation by reactions of iron mono-sulfides with dissolved inorganic and organic sulfur species. *Geochimica et Cosmochimica Acta*, *60*, 4167–4179. doi:10.1016/S0016-7037(97)81466-4.

Wu, R., Zheng, Y., Zhang, X., Sun, Y., Xu, J., & Jian, J. (2004). Hydrothermal synthesis and crystal structure of pyrite. *Journal of Crystal Growth*, *266*, 523–527. doi:10.1016/j.jcrysgro.2004.02.020.

Zachariasen, W. H. (1934). Note on the Structure of the Trithionate Group, $(S_3O_6)^{-2}$. *The Journal of Chemical Physics*, *2*, 109–111. doi:10.1063/1.1749428.

Zeebe, R. E. (2009). Hydration in solution is critical for stable oxygen isotope fractionation between carbonate ion and water. *Geochimica et Cosmochimica Acta*, *73*, 5283–5291. doi:10.1016/j.gca.2009.06.013.

Zeebe, R. E. (2010). A new value for the stable oxygen isotope fractionation between dissolved sulfate ion and water. *Geochimica et Cosmochimica Acta*, *74*, 818–828. doi:10.1016/j.gca.2009.10.034.

Zopfi, J., Ferdelman, T., & Fossing, H. (2004). Distribution and fate of sulfur intermediates—sulfite, tetrathionate, thiosulfate, and elemental sulfur—in marine sediments. In *Sulfur Biogeochemistry - Past and Present* (pp. 97–116). Geological Society of America volume 379. doi:10.1130/0-8137-2379-5.97.

Table 1: List of sulfur compounds and corresponding water cluster sizes (nH_2O).

Polysulfides (S_x^{2-}, HS_x^-)
$S_2^{2-} \bullet nH_2O$ (n = 30, 34, 38, 42, 45, 46, 50, 50)
$S_3^{2-} \bullet nH_2O$ (n = 34, 38, 42, 45, 46, 50)
$S_4^{2-} \bullet nH_2O$ (n = 34, 38, 42, 45)
$S_5^{2-} \bullet nH_2O$ (n = 38, 41, 42, 46, 50, 50, 50)
$S_6^{2-} \bullet nH_2O$ (n = 40, 42, 45, 46, 50, 50, 50)
$S_7^{2-} \bullet nH_2O$ (n = 45, 46, 48, 50, 50, 52)
$S_8^{2-} \bullet nH_2O$ (n = 50)
$HS_2^- \bullet nH_2O$ (n = 34, 38, 42, 46, 50)
$HS_3^- \bullet nH_2O$ (n = 34, 38, 42, 46, 50)
Polysulfur radical ions ($S_x^{\cdot -}$)
$S_2^{\cdot -} \bullet nH_2O$ (n = 30, 34, 38, 42, 46, 50)
$S_3^{\cdot -} \bullet nH_2O$ (n = 34, 38, 42, 46, 50)
Sulfide
$H_2S \bullet nH_2O$ ($n = 30^*, 35, 40, 45$)
$HS^- \bullet nH_2O$ ($n = 30^*, 30, 35, 40, 45, 45$)
$S^{2-} \bullet nH_2O$ ($n = 30^*$)
$FeSH^+ \bullet nH_2O$ (n = 34, 38, 42, 46, 50)
$FeS_{(aq)} \bullet nH_2O$ (n = 31, 34, 38, 40, 48, 50)
$(Na^+HS^-)^0 \bullet nH_2O$ (n = 30, 32, 35, 38, 41, 45)
Sulfate
$HSO_4^- \bullet nH_2O$ (n = 36, 40, 44, 48, 52)
$SO_4^{2-} \bullet nH_2O$ ($n = 30^*, 36, 40, 44, 48, 52$)
$(Na^+SO_4^{2-})^- \bullet nH_2O$ (n = 43, 48, 52)
$(Mg^{2+}SO_4^{2-})^0 \bullet nH_2O$ (n = 41, 43, 50)
Polythionates
$S_3O_6^{2-} \bullet nH_2O$ (n = 42, 44, 46, 48, 50, 52)
$S_4O_6^{2-} \bullet nH_2O$ (n = 42, 46, 48, 50, 52)
Elemental Sulfur
$S_8 \bullet nH_2O$ (n = 50)

* Incorporated from Eldridge et al. (2016)

Table 2: Mean geometry parameters of compounds modeled in water clusters.

Compound	Bond	R(Å)	1 s.d.	Angle	∠(°)	1 s.d.	Angle	Dihedral(°)	1 s.d.
$S_2^{2-}(nH_2O)$	S-S	2.167	0.008						
S_2^{2-}(g)	S-S	2.216							
$S_3^{2-}(nH_2O)$	S-S	2.121	0.006	S-S-S	111.1	1.0			
S_3^{2-}(g)	S-S	2.158		S-S-S	114.8				
$S_4^{2-}(nH_2O)$	S-S	2.112	0.009	S-S-S	111.1	1.7	S-S-S-S	96	9
S_4^{2-}(g)	S-S	2.137	0.018	S-S-S	116.6		S-S-S-S	95	
$S_5^{2-}(nH_2O)$	S-S	2.104	0.016	S-S-S	109.9	1.8	S-S-S-S	92	12
S_5^{2-}(g)	S-S	2.130	0.032	S-S-S	115.3	1.8	S-S-S-S	91	
$S_6^{2-}(nH_2O)$	S-S	2.105	0.014	S-S-S	108.7	1.1	S-S-S-S	86	9
S_6^{2-}(g)	S-S	2.123	0.037	S-S-S	114.3	0.1	S-S-S-S	88	
$S_7^{2-}(nH_2O)$	S-S	2.101	0.012	S-S-S	110.1	1.7	S-S-S-S	80	8
S_7^{2-}(g)	S-S	2.119	0.031	S-S-S	113.7	1.2	S-S-S-S	86	
$S_8^{2-}(nH_2O)$	S-S	2.099	0.015	S-S-S	109.5	2.4	S-S-S-S	81	11
S_8^{2-}(g)	S-S	2.117	0.038	S-S-S	113.4	1.6	S-S-S-S	86	1
$HS_2^-(nH_2O)$	S-SH	2.124	0.003	S-S-H	99.6	0.6			
	S-H	1.353	<0.001						
$HS_3^-(nH_2O)$	S-S	2.085	0.003	S-S-SH	109.8	0.4	S-S-S-H	90	3
	S-SH	2.120	0.003	S-S-H	97.4	0.6			
	S-H	1.366	0.003						
$S_2^{\cdot-}(nH_2O)$	S-S	2.032	0.001						
$S_3^{\cdot-}(nH_2O)$	S-S	2.031	0.011	S-S-S	114.3	1.1			
$S_8(nH_2O)$	S-S	2.10	0.01	S-S-S	108.7	1.1	S-S-S-S	97.8	3.3
$H_2S(nH_2O)$	S-H	1.347	0.002	H-S-H	92.9	0.5			
$HS^-(nH_2O)$	S-H	1.349	0.002						
$FeSH^+(nH_2O)$	S-H	1.349	<0.001	H-S-Fe	103.7	0.9			
	Fe-S	2.27	0.02						
$FeS^0_{aq}(nH_2O)$	Fe-S	2.140	0.004						
$(Na^+HS^-)^0(nH_2O)$	S-H	1.345	0.003	H-S-Na	95	11			
	S-Na	2.76	0.02			(range: 75-105°)			
$SO_4^{2-}(nH_2O)$	S-O	1.52	0.01	O-S-O	109.5	1.2			
$HSO_4^-(nH_2O)$	S-O	1.49	0.01	O-S-O	109.4	3.6			
	S-OH	1.596	0.002						
	O-H	1.03	0.01						
$(Na^+SO_4^{2-})^-(nH_2O)$	S-O	1.52	0.01	O-S-O	109.5	1.0			
	S-O(Na)	1.496	<0.001						
	O-Na	2.248	0.005						
$(Mg^{2+}SO_4^{2-})^0(nH_2O)$	S-O	1.51	0.02	O-S-O	109.4	1.9			
	S-O(Mg)	1.547	0.001						
	O-Mg	2.05	0.02						
$S_3O_6^{2-}(nH_2O)$	S-S(O_3)	2.17	0.02	S-S-S	104.2	1.3			
	S-O	1.49	0.01	O-S-O	113.7	1.5			
$S_4O_6^{2-}(nH_2O)$	S-S(O_3)	2.20	0.02	S-S-S	104.4	2.1	S-S-S-S	104.0	2.9
	S-S	2.036	0.003	O-S-O	113.6	1.7			
	S-O	1.49	0.02						

Table 3: Average reduced partition function ratios (RPFRs) for singly substituted isotopologues of sulfide and polysulfide compounds modeled in water clusters at $T = 25°C$. '33/34'= $\ln(^{33}\text{RPFR})/\ln(^{34}\text{RPFR})$, '36/34'=$\ln(^{36}\text{RPFR})/\ln(^{34}\text{RPFR})$, MWCN=Mean Water Coordination Number that refers to the mean number of water molecules that are hydrogen-bonded to the specified sulfur atom (range given in parentheses).

	nH_2O	Atom Position	Schematic	MWCN	^{33}RPFR	1 s.d.	^{34}RPFR	1 s.d.	^{36}RPFR	1 s.d.	33/34	36/34
S_2^{2-}	30-50	outer	*S-S	5.00(4-6)	1.0044	0.0002	1.0086	0.0004	1.0164	0.0008	0.51571	1.8917
		outer	S-*S	5.25(5-6)	1.0045	0.0002	1.0087	0.0004	1.0164	0.0008	0.51572	1.8920
S_3^{2-}	34-50	outer	*S-S-S	4.33(4-5)	1.0045	0.0001	1.0088	0.0002	1.0167	0.0004	0.51565	1.8919
		center	S-*S-S	2.00(1-3)	1.0069	0.0001	1.0134	0.0002	1.0256	0.0004	0.51558	1.8923
		outer	S-S-*S	4.67(4-5)	1.0046	0.0002	1.0090	0.0003	1.0171	0.0006	0.51567	1.8919
S_4^{2-}	34-45	outer	*S-S-S-S	4.75(4-5)	1.0047	0.0001	1.0091	0.0002	1.0174	0.0003	0.51561	1.8918
		inner	S-*S-S-S	1.00	1.0065	0.0000	1.0127	0.0001	1.0242	0.0001	0.51561	1.8921
		inner	S-S-*S-S	1.25(1-2)	1.0064	0.0000	1.0125	0.0001	1.0238	0.0001	0.51561	1.8920
		outer	S-S-S-*S	4.75(4-5)	1.0045	0.0001	1.0087	0.0002	1.0165	0.0003	0.51569	1.8918
S_5^{2-}	38-50	outer	*S-S-S-S-S	4.29(4-6)	1.0048	0.0003	1.0094	0.0005	1.0178	0.0009	0.51565	1.8920
		inner	S-*S-S-S-S	0.86(0-1)	1.0067	0.0003	1.0129	0.0005	1.0246	0.0010	0.51563	1.8922
		center	S-S-*S-S-S	1.14(0-2)	1.0061	0.0003	1.0118	0.0005	1.0224	0.0010	0.51562	1.8920
		inner	S-S-S-*S-S	0.57(0-1)	1.0066	0.0002	1.0129	0.0004	1.0246	0.0008	0.51563	1.8922
		outer	S-S-S-S-*S	4.29(4-5)	1.0047	0.0002	1.0091	0.0004	1.0174	0.0008	0.51564	1.8919
S_6^{2-}	40-50	outer	*S-S-S-S-S-S	4.14(3-6)	1.0046	0.0002	1.0089	0.0004	1.0169	0.0007	0.51570	1.8921
		inner(2)	S-*S-S-S-S-S	1.00(0-2)	1.0069	0.0002	1.0135	0.0003	1.0256	0.0006	0.51562	1.8923
		inner(1)	S-S-*S-S-S-S	0.71(0-1)	1.0060	0.0002	1.0117	0.0005	1.0222	0.0009	0.51564	1.8918
		inner(1)	S-S-S-*S-S-S	0.86(0-1)	1.0060	0.0002	1.0117	0.0004	1.0223	0.0008	0.51567	1.8920
		inner(2)	S-S-S-S-*S-S	0.86(0-1)	1.0067	0.0002	1.0131	0.0003	1.0249	0.0006	0.51563	1.8922
		outer	S-S-S-S-S-*S	4.86(4-5)	1.0046	0.0001	1.0090	0.0003	1.0171	0.0005	0.51560	1.8919
S_7^{2-}	45-52	outer	*S-S-S-S-S-S-S	4.83(4-6)	1.0046	0.0002	1.0089	0.0003	1.0170	0.0006	0.51565	1.8921
		inner(2)	S-*S-S-S-S-S-S	1.33(1-2)	1.0070	0.0002	1.0136	0.0004	1.0259	0.0007	0.51562	1.8923
		inner(1)	S-S-*S-S-S-S-S	0.67(0-1)	1.0062	0.0001	1.0121	0.0001	1.0230	0.0003	0.51565	1.8919
		center	S-S-S-*S-S-S-S	0.33(0-1)	1.0059	0.0002	1.0116	0.0004	1.0220	0.0007	0.51569	1.8919
		inner(1)	S-S-S-S-*S-S-S	1.17(1-2)	1.0062	0.0000	1.0120	0.0001	1.0228	0.0001	0.51567	1.8918
		inner(2)	S-S-S-S-S-*S-S	0.83(0-1)	1.0067	0.0002	1.0130	0.0004	1.0248	0.0008	0.51560	1.8923
		outer	S-S-S-S-S-S-*S	4.17(4-5)	1.0046	0.0001	1.0090	0.0002	1.0172	0.0004	0.51566	1.8920
S_8^{2-}	50	outer	*S-S-S-S-S-S-S-S	4.00	1.0049	-	1.0094	-	1.0180	-	0.51564	1.8920
		inner(3)	S-*S-S-S-S-S-S-S	2.00	1.0072	-	1.0140	-	1.0267	-	0.51557	1.8923
		inner(2)	S-S-*S-S-S-S-S-S	0.00	1.0062	-	1.0121	-	1.0229	-	0.51552	1.8918
		inner(1)	S-S-S-*S-S-S-S-S	0.00	1.0065	-	1.0126	-	1.0240	-	0.51568	1.8920
		inner(1)	S-S-S-S-*S-S-S-S	0.00	1.0062	-	1.0120	-	1.0229	-	0.51567	1.8918
		inner(2)	S-S-S-S-S-*S-S-S	0.00	1.0058	-	1.0113	-	1.0215	-	0.51568	1.8920
		inner(3)	S-S-S-S-S-S-*S-S	2.00	1.0069	-	1.0135	-	1.0256	-	0.51560	1.8922
		outer	S-S-S-S-S-S-S-*S	4.00	1.0045	-	1.0088	-	1.0167	-	0.51566	1.8919
HS_2^-	34-50	outer	*S-S-H	4.00	1.0051	0.0001	1.0100	0.0002	1.0190	0.0003	0.51562	1.8920
		HS-bonded	S-*S-H	1.60(1-2)	1.0068	0.0001	1.0133	0.0001	1.0253	0.0002	0.51566	1.8919
HS_3^-	34-50	outer	*S-S-S-H	4.00	1.0049	0.0002	1.0095	0.0004	1.0180	0.0008	0.51560	1.8921
		inner	S-*S-S-H	2.00	1.0073	0.0000	1.0141	0.0001	1.0269	0.0001	0.51558	1.8924
		HS-bonded	S-S-*S-H	2.00	1.0067	0.0001	1.0131	0.0002	1.0249	0.0003	0.51571	1.8917
$S_2^{\cdot-}$	30-50	outer	*S-S	4.83(4-5)	1.0052	0.0001	1.0100	0.0002	1.0190	0.0004	0.51552	1.8927
		outer	S-*S	4.83(3-6)	1.0052	0.0002	1.0102	0.0004	1.0193	0.0007	0.51556	1.8928
$S_3^{\cdot-}$	34-50	outer	*S-S-S	3.40(3-4)	1.0051	0.0001	1.0099	0.0003	1.0188	0.0006	0.51555	1.8924
		center	S-*S-S	1.60(1-2)	1.0085	0.0002	1.0165	0.0003	1.0314	0.0006	0.51553	1.8930
		outer	S-S-*S	4.40(4-5)	1.0050	0.0001	1.0097	0.0002	1.0184	0.0005	0.51554	1.8925
$FeSH^+$	34-50	N/A	Fe-*S-H	1.60(1-2)	1.0061	0.0001	1.0119	0.0003	1.0227	0.0005	0.51573	1.8914
$FeS_{(aq)}$	31-50	N/A	Fe-*S	4.00(3-5)	1.0046	0.0001	1.0089	0.0003	1.0169	0.0005	0.51564	1.8920
$(Na^+HS^-)^0$	30-45	N/A	Na-*S-H	1.5(1-4)	1.0045	0.0001	1.0088	0.0003	1.0167	0.0005	0.51578	1.8912
H_2S	30-45	N/A	H-*S-H	0.5(0-1)	1.0067	0.0002	1.0129	0.0003	1.0246	0.0006	0.51571	1.8912
HS^-	30-45	N/A	H-*S	3.00(2-4)	1.0045	0.0003	1.0087	0.0005	1.0166	0.0010	0.51580	1.8912
S^{2-}	30	N/A	*S	6	1.0039	-	1.0076	-	1.0145	-	0.51576	1.8916

Table 4: Coefficients of polynomial fits to mean β-values (or related κ values) and standard deviation of the mean (1 s.d.) of β-values for aqueous sulfur compounds computed at the B3LYP/6-31+G(d,p) level in numerous water clusters each over T = 0-5000°C. Quantities are computed using the coefficients via: ${}^{34}\beta$ or ${}^{33/34}\kappa$ or ${}^{36/34}\kappa$ or 1 s.d. $= A/T^4 + B/T^3 + C/T^2 + D/T + E$ where T is temperature in Kelvin (K). Values for ${}^{33}\beta$ and ${}^{36}\beta$ are computed from the ${}^{33/34}\kappa$ and ${}^{36/34}\kappa$ exponents, respectively, using: ${}^{33}\beta = {}^{34}\beta^{({}^{33/34}\kappa)}$ and ${}^{36}\beta = {}^{36}\beta^{({}^{36/34}\kappa)}$ at a given temperature. Note that the 1 s.d. are given for ${}^{33}\beta$ and ${}^{36}\beta$ values rather than for κ values. To compute a coefficient, treat column headers and tabulated values as equations where you solve for the coefficient. For example, to compute A for the ${}^{34}\beta$ of S_2^{2-} we begin with A$\times 10^{-4}$ = -176.026 from the table and then solve for A: A = -176.026$\times 10^4$ = -1.76026$\times 10^6$ (or -1760260). Extra significant figures are given for the coefficients to minimize rounding errors.

		${}^{34}\beta$					${}^{33/34}\kappa$					${}^{36/34}\kappa$				
Compound	nH_2O	$A\times10^{-4}$	$B\times10^{-2}$	C	$D\times10^{3}$	E	$A\times10^{-4}$	$B\times10^{-2}$	C	$D\times10^{3}$	E	$A\times10^{-4}$	$B\times10^{-2}$	C	$D\times10^{3}$	E
S_2^{2-} (8 clusters)	30-50	-176.026	-131.764	835.008	-9.99974	1.0000	-32.5449	45.1775	-31.4688	-7.37587	0.51597	-23.5069	-78.2557	150.006	25.9227	1.8904
S_2^{2-}- (6 clusters)	34-50	-246.675	-148.339	1006.37	-13.8127	1.0000	101.256	-75.1225	-1.01774	12.832	0.51569	-359.942	147.689	137.632	-138.77	1.8909
S_3^{2-}(4 clusters)	34-45	-258.782	-129.593	1032.35	-12.5886	1.0000	95.0159	-54.2567	-15.9062	33.8974	0.51577	-57.1913	-75.3122	175.746	-7.89257	1.8904
S_5^{2-}(7 clusters)	38-50	-276.15	-133.658	1077.82	-13.3699	1.0000	11.1501	7.38309	-24.4208	-1.95696	0.51587	-105.385	-38.1416	171.658	-17.3883	1.8905
S_6^{2-}(7 clusters)	40-50	-278.962	-125.483	1082.27	-12.9053	1.0000	9.34265	9.69746	-25.3974	-0.690149	0.51588	-89.55	-45.1938	169.906	-13.6531	1.8905
S_7^{2-}(6 clusters)	45-52	-285.546	-124.641	1097.09	-13.0559	1.0000	23.8421	1.46416	-26.135	8.99564	0.51588	-121.818	-23.7279	169.565	-28.5768	1.8905
S_8^{2-}(1 cluster)	50	-293.406	-129.258	1121.42	-13.6248	1.0000	56.473	-24.2593	-21.8124	20.4013	0.51582	-104.941	-34.429	171.069	-11.2637	1.8904
HS_2^- (5 clusters)	34-50	1114.14	-1527.72	1396.61	91.3744	1.0000	14.6488	-6.45365	-12.9689	-9.82894	0.51583	60.2784	-100.085	125.739	94.8934	1.8905
HS_3^- (5 clusters)	34-50	586.29	-1047.59	1363.96	32.1762	1.0000	-30.2866	37.0042	-27.4032	-15.5142	0.51589	99.1276	-165.126	169.89	74.34	1.8904
S_2^-(6 clusters)	30-50	-286.31	-282.441	1032.71	-29.9483	1.0000	10.2399	31.197	-42.0312	0.306661	0.51588	-124.467	-166.497	277.408	-22.9975	1.8905
S_3^-(5 clusters)	34-50	-342.187	-262.552	1202.46	-27.5626	1.0000	29.7163	9.37457	-36.0811	7.32133	0.51585	-149.804	-102.735	251.851	-31.2004	1.8905
H_2S (4 clusters)	30-45	5417.73	-5579.69	2286.1	451.276	0.9999	-148.615	122.638	-27.4387	-30.0089	0.51584	1080.9	-884.604	192.046	232.349	1.8903
HS^- (6 clusters)	30-45	2578.83	-2660.81	1313.42	236.104	0.9999	-86.8794	60.8481	-11.2387	-29.918	0.51590	724.748	-534.609	106.095	215.845	1.8904
$FeSH^+$ (5 clusters)	34-50	2470.5	-2659.03	1609.72	227.84	1.0000	-76.8008	57.6489	-17.3365	-26.3414	0.51590	527.886	-390.982	114.217	187.909	1.8903
$FeS^0_{(aq)}$ (6 clusters)	31-50	-172.918	-114.989	850.736	-7.16277	1.0000	-38.0652	49.7996	-35.3566	-9.03733	0.51593	26.6346	-132.151	189.678	30.0563	1.8903
$(Na^+HS^-)^0$ (6 clusters)	30-45	2590.13	-2645	1304.22	254.946	0.9999	-105.404	73.289	-11.8137	-36.7142	0.51589	695.769	-508.518	97.181	217.75	1.8904
HSO_4^- (5 clusters)	36-52	6544.64	-13394.1	11163	-1048.25	1.0002	-351.093	496.74	-223.816	37.3413	0.51586	2339.32	-3326.15	1508.23	-232.835	1.8905
SO_4^{2-} (6 clusters)	30-52	5055.38	-11886.9	10728.1	-962.399	1.0002	-285.366	438.566	-210.52	32.621	0.51588	1822.79	-2875.94	1408.93	-223.382	1.8905
$(Na^+SO_4^{2-})^-$ (3 clusters)	43-52	5308.74	-12158.2	10823.9	-981.142	1.0002	-304.288	454.17	-213.606	30.3202	0.51589	1937.65	-2974.47	1430.5	-215.099	1.8904
$(Mg^{2+}SO_4^{2-})^0$ (3 clusters)	41-50	5389.1	-12219.9	10835.4	-994.01	1.0002	-296.251	449.626	-214.036	37.7653	0.51587	1938.67	-2980.84	1435.7	-236.773	1.8905
S_8 (1 cluster)	50	-321.316	-119.192	1218.68	-13.3141	1.0000	20.8403	13.2180	-42.6863	0.454824	0.5159	-174.863	-57.5431	283.012	-17.5569	1.8905
Intercept (E) Avg.						1.0000					0.51587					1.8904
Intercept (E) 1 s.d.						0.0001					0.00006					0.0001

		1 s.d.: ${}^{34}\beta$					1 s.d.: ${}^{33}\beta$					1 s.d.: ${}^{36}\beta$				
Compound	nH_2O	$A\times10^{-4}$	$B\times10^{-2}$	C	$D\times10^{3}$	E	$A\times10^{-4}$	$B\times10^{-2}$	C	$D\times10^{3}$	E	$A\times10^{-4}$	$B\times10^{-2}$	C	$D\times10^{3}$	E
S_2^{2-}(8 clusters)	30-50	-7.29970	-11.5193	40.8895	-0.869774	0.0000	-4.06321	-6.2170	21.1263	-0.481825	0.0000	-11.5355	-20.0121	76.9874	-1.46660	0.0000
S_2^{2-}- (6 clusters)	34-50	-2.76210	-4.79241	19.1476	-0.400900	0.0000	-1.47558	-2.7439	9.94918	-0.200806	0.0000	-3.9795	-8.07180	36.0233	-0.701843	0.0000
S_3^{2-}(4 clusters)	34-45	-2.91292	-1.59154	8.46982	-0.330178	0.0000	-1.61646	-0.8459	4.36302	-0.170081	0.0000	-4.6961	-2.78582	16.0062	-0.512866	0.0000
S_5^{2-}(7 clusters)	38-50	-11.1954	-7.58168	38.0334	-0.755429	0.0000	-6.09852	-4.2968	19.7074	-0.416844	0.0000	-18.4886	-12.1265	71.521	-1.23223	0.0000
S_6^{2-}(7 clusters)	40-50	-4.8396	-0.76162	14.8763	-0.136978	0.0000	-2.67478	-0.5174	7.68917	-0.0823192	0.0000	-7.6688	-0.784058	28.0563	-0.169643	0.0000
S_7^{2-}(6 clusters)	45-52	-4.14796	-4.04084	14.3328	-0.371715	0.0000	-2.22879	-2.27	7.45526	-0.199382	0.0000	-7.1006	-6.56316	26.8259	-0.610642	0.0000
S_8^{2-}(1 cluster)	50	-	-	-	-	-	-	-	-	-	-	-	-	-	-	-
HS_2^- (5 clusters)	34-50	3.1678	-3.26392	8.65037	1.43031	0.0000	1.49386	-1.66106	4.425	0.724016	0.0000	6.53562	-5.61311	16.2124	2.75836	0.0000
HS_3^- (5 clusters)	34-50	-3.51532	-5.35512	22.1104	-4.23011	0.0000	-2.05999	-2.93482	11.4488	-2.21219	0.0000	-5.46904	-8.53416	41.4894	-7.94822	0.0000
S_2^-(6 clusters)	30-50	-0.952074	-4.56027	25.4454	-0.287889	0.0000	-0.620231	-2.66981	13.2184	-0.163996	0.0000	0.0806251	-7.50837	47.8817	-0.390603	0.0000
S_3^-(5 clusters)	34-50	-3.34442	-5.33201	23.026	-0.396108	0.0000	-2.04928	-2.8871	11.9135	-0.23299	0.0000	-4.6576	-8.63573	43.2743	-0.606331	0.0000
H_2S (4 clusters)	30-45	-28.8036	29.82	17.9267	15.8468	0.0000	-14.9037	15.0587	9.21893	8.18888	0.0000	-53.5242	58.3478	33.7535	30.0296	0.0000
HS^- (6 clusters)	30-45	-20.6106	4.17215	48.572	1.36225	0.0000	-10.7393	1.65078	25.1641	0.646344	0.0000	-37.5342	10.2169	91.6611	2.61754	0.0000
$FeSH^+$ (5 clusters)	34-50	-7.33082	-7.63827	27.5078	-0.800905	0.0000	-3.91796	-4.19128	14.2278	-0.424076	0.0000	-13.0875	-12.5153	51.7517	-1.42863	0.0000
$FeS^0_{(aq)}$ (6 clusters)	31-50	-6.95111	-2.67824	25.6918	-0.826832	0.0000	-3.81962	-1.56389	13.2941	-0.428178	0.0000	-11.0192	-4.30296	48.4865	-1.46222	0.0000
$(Na^+HS^-)^0$ (6 clusters)	30-45	-18.9943	8.94416	25.617	-7.53472	0.0000	-9.87589	4.37759	13.2475	-3.88168	0.0000	-34.978	18.1784	48.2611	-14.1717	0.0000
HSO_4^- (5 clusters)	36-52	11.727	-32.7357	25.5003	-3.95198	0.0000	7.99022	-19.2844	13.5129	-2.21075	0.0000	10.5427	-45.9072	45.8225	-6.463921	0.0000
SO_4^{2-} (6 clusters)	30-52	78.8748	-84.6744	35.7615	-2.32904	0.0000	42.118	-45.4037	18.5233	-1.23343	0.0000	140.822	-148.031	66.7119	-4.18088	0.0000
$(Na^+SO_4^{2-})^-$ (3 clusters)	43-52	16.9268	-19.6855	9.41901	-1.5102	0.0000	9.46145	-11.0284	5.05119	-0.759651	0.0000	30.204	-34.1054	17.4299	-2.68508	0.0000
$(Mg^{2+}SO_4^{2-})^0$ (3 clusters)	41-50	-11.7906	7.16296	5.33021	3.92685	0.0000	-5.76953	2.66752	2.99964	1.92179	0.0000	-22.6473	18.76637	9.57099	7.81303	0.0000
S_8 (1 cluster)	50	-	-	-	-	-	-	-	-	-	-	-	-	-	-	-

Table 5: Coefficients from polynomial fits to mean and standard deviation of the mean of RPFR-values for polythionates computed at the B3LYP/6-31+G(d,p) level in numerous water clusters each over T = 0-5000℃. Values are computed using the coefficients via: ^{34}RPFR or ln(^{33}RPFR)/ln(^{34}RPFR) or ln(^{36}RPFR)/ln(^{34}RPFR) or 1 s.d. $= A/T^4 + B/T^3 + C/T^2 + D/T + E$ where T is temperature in Kelvin (K). Extra significant figures are given for the coefficients to minimize rounding errors.

		$^{34}RPFR$					$\frac{ln(^{33}RPFR)}{ln(^{34}RPFR)}$					$\frac{ln(^{36}RPFR)}{ln(^{34}RPFR)}$				
Compound	nH_2O	$A \times 10^{-4}$	$B \times 10^{-2}$	C	$D \times 10^{3}$	E	$A \times 10^{-4}$	$B \times 10^{-2}$	C	$D \times 10^{3}$	E	$A \times 10^{-4}$	$B \times 10^{-2}$	C	$D \times 10^{3}$	E
$S_3O_6^{2-}$																
Outer ('sulfonate')	42-52	6638.18	-12577.5	10099.9	-973.35	1.0002	-411.349	530.434	-222.115	29.4818	0.51590	2613.62	-3460.68	1486.33	-241.351	1.8905
Center ('sulfanyl')	42-52	-327.777	-150.407	1354.914	-15.61672	1.0000	6.38566	8.40783	-25.3466	-8.61598	0.51590	-39.3292	-86.858	194.783	7.97193	1.8903
Outer ('sulfonate')	42-52	6080.7	-11974.2	9896.42	-937.023	1.0002	-365.737	490.741	-213.596	36.5594	0.51587	2422.02	-3271.69	1434.92	-228.263	1.8905
$S_4O_6^{2-}$																
Outer ('sulfonate')	42-52	6401.64	-12333.1	10033.9	-959.236	1.0002	-393.105	514.744	-218.909	32.1914	0.51588	2517.7	-3373.78	1466.27	-245.219	1.8905
Inner	42-52	-358.36	-201.597	1359.88	-22.0887	1.0000	22.5274	5.00042	-30.033	2.35247	0.51587	-133.632	-60.4634	216.176	-27.4184	1.8905
Inner	42-52	-383.145	-219.193	1460.05	-23.8966	1.0000	11.9535	18.3264	-35.6729	4.65989	0.51593	-94.2731	-83.128	216.345	-2.72562	1.8905
Outer ('sulfonate')	42-52	5820.26	-11682.1	9786.69	-918.552	1.0001	-361.789	484.035	-210.495	31.0217	0.51589	2340.23	-3192.6	1414.41	-228.677	1.8905
Intercept (E) Avg.						1.0001					0.51589					1.8905
Intercept (E) 1 s.d.						0.0001					0.00002					0.0001

		1 s.d.: ^{34}RPFR					1 s.d.: ^{33}RPFR					1 s.d.: ^{36}RPFR				
Compound	nH_2O	$A \times 10^{-4}$	$B \times 10^{-2}$	C	$D \times 10^{3}$	E	$A \times 10^{-4}$	$B \times 10^{-2}$	C	$D \times 10^{3}$	E	$A \times 10^{-4}$	$B \times 10^{-2}$	C	$D \times 10^{3}$	E
$S_3O_6^{2-}$																
Outer ('sulfonate')	42-52	15.1238	76.3898	-22.608	49.7611	0.0000	-1.85982	44.0515	-12.6214	26.1783	0.0000	91.3597	117.441	-37.5545	90.9992	0.0000
Center ('sulfanyl')	42-52	-3.92357	-6.54289	22.9726	-0.673392	0.0000	-2.35804	-3.51986	11.8243	-0.363225	0.0000	-5.2369	-10.7863	43.1014	-1.07264	0.0000
Outer ('sulfonate')	42-52	125.374	-156.693	82.8116	-7.12916	0.0000	68.0524	-85.5122	43.2176	-3.88146	0.0000	218.554	-265.655	153.601	-11.9924	0.0000
$S_4O_6^{2-}$																
Outer ('sulfonate')	42-52	51.5253	-49.5753	23.5354	-1.88015	0.0000	26.7618	-26.3607	12.1135	-1.01509	0.0000	96.9131	-87.4455	44.0097	-3.60482	0.0000
Inner	42-52	-6.54691	-6.23833	22.6332	-0.660979	0.0000	-3.64656	-3.41165	11.6876	-0.363399	0.0000	-10.7528	-10.0017	42.4437	-1.08237	0.0000
Inner	42-52	-7.15153	-9.96721	24.9752	-1.04215	0.0000	-3.70783	-5.62526	12.9802	-0.564309	0.0000	-12.1468	-16.4619	46.7466	-1.73977	0.0000
Outer ('sulfonate')	42-52	-49.5241	16.8282	21.2963	-3.01357	0.0000	-23.8494	5.81412	11.4489	-1.87217	0.0000	-101.886	50.2571	37.0783	-3.63496	0.0000

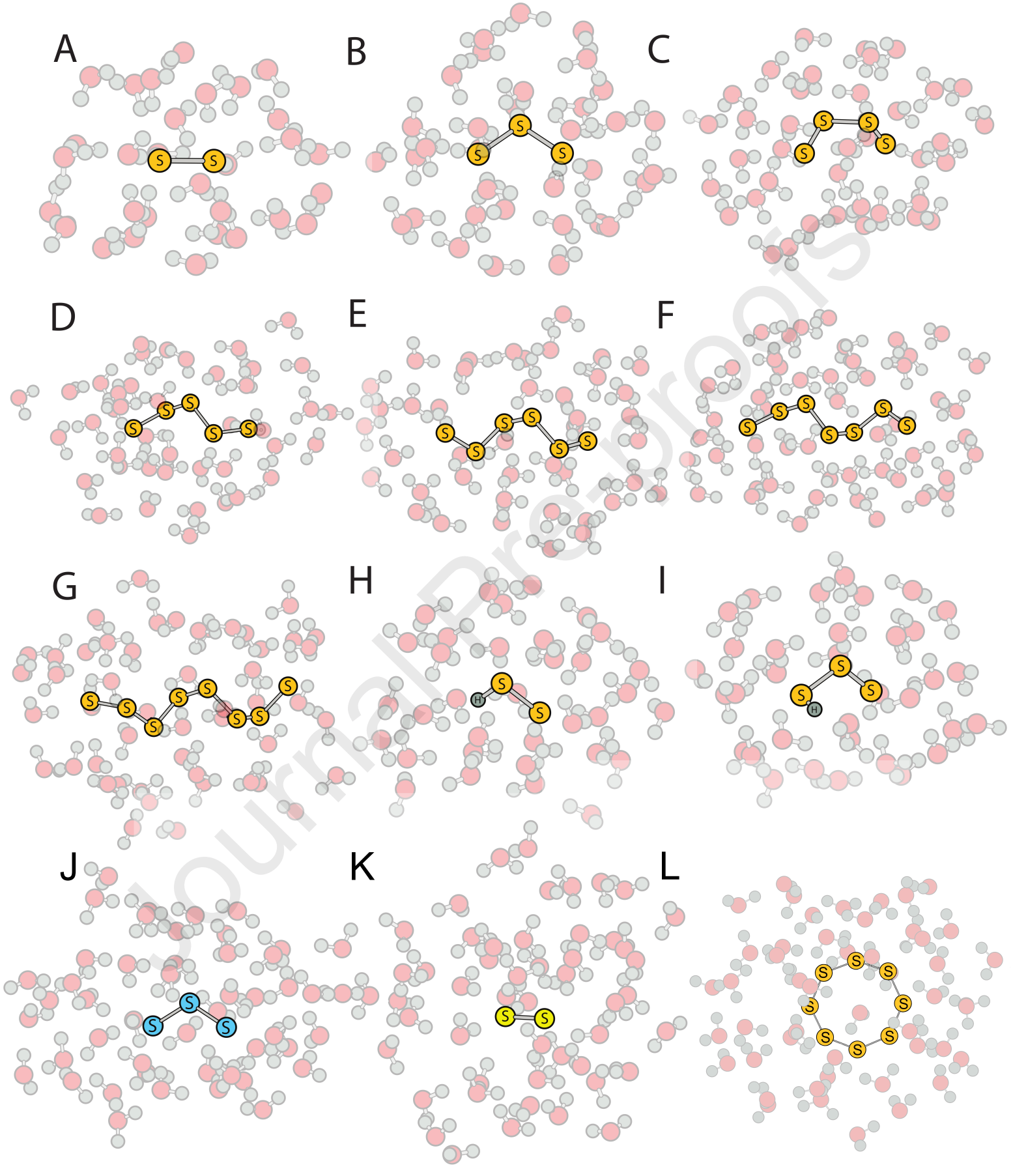

Figure2

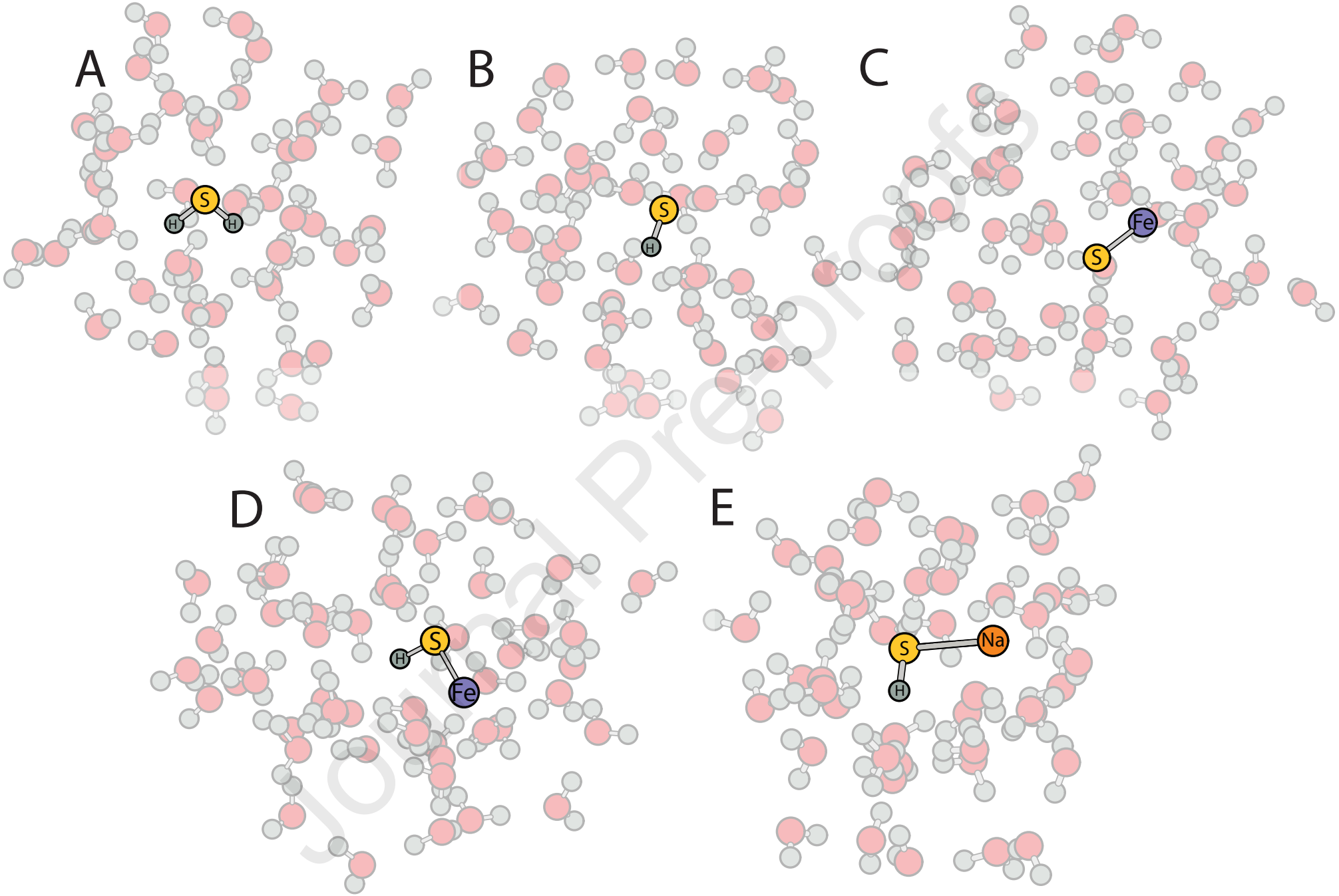

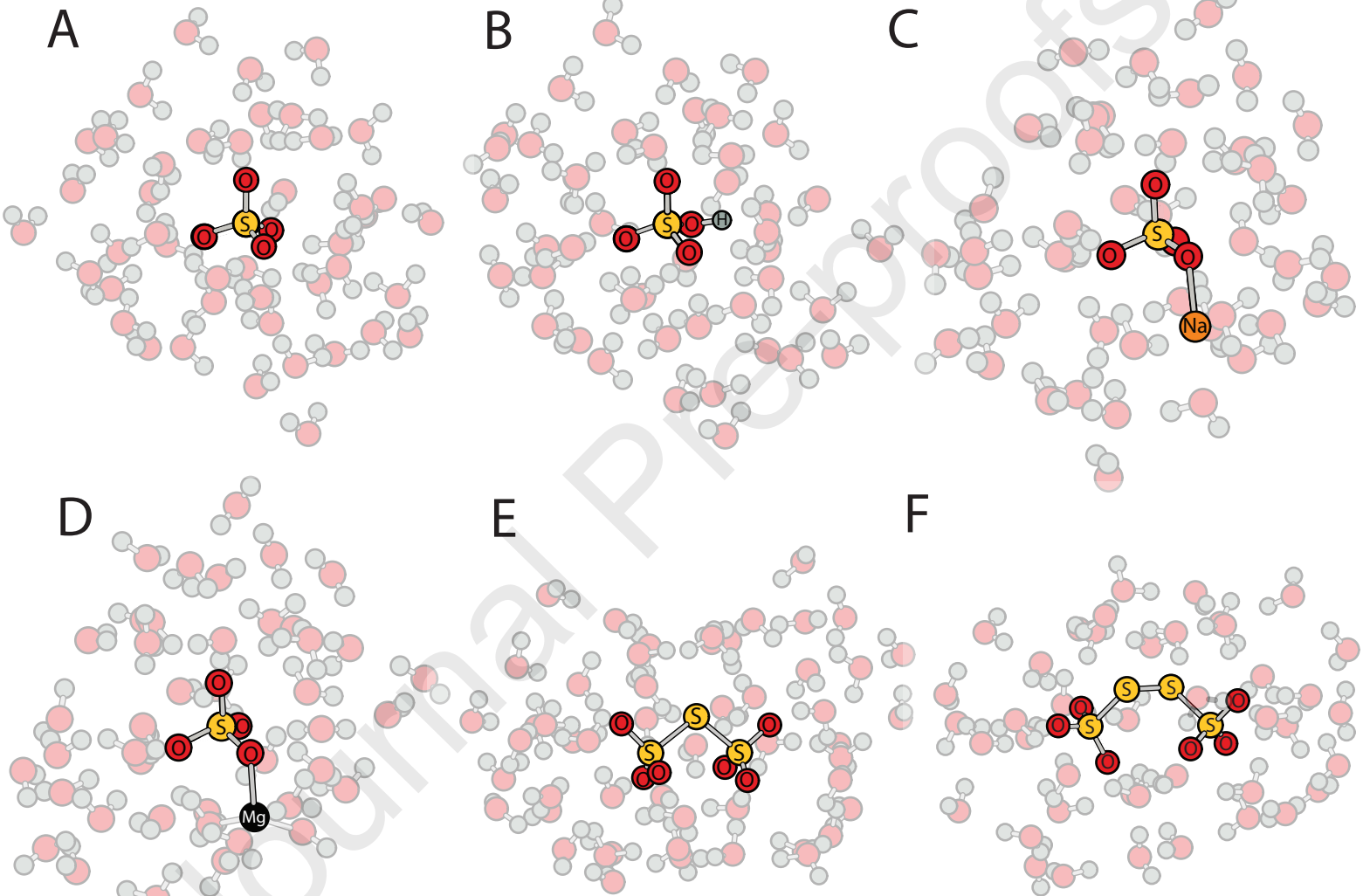

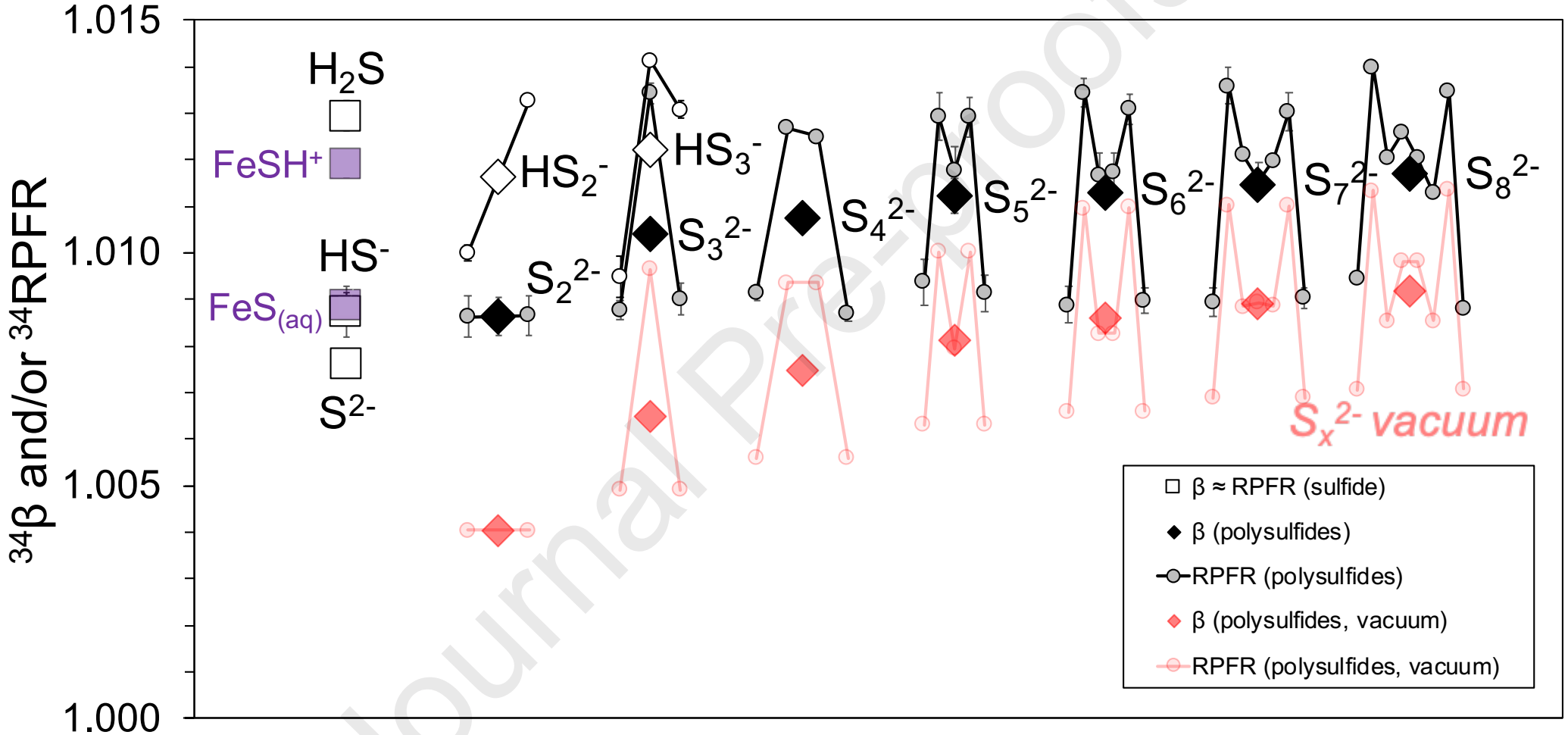

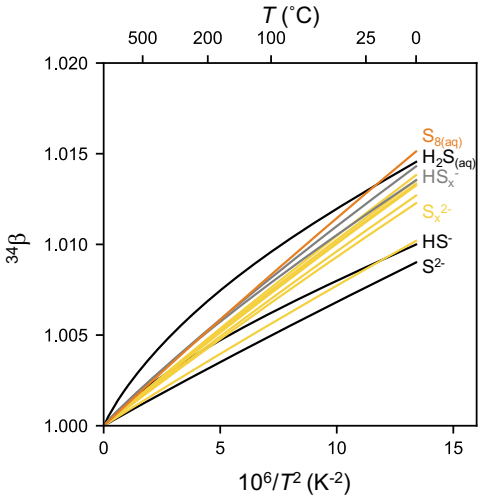

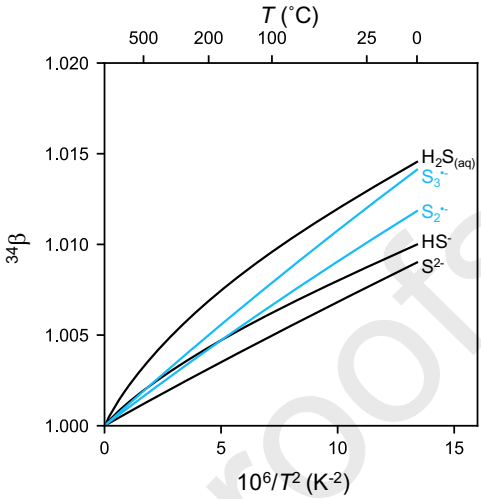

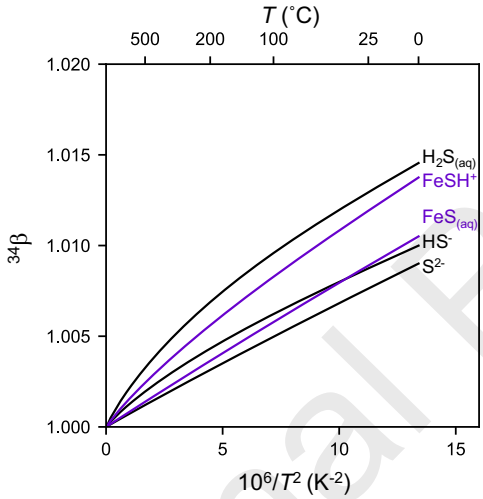

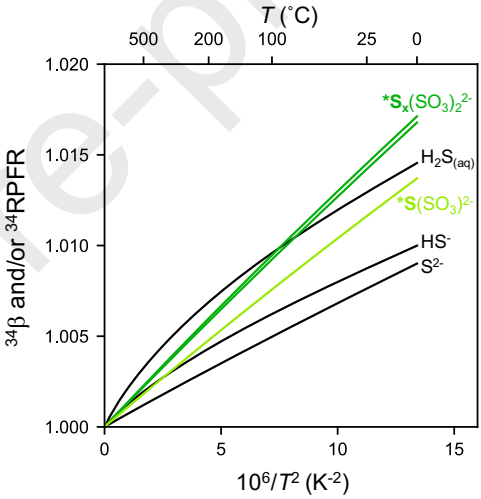

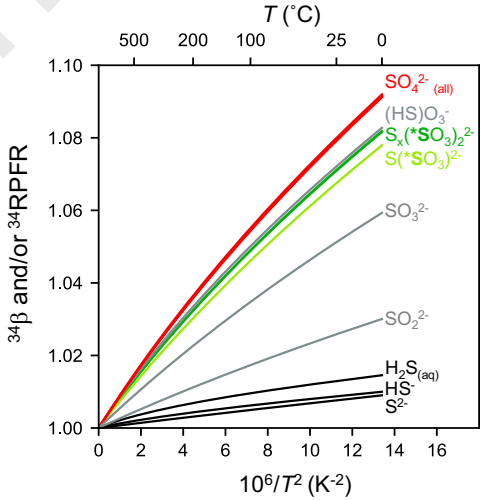

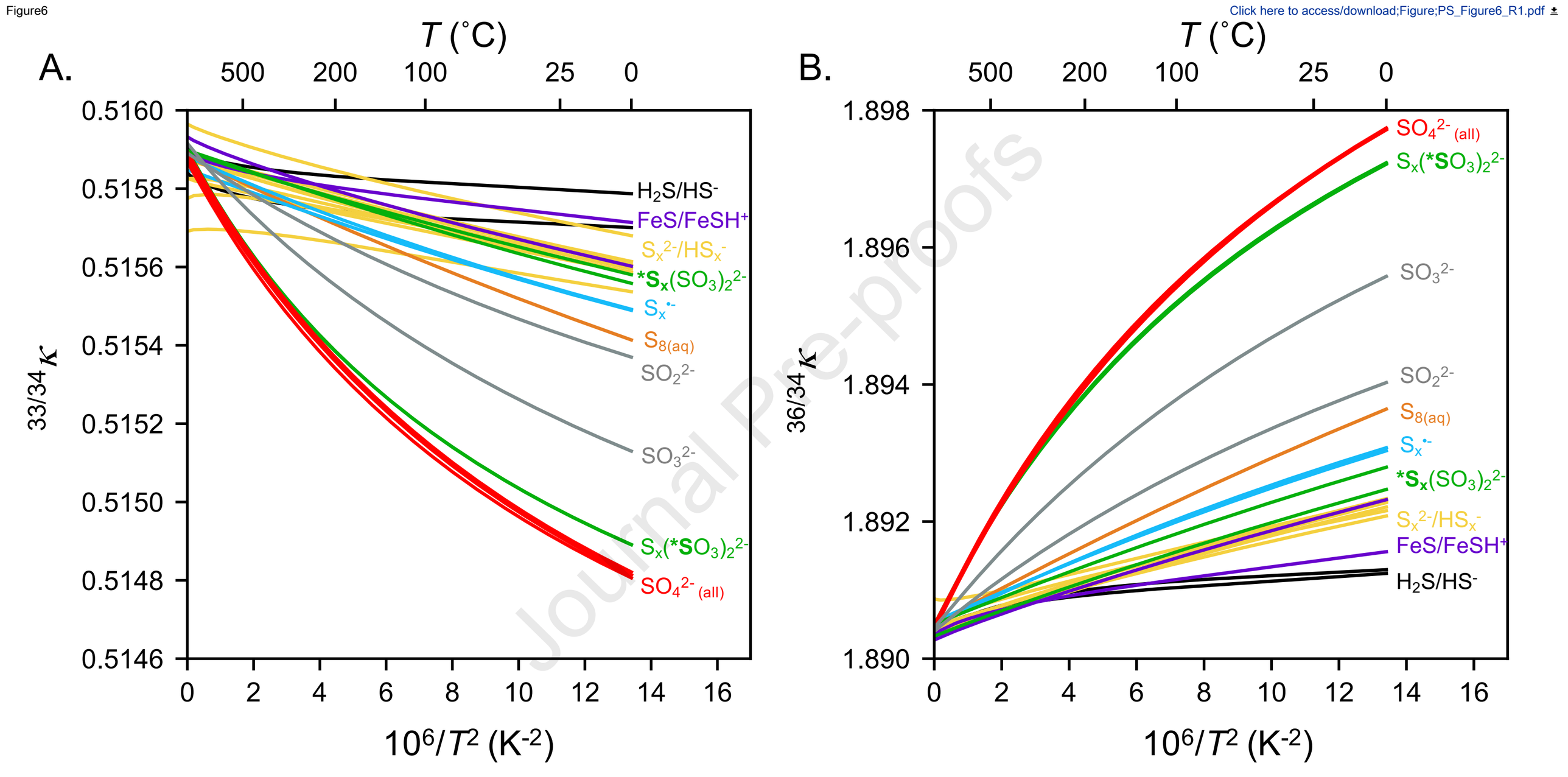

Figure7

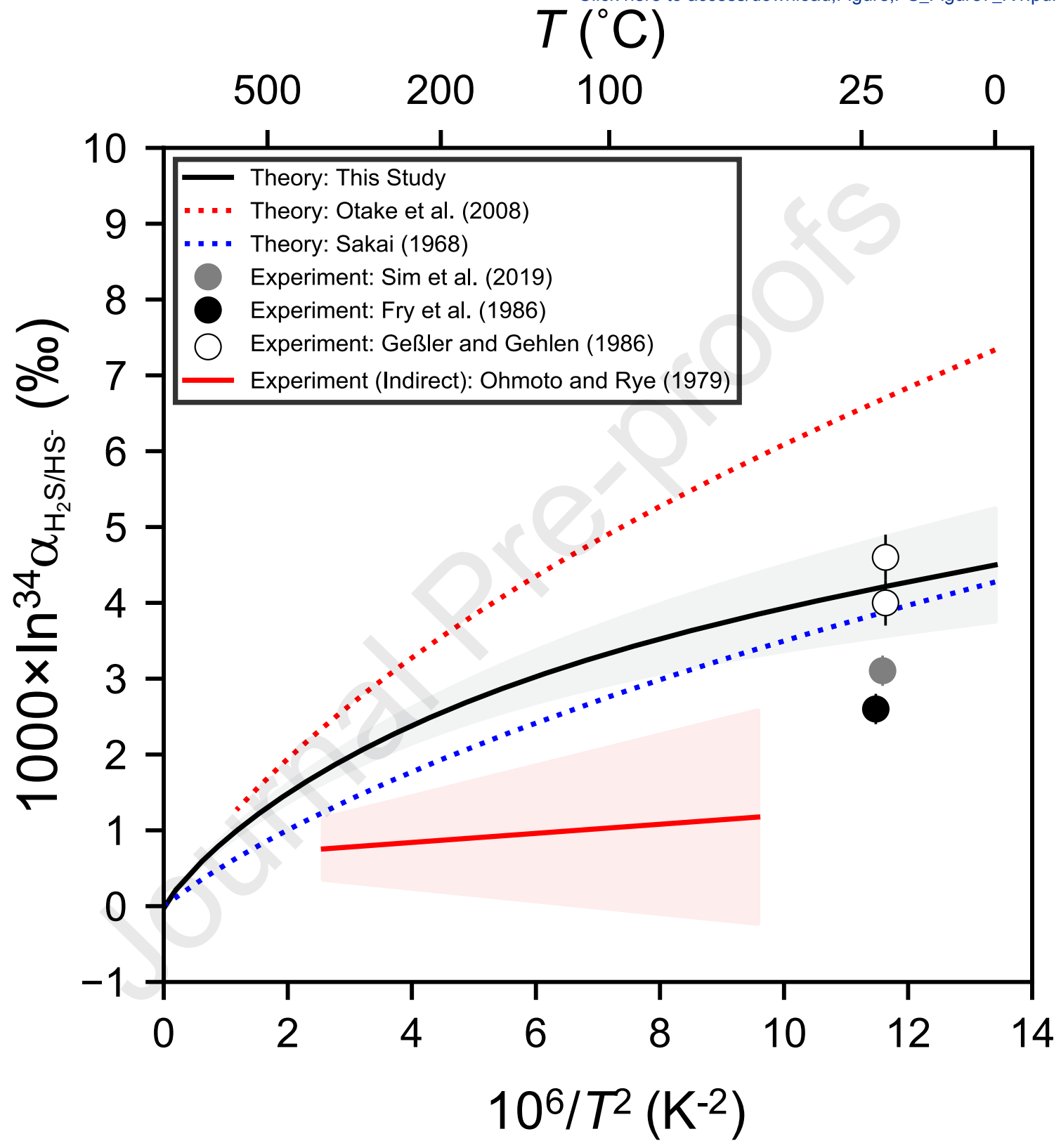

Figure8

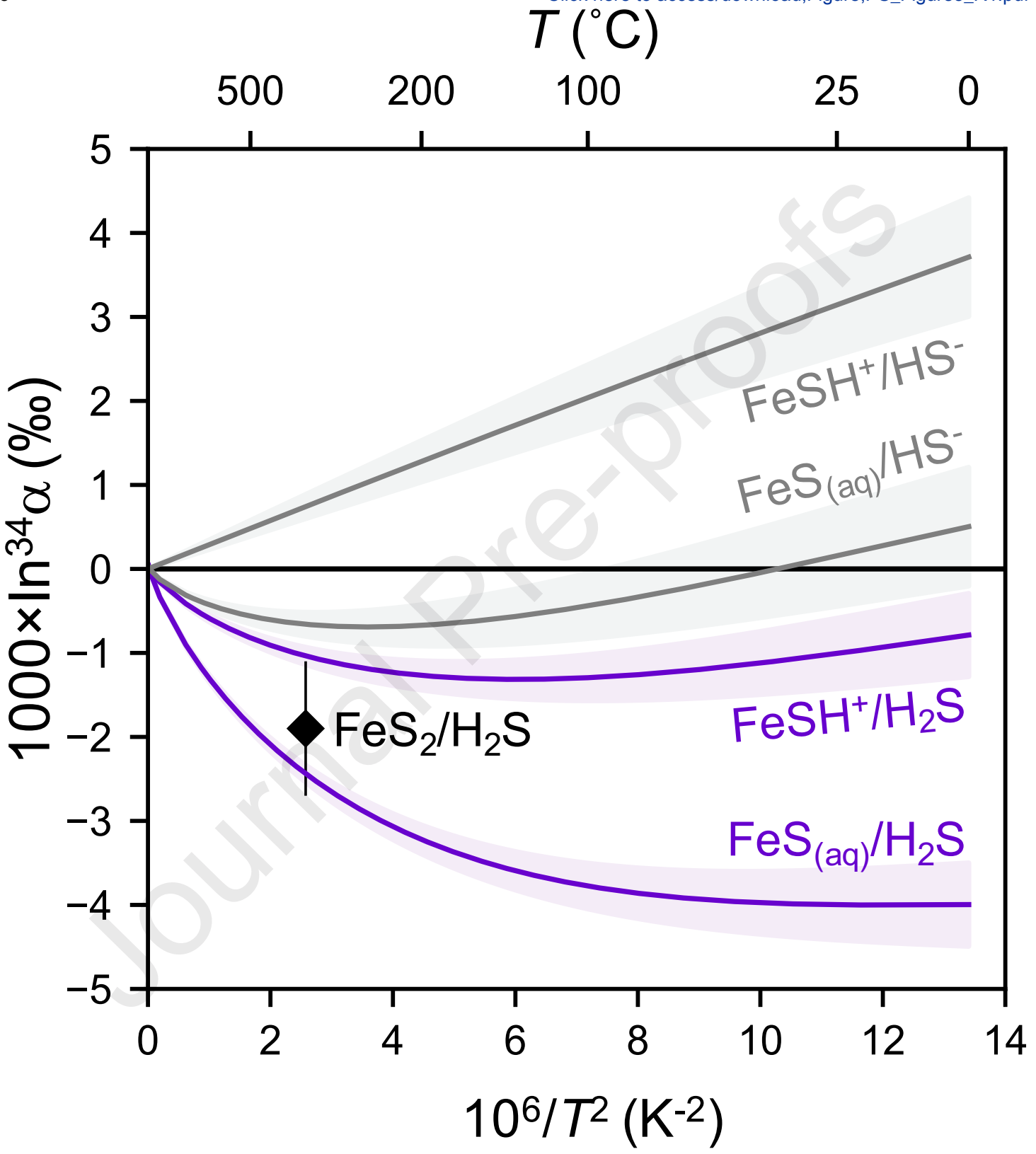

Figure9

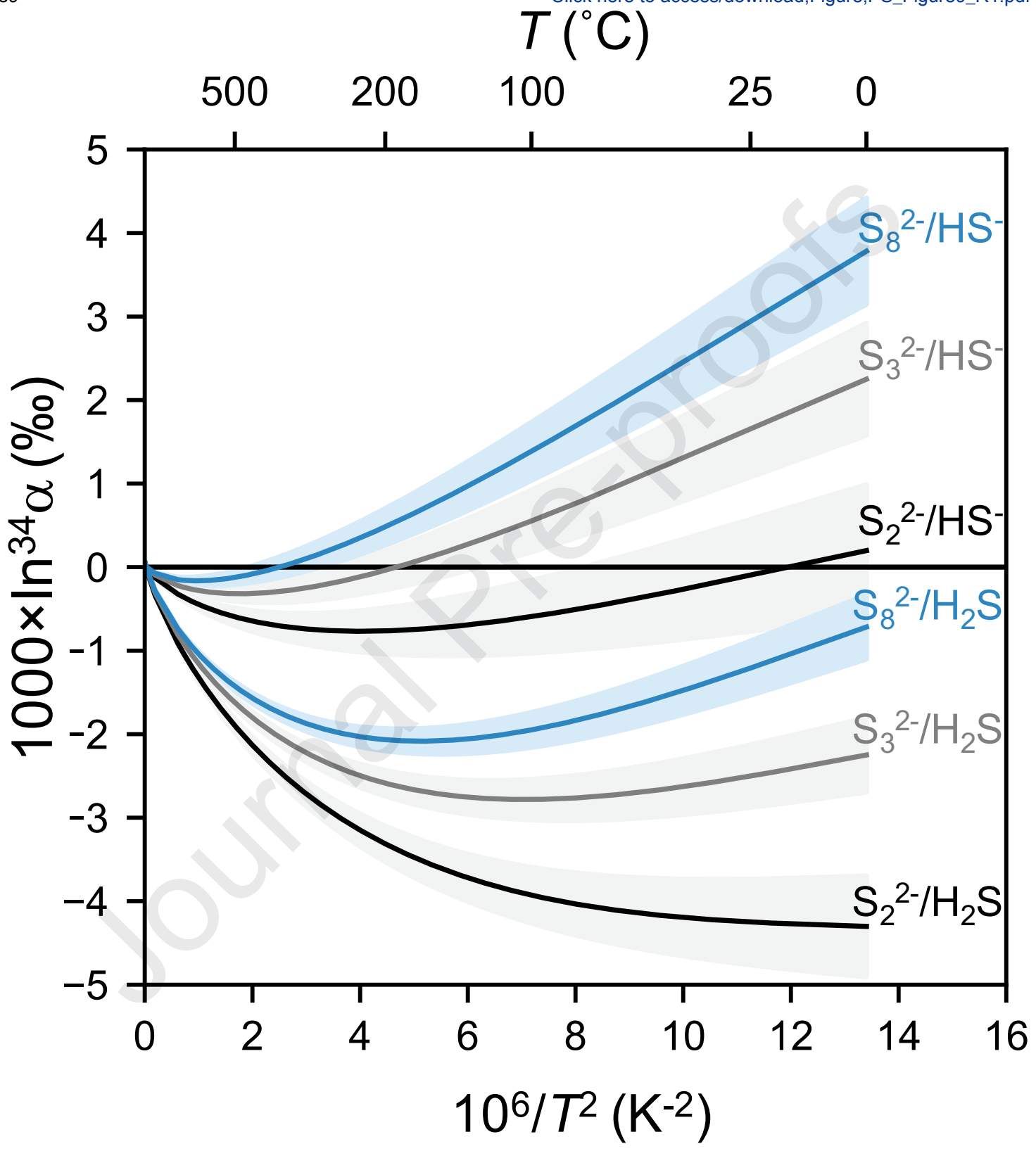

Figure10

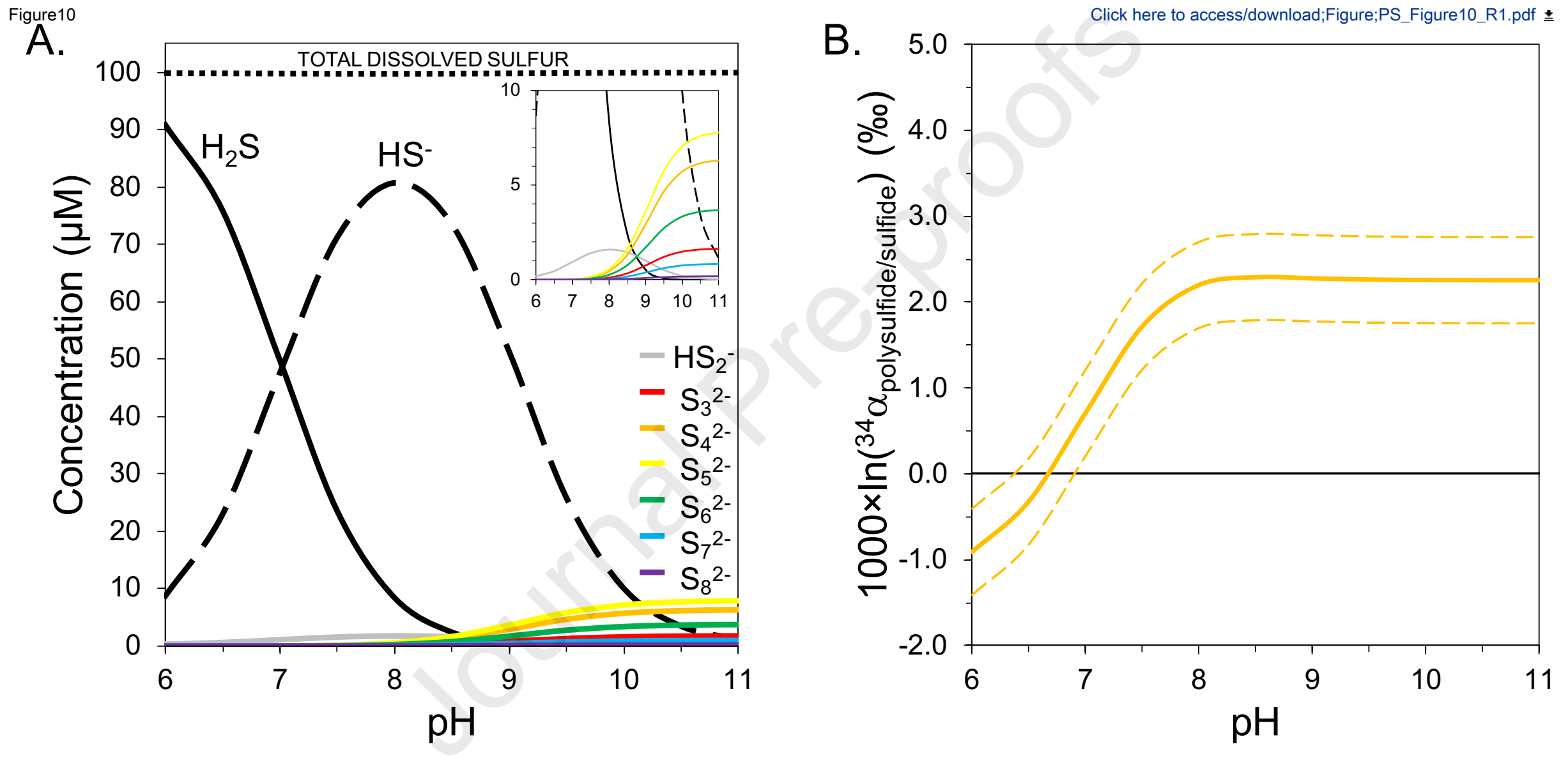

Figure11

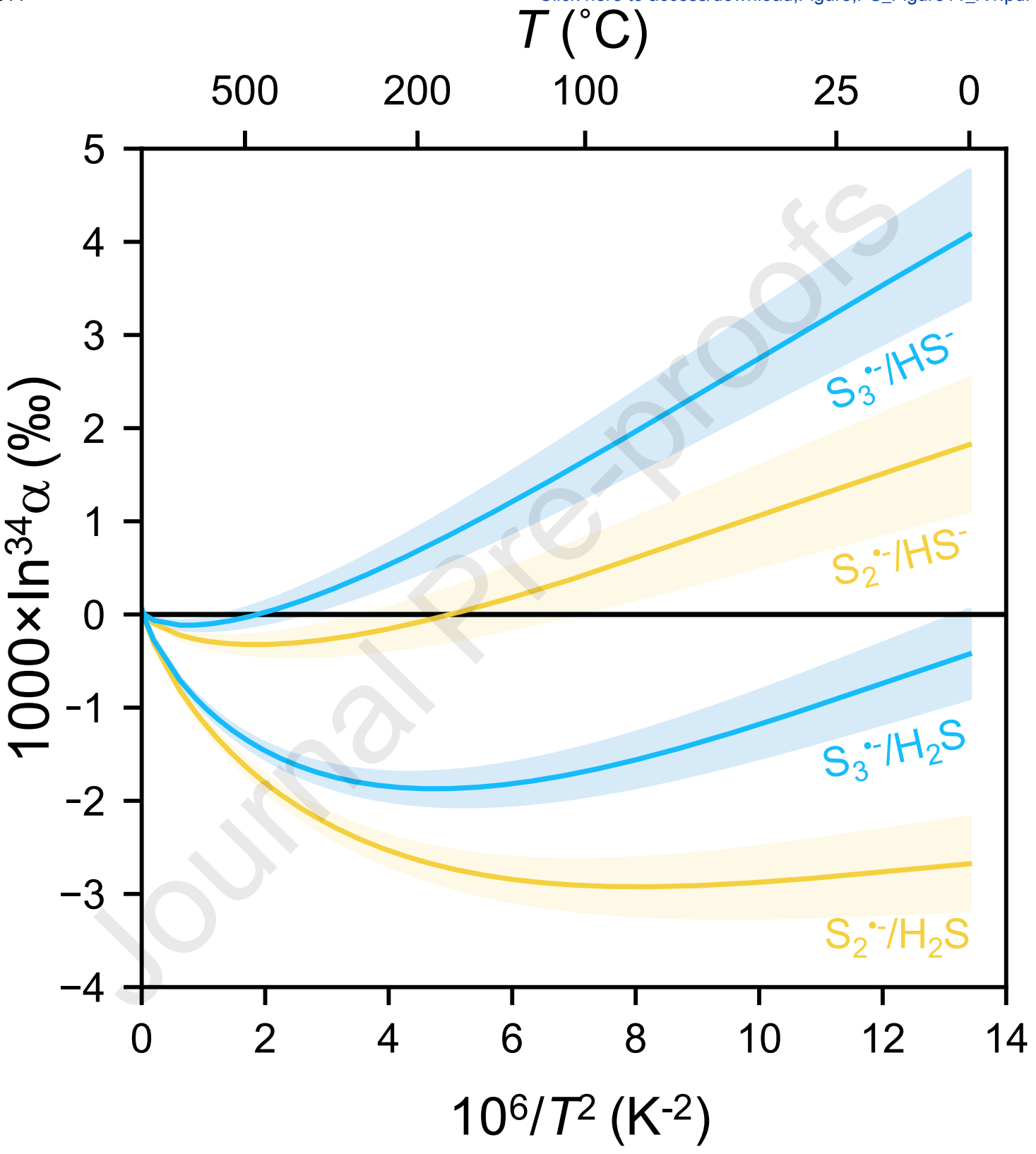

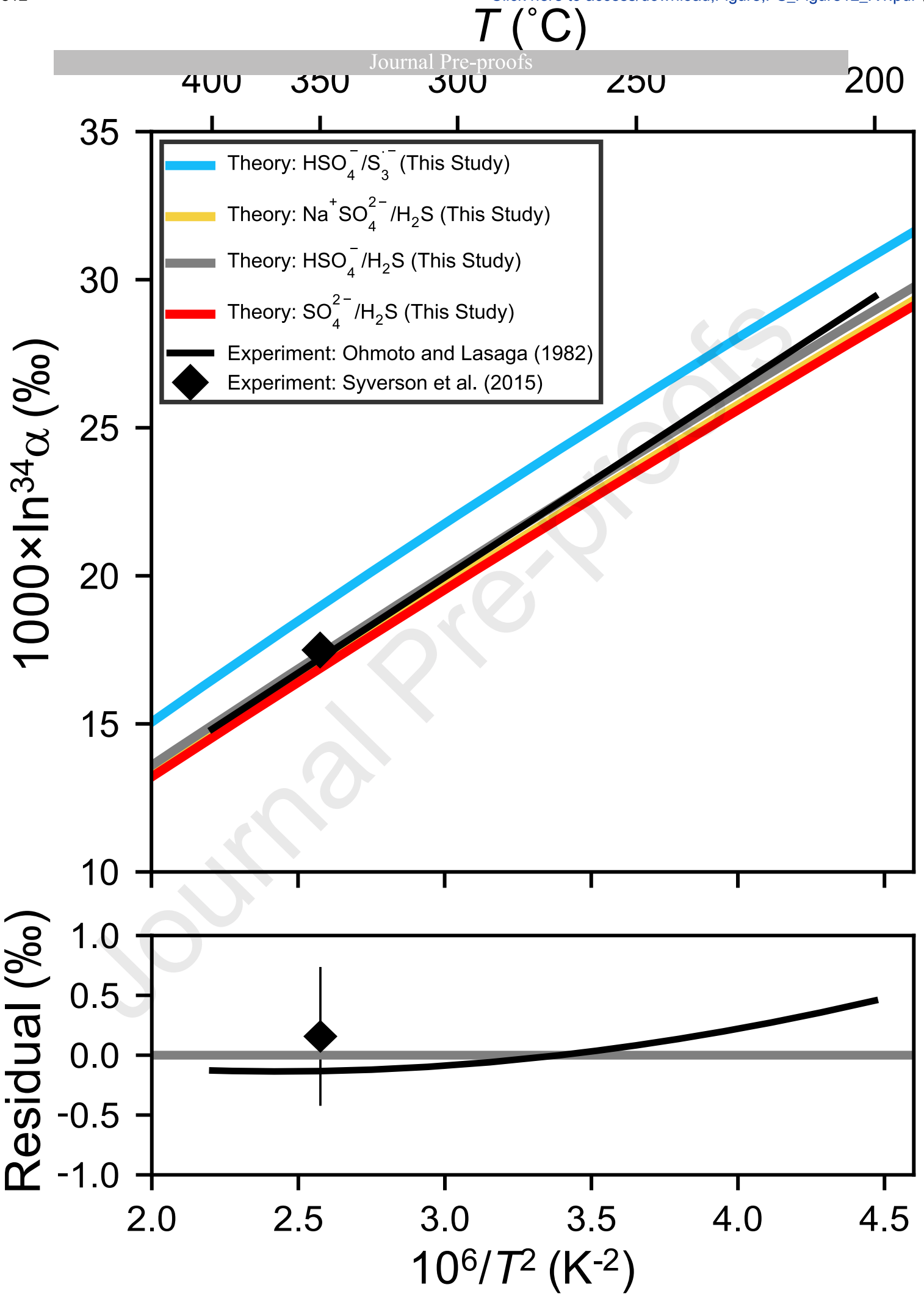

Figure13

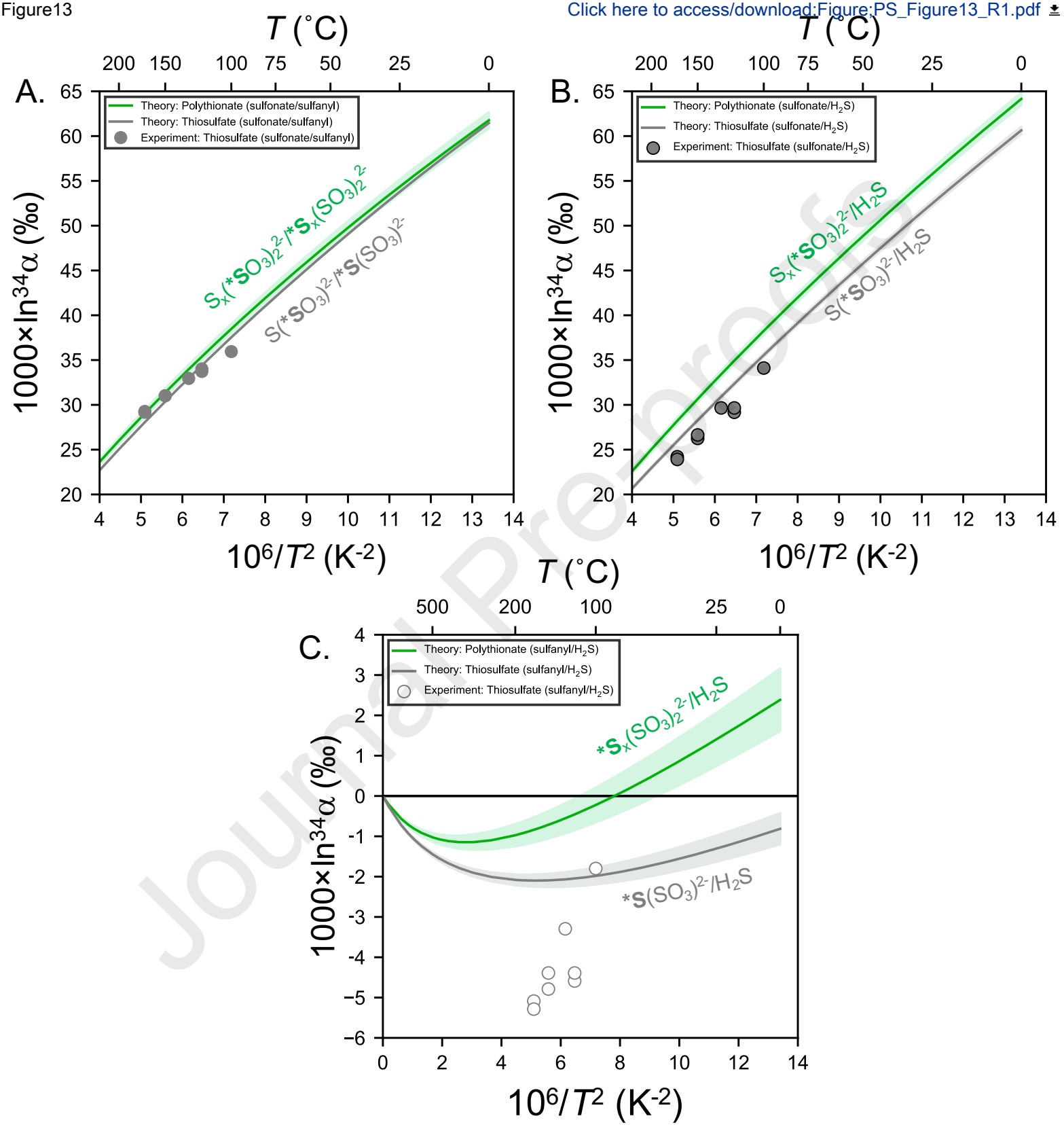

Figure14

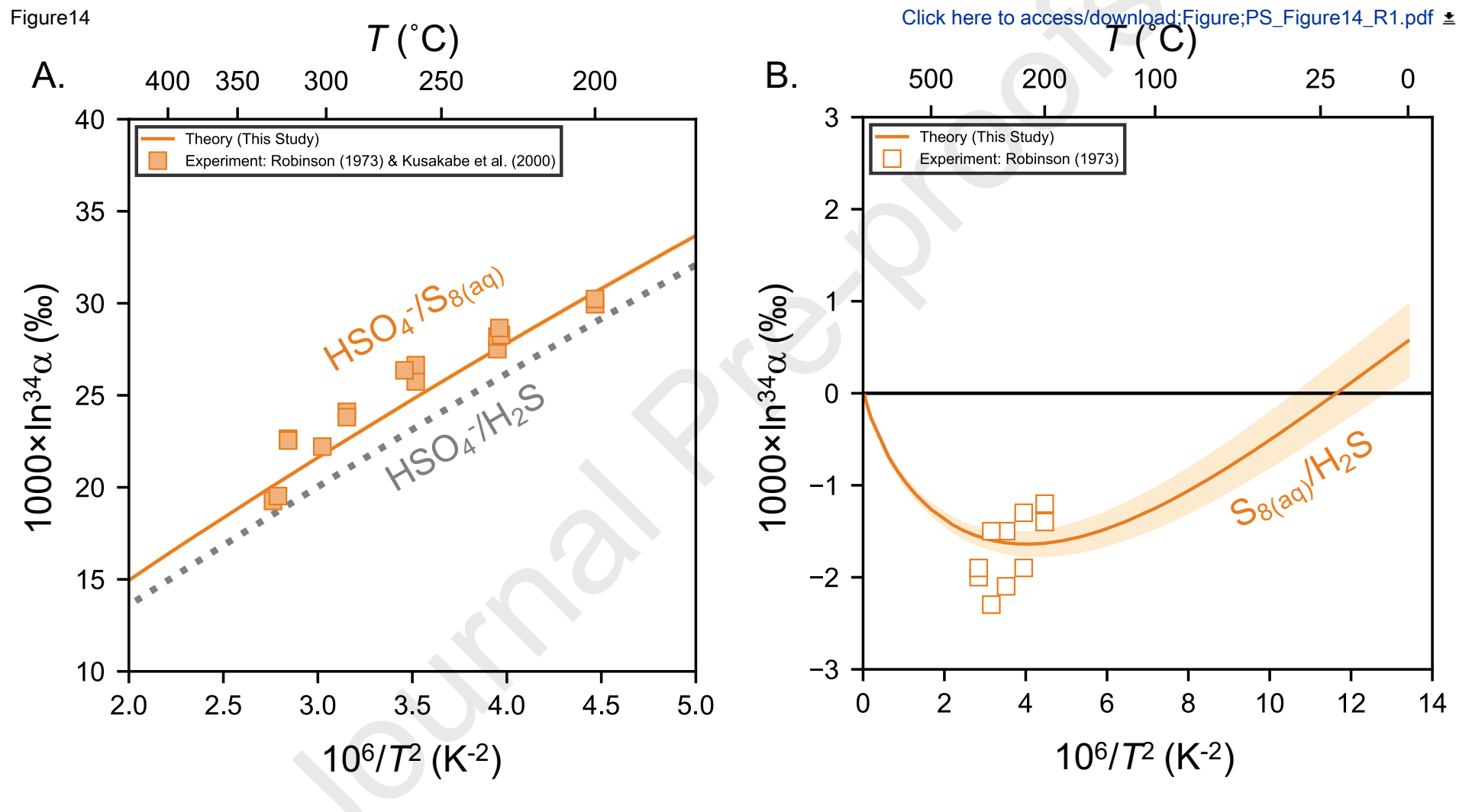

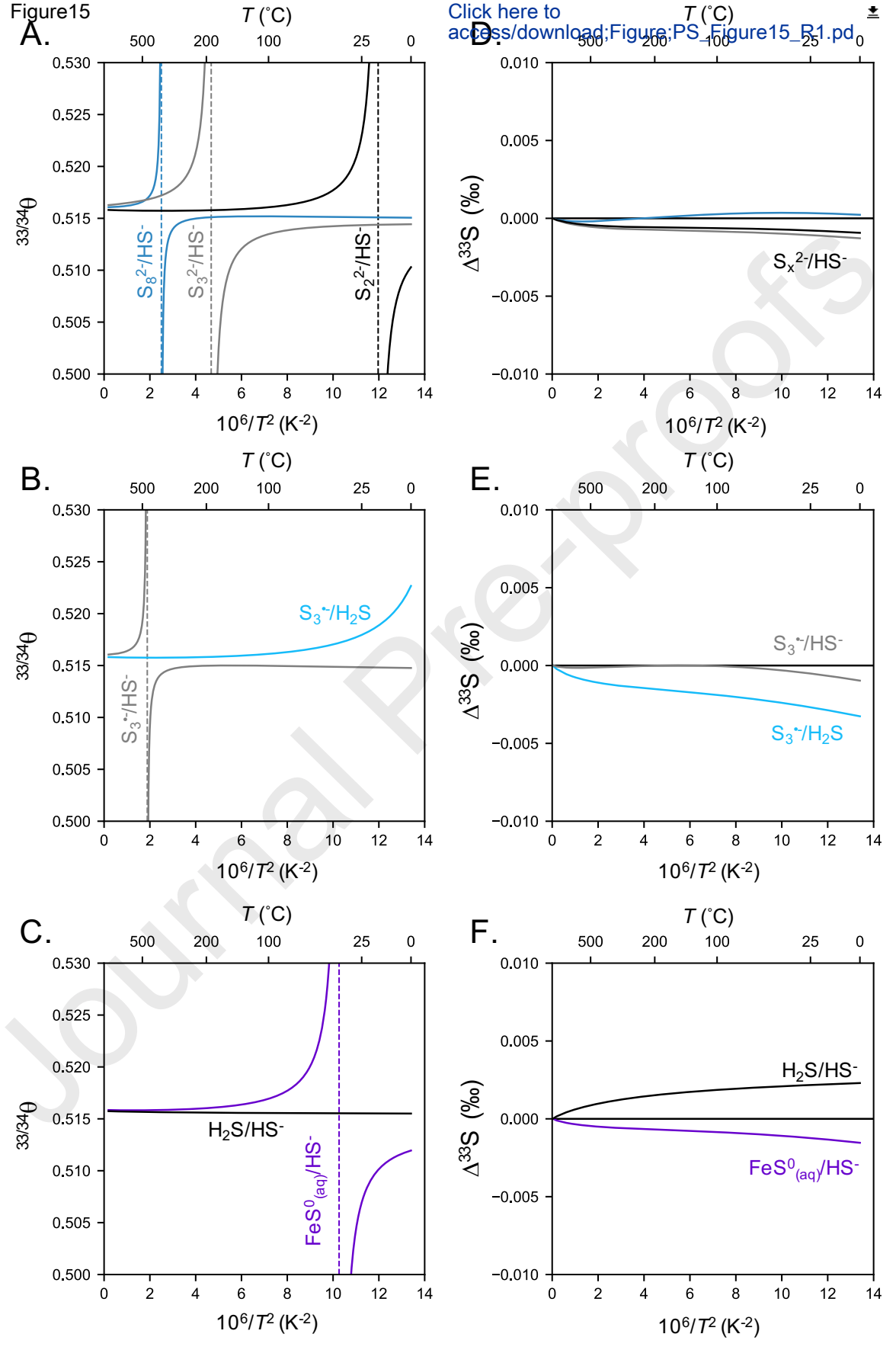

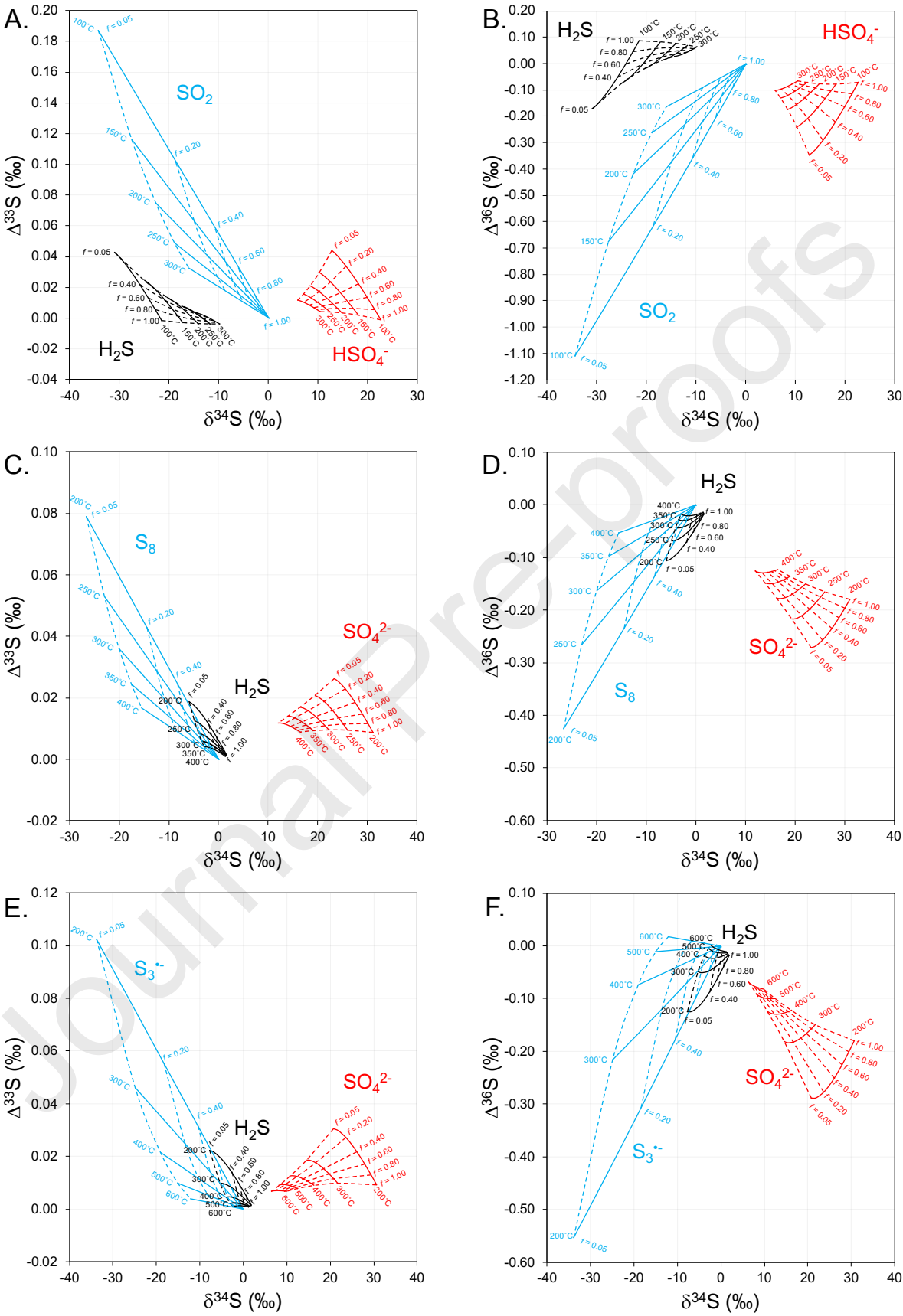

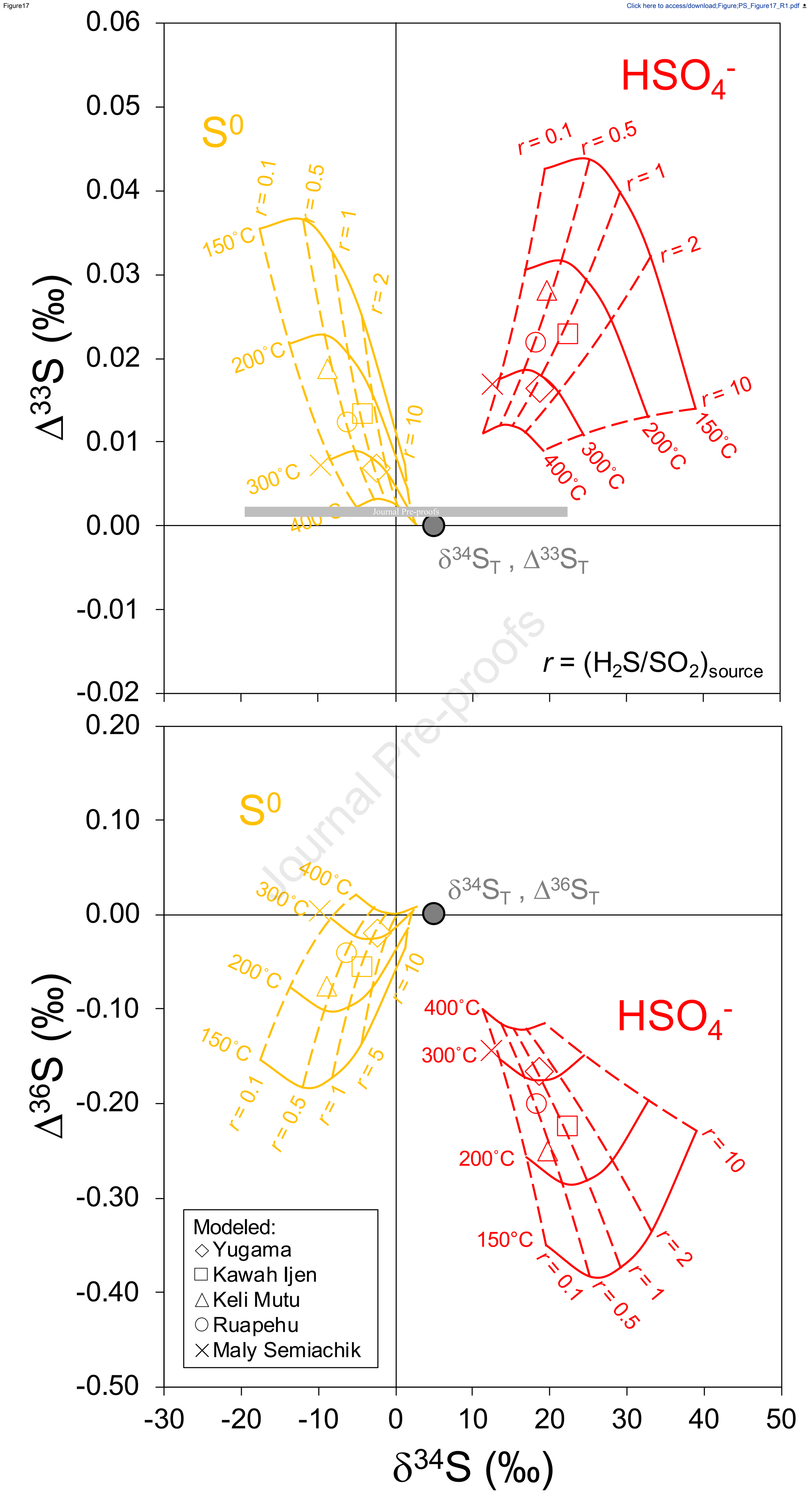

*Declaration of Interest Statement

Declaration of interests

☒ The authors declare that they have no known competing financial interests or personal relationships that could have appeared to influence the work reported in this paper.

☐The authors declare the following financial interests/personal relationships which may be considered as potential competing interests: